2017

Quaternary dynamics underlie the chaperone function of Hsp27 and αB-crystallin in maintaining proteostasis

Blagojce Jovcevski
University of Wollongong

Quaternary dynamics underlie the chaperone function of Hsp27 and αB-crystallin in maintaining proteostasis

A thesis submitted in (partial) fulfilment of the requirements for the award of the degree of

Doctor of Philosophy

from

University of Wollongong

School of Biological Sciences

By

Blagojce Jovcevski

Bachelor of Science (Biological Sciences) (Honours)

Supervisors:
Assoc. Prof. Heath Ecroyd
Dr. Andrew Aquilina

2017

Author Declaration

This thesis is submitted in line with the regulations of the University of Wollongong in partial fulfilment of the degree of Doctor of Philosophy. This thesis does not contain any material published by another person except where due reference is made in text. The experimental work described in this thesis is original work and has not been submitted for a degree or diploma at any other university.

Blagojce Jovcevski

February 2017

Acknowledgments

Firstly, I have to thank my supervisors Heath Ecroyd and Andrew Aquilina (Madge). Both of you have been incredible in dealing with me for these last five years including from Honours. But extra mention to you Heath in taking me on board full-time in the business end of things, I can't thank you enough! The same also goes to Justin Benesch; you've been there early on as well and gave me the opportunity to work with you in your lab at Oxford, which is something I never thought I'd ever achieve in my life. For that I will be always grateful. Even though he might have only just finished, I rate you on the same level as well Luke, been there from day one all the way to the end, we pretty much supervised each other, we kept each other sane throughout. It's quite simple, if it weren't for you four, I would not be able to have this thing written up! For that I'm deeply thankful. I also want to thank the Henning Family Foundation and Australian Rotary Health for providing me my PhD scholarship and continuing support.

These five years have also shown me how great and amazing other people in the work that we all do, it's pretty much a lab family. There have been so many people I could thank and mention because you've all helped and taught me a lot along the way; Anthea, Di, Dez, Bec, Caitlin, Tracey, Megan, Mick, Jeremy, Simon, Aleta, Dave, Nat, Dzung... I could be here all day really, but you are all legends and have been great friends, PhD would have been nowhere near as much enjoyable without you all. Also same shout out goes to my close friends (Jacki, Maree, Spence, Ryan, Reidsy, Rob) you all have made your mark on me and shaped me to the person I am now.

Have to mention the family here, both Mum and Dad. You have supported me and kept me clothed and fed all my life. I care and love you both so much. So I hope this 100+ page document means something to you, even though you both have no idea what I've been studying (no matter how many times I explain it in two languages!)

Also, to Emily, thank you. Honestly, words cannot even express how much it means to me to have you there. Thank you.

Thank you all

List of Publications

Conference Proceedings

Jovcevski, B., M. A. Kelly, J. A. Aquilina and H. Ecroyd. "ASPiring to a 3D view of Hsp27". 39th Lorne Conference on Protein Structure and Function, Lorne, AUS, February 2014. *Poster Presentation.*

Jovcevski, B., M. A. Kelly, J. A. Aquilina and H. Ecroyd. "Phosphorylation unveils an unique dimeric core of Hsp27". 2nd International Proteostasis and Disease Symposium, Wollongong, AUS, November 2014. *Poster Presentation.*

Jovcevski, B., M. A. Kelly, A. P. Rote, T. Berg, H. Y. Gastall, J. L. Benesch, J. A. Aquilina and H. Ecroyd. "Using native MS to delineate the structural heterogeneity and dynamics of small heat-shock proteins". 31st ASMS Asilomar Conference on Native Mass Spectrometry, Pacific Grove, USA, October 2015. *Oral/Poster Presentation.*

Jovcevski, B., M. A. Kelly, J. A. Aquilina and H. Ecroyd. "Post-translational modifications alter the structure and dynamics of Hsp27 dimers and oligomers". 42nd Lorne Conference on Protein Structure and Function, Lorne, AUS, February 2017. *Poster Presentation.*

Published Research Publications

Jovcevski, B., M. A. Kelly, A. P. Rote, T. Berg, H. Y. Gastall, J. L. Benesch, J. A. Aquilina and H. Ecroyd (2015). "Phosphomimics destabilize hsp27 oligomeric assemblies and enhance chaperone activity." *Cell Chem. Biol.* 22(2): 186-195.

Henningham, A., D. J. Ericsson, K. Langer, L. W. Casey, **B. Jovcevski**, G. S. Chhatwal, J. A. Aquilina, M. R. Batzloff, B. Kobe and M. J. Walker (2013). "Structure-informed design of an enzymatically inactive vaccine component for group A Streptococcus." *MBio* 4(4).

Cork, A. J., D. J. Ericsson, R. H. P. Law, L. W. Casey, E. Valkov, C. Bertozzi, A. Stamp, **B. Jovcevski**, J. A. Aquilina, J. C. Whisstock, M. J. Walker and B. Kobe (2015). "Stability of the octameric structure Affects Plasminogen-Binding Capacity of Streptococcal Enolase." *PLoS ONE* 10(3): e0121764.

Manuscripts in Preparation

Jovcevski B., J.A. Aquilina, J.L.P. Benesch and H. Ecroyd – Post-translational modifications alter the structure and dynamics of Hsp27 dimers and oligomers.

Jovcevski B., J.A. Aquilina, J.L.P. Benesch and H. Ecroyd – N-terminal mutations alter the structure and chaperone function of αB-crystallin.

Abstract

The pathogenesis of neurodegenerative diseases, such as Alzheimer's disease and amyotrophic lateral sclerosis, is believed to be caused by the aggregation of non-native proteins. The small heat shock proteins (sHsps) are a class of molecular chaperones which act as the first line of defence against intracellular protein aggregation. Defining the structure-function relationship of sHsps is critical to understanding the molecular mechanisms by which they inhibit protein aggregation. This thesis primarily utilised native mass spectrometry (MS) to study the structure and dynamics of the human sHsps Hsp27 (HSPB1) and αB-crystallin (αB-c, HSPB5).

Post-translational modifications (PTM) regulate the function of sHsps by inducing a range of structural changes from the secondary to the quaternary level. Serine phosphorylation of Hsp27 occurs at residues 15, 78 and 82. However, the site-specific effect of phosphorylation at each site and how the degree of phosphorylation affects Hsp27 structure and function had not been extensively characterised. One aspect of this thesis was to explore how phosphorylation affects the structure and function of Hsp27 by using mutations that mimic phosphorylation (MMP), where serine residues were substituted for aspartic acid. Utilising native MS and other biophysical techniques, this work shows that increasing the number of MMP alters the dimer-oligomer equilibrium of Hsp27, such that the proportion of dimer increases. The increase in dimer abundance correlates with an enhanced capacity of Hsp27 to inhibit amorphous and fibrillar aggregation of client proteins. Thus, based on this work it is concluded that phosphorylation of Hsp27 *in vivo* induces dissociation of large oligomers into chaperone 'active' dimers. Phosphorylation of Hsp27 can therefore be regarded as a 'molecular

switch'; during periods of cellular stress phosphorylation of Hsp27 occurs in order to help maintain intracellular proteostasis.

Whilst establishing that the dimer is likely the chaperone-active species of Hsp27, it was unclear whether dissociation of the oligomer (i.e. changes in quaternary structure) or changes in the conformation of the dimer (i.e. changes in tertiary structure) was responsible for the enhanced chaperone activity of phosphorylated Hsp27. By using MMP of Hsp27, ion-mobility MS was utilised to observe the conformation of Hsp27 dimers and oligomers. Increased levels of MMP resulted in an increase in both the unstructured state and stability of Hsp27 dimers; however, there were no differences in a larger oligomeric (12-mer) form. These changes in the tertiary structure of Hsp27 dimers did not translate to gross changes in the conformation of Hsp27 oligomers with MMP. It is concluded that the observed increase in unstructured state of Hsp27 dimers upon phosphorylation enhances the flexibility of the dimer, potentially improves its capacity to recognise and interact with misfolded client proteins to prevent aggregation. Another key PTM of Hsp27 is the stabilisation of the dimer via an inter-molecular disulfide bond mediated by Cys137. Reduction of this disulfide-bond in mutated forms of Hsp27 has been associated with motor neuropathies. The effect of reduction on the quaternary structure of Hsp27 was examined by thiol-blocking of Cys137. Reduction and thiol-blocking substantially shifts the oligomeric distribution and equilibrium of Hsp27 toward smaller odd-sized stoichiometries. This shift in the distribution ultimately results in an increased abundance of monomeric Hsp27. Overall, the data demonstrates that PTMs are crucial in modulating the structure and dynamics of Hsp27, which in turn regulates its chaperone activity and its role in proteostasis.

The N-terminal domain (residues 1 – 65) of αB-c regulates its oligomerisation and contributes to its polydispersity. The quaternary dynamics of αB-c also serve as a determinant of chaperone activity. Mutations in the N-terminal domain of αB-c at residues 54-60 were designed to identify residues involved in maintaining αB-c oligomers and chaperone function. These N-terminal domain mutant isoforms had a similar secondary structure to αB-c WT, with the exception of a 54-60 inversion mutant, which had decreased hydrophobic exposure compared to αB-c WT. All mutant isoforms were found to have a similar oligomeric distribution to αB-c WT, again with the exception of the 54-60 inversion mutant, which formed larger oligomers. The quaternary structure of the αB-c isoforms correlated strongly with chaperone activity; all the mutant isoforms had a similar ability to αB-c WT to inhibit the amorphous aggregation of insulin and seeded fibrillar aggregation of α-synuclein, except for the 54-60 inversion mutant, which had a decreased capacity to prevent the amorphous aggregation of insulin. Together, the data indicates that the quaternary structure of αB-c is a major determinant of chaperone function.

Overall, the results of this work demonstrate that the N-terminal domain is crucial in regulating the structure, function and interactions of the mammalian sHsps Hsp27 and αB-c. This is highlighted by the effect phosphorylation has on the structure and functional dynamics of Hsp27 in which increasing levels of phosphorylation induces oligomeric dissociation and enhancing chaperone activity. This work shows that the quaternary dynamics of Hsp27 and αB-c underlie their chaperone activity and therefore play a crucial role in maintaining intracellular proteostasis. Native MS-based techniques provide an ideal tool to probe these fundamental aspects of this highly dynamic family of molecular chaperone proteins.

List of Abbreviations

αB-c	αB-crystallin
αCD	α-crystallin domain
αS	α-synuclein
Aβ	amyloid β peptide
AP	antiparallel interaction
ATD	arrival time distribution
CID	collision-induced dissociation
CIU	collision-induced unfolding
DTT	dithiothreitol
E. coli	Escherichia coli
EDTA	ethylenediaminetetraacetic acid
h	hours
Hsp	heat shock protein(s)
Hsp27	heat shock protein 27
IM-MS	ion mobility – mass spectrometry
LB	Luria Bertani
MS	mass spectrometry
MS/MS	tandem mass spectrometry
m/z	mass to charge ratio
nanoESI-MS	nanoelectrospray ionisation – mass spectrometry
NH_4OAc	ammonium acetate
NMR	nuclear magnetic resonance
PB	phosphate buffer
PBS	phosphate buffered saline
PES	polyethersulfone
PMF	peptide mass fingerprint(s)
PMSF	phenylmethylsulfonyl fluoride
PTM	post-translational modification
Q-TOF	quadrupole - time of flight
s	seconds

SEC	size-exclusion chromatography
SDS-PAGE	sodium dodecyl sulfate - polyacrylamide gel electrophoresis
sHsp	small heat shock protein(s)
TCEP	tris(2-carboxyethyl)phosphine
TEM	transmission electron microscopy
TEMED	tetramethyl-ethlenediamine
V	volts
WH	waveheight

List of Tables

List of Figures

Table of Contents

Chapter 1:

Introduction

Chapter 1: Introduction

The aggregation and deposition of proteins into intracellular inclusions or extracellular plaques is associated with numerous diseases, including Alzheimer's disease, Amyotrophic Lateral Sclerosis and some cardiac myopathies (Dobson, 1999, Evgrafov *et al.*, 2004, Vicart *et al.*, 1998). The pathogenesis of these diseases is believed to be caused by the aggregation of non-native (misfolded or partially-folded) proteins, thereby disrupting cell/tissue function (Caughey and Lansbury, 2003, Guo *et al.*, 2009, Walsh *et al.*, 2002). It is well known that the body has control mechanisms that act to ensure that proteins are kept in their native (functional) state, thereby avoiding aggregation. Chaperones play a key role in this protein quality control (PQC) network, preventing protein aggregation and, in some cases, refolding misfolded proteins back to their native state (Buchner, 1996). The small heat shock proteins (sHsps) are a class of molecular chaperones that are one of the first lines of defence against protein aggregation in cells. Characterisation of the structure and function of sHsps is critical in understanding how these proteins minimise aggregation and contribute to overall PQC in the cell. What has made this difficult in the past is that the sHsps are typically large, oligomeric dynamic proteins and therefore challenging to study using traditional structural biology approaches. However, with the development and use of native mass spectrometry (MS) as a structural biology tool, the structure and dynamics of non-covalent macromolecular assemblies can now be interrogated. The focus of the work described in this thesis was the use of native MS to study the structure and dynamics of the human sHsps Hsp27 and αB-crystallin.

1.1 Protein folding, misfolding and aggregation

1.1.1 Protein folding

Proteins are polypeptide chains that are typically folded into tertiary structures in which the hydrophobic regions are shielded from the aqueous environment (Dobson, 2003). This is essential to ensure the stability and optimal function of the protein. When proteins are not folded correctly, function becomes impaired and, in some cases, this results in disease (Dobson, 2003, Stirling *et al.*, 2003). Small proteins typically fold spontaneously, however, large proteins (i.e. >100 amino acid residues) typically fold through a series of transition states, forming stable intermediates that display distinct secondary structures (Dobson, 2003, Radford and Dobson, 1999, Stirling *et al.*, 2003).

Early work on protein folding revolved around understanding the kinetics which drive the process and identified protein folding as a sequential and spontaneous process with defined intermediates (Anfinsen, 1973, Kim and Baldwin, 1982). The initiating step of protein folding involves hydrogen-bonding between key residues in the primary structure of the protein; this drives the formation of secondary structures such as α-helices and β-sheets. The polypeptide backbone subsequently undergoes hydrophobic collapse, forming a stable intermediate (molten globule), in which most of the hydrophobic regions are protected from the aqueous environment (Anfinsen, 1973, Csermely *et al.*, 2003, Fink, 1999, Yang and Gruebele, 2003). The inner hydrophobic core is then rearranged and water is removed to form the native tertiary structure. The advances in methodologies used to study protein folding, such as solid state nuclear magnetic resonance (NMR) spectroscopy and *ab-initio* computer modelling, have introduced the concept of the 'energy landscape' with regards to protein folding (Figure 1.1) (Dobson, 2003, Krishna *et al.*, 2004). This energy landscape

model describes why, when a polypeptide chain folds, native conformations, which are more thermodynamically stable, are favoured (Figure 1.1) (Dinner *et al.*, 2000).

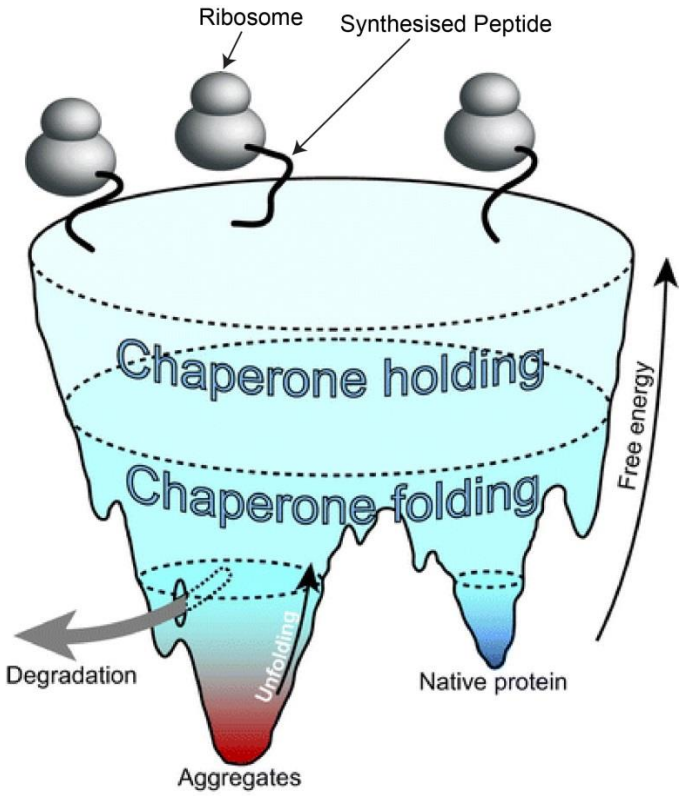

Figure 1.1: Representation of the free energy landscape of protein folding.
Synthesised peptides 'funnel' towards their native conformation, distinguished by a state of minimal free energy (enthalpy and entropy). Various 'funnels' indicate possible pathways that proteins may take (degradation, aggregation and native conformations). Regions highlighted as chaperone 'holding' (sHsps) and 'folding' (e.g. Hsp60, Hsp70) indicate the points where these chaperones act in the folding landscape. Modified from Gregersen *et al.*, (2006).

1.1.2 Protein misfolding and aggregation

Factors that induce the unfolding and misfolding of proteins include mutations and post-translational modifications, as well as environmental changes (e.g. temperature, pH and oxidation state) (Dobson, 1999). These non-native states have an increased amount of exposed hydrophobicity (which would normally be buried into the core of the native state of the protein), and therefore a high propensity to self-associate, leading to aggregation (Stirling *et al.*, 2003). The formation of these aggregates, which can be amorphous or fibrillar

in nature, is believed to disrupt cell function and be cytotoxic (Stefani and Dobson, 2003). Such aggregates are a hallmark of numerous neurodegenerative diseases, such as Alzheimer's disease, Amyotrophic Lateral Sclerosis and lens cataract (Iwaki *et al.*, 1992, Liu *et al.*, 2006, Renkawek *et al.*, 1994b).

Amorphous aggregates arise from the disordered accumulation of misfolded monomeric units which have increased regions of exposed hydrophobicity, such that the aggregate has no defined 3D structure (Dobson, 2004). Models have been proposed for the mechanisms by which bovine α-lactalbumin forms amorphous aggregates (based on experiments that measured the turbidity of the solution at 340 nm as a reporter of aggregation) (Stranks *et al.*, 2009). Bovine α-lactalbumin forms amorphous aggregates under reducing conditions and is commonly used in aggregation assays *in vitro* to assess the ability of molecular chaperones to prevent protein aggregation (Lindner *et al.*, 1997, Treweek *et al.*, 2005). The model to describe the aggregation of α-lactalbumin suggests that monomeric units associate with the growing aggregate, resulting in increased aggregate surface area and an increase in the rate of aggregation (Stranks *et al.*, 2009). In addition, this model suggests that monomers can associate to the growing aggregate from any direction, and thus formation of the amorphous aggregate occurs three-dimensionally (Stranks *et al.*, 2009).

Fibrillar aggregates arise from the ordered aggregation of partially-folded proteins and/or peptides (Kelly, 1997). The most common type of fibrillar aggregate are amyloid fibrils, which are structurally ordered filaments ~10 nm in width and 0.1–10 μm in length (Figure 1.2A) (Makin *et al.*, 2005, Ross and Poirier, 2004). X-ray fibre diffraction analysis identified a generic structural motif in amyloid fibrils consisting of β-sheets running perpendicular to the long fibril axis and hydrogen-bonds running parallel to this long axis

(Fitzpatrick *et al.*, 2013, Serpell *et al.*, 1997, Sunde *et al.*, 1997). These structural motifs result in the diagnostic 'cross β-sheet' array of fibrillar aggregates. Morphologically, most fibrils exhibit a twisted appearance when observed by atomic force microscopy and transmission electron microscopy (TEM) (Figure 1.2) (Fitzpatrick *et al.*, 2013, Ross and Poirier, 2004).

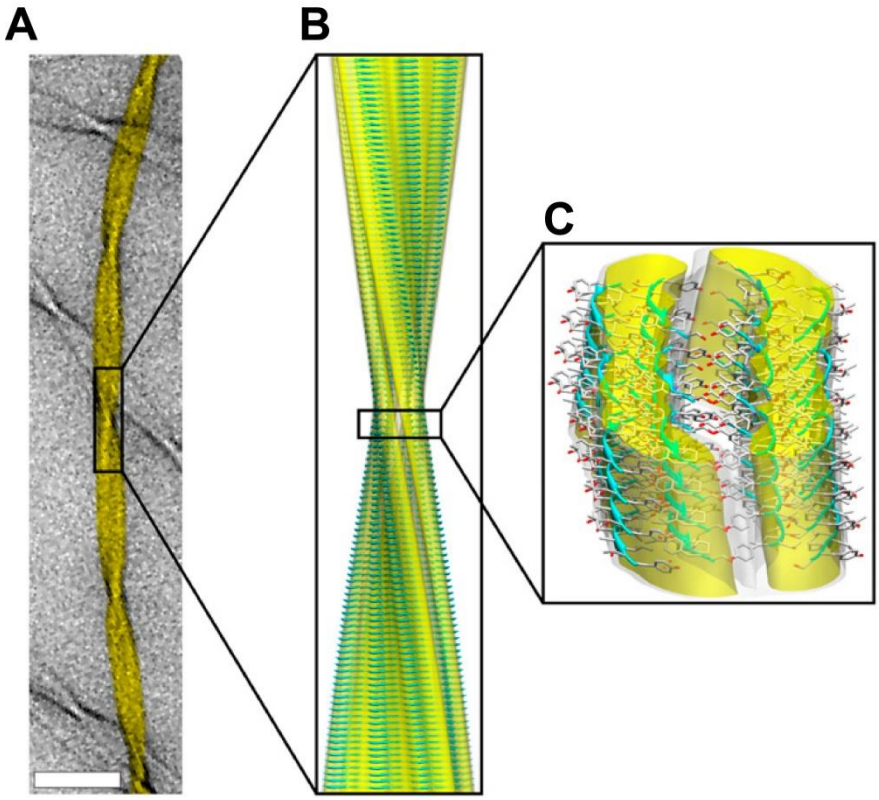

Figure 1.2: TEM image and a high-resolution model of amyloid fibrils
A: TEM image of amyloid fibrils formed using transthyretin (TTR) peptides (residues 105-115) (scale bar 50 μm) **B:** TEM image of the amyloid fibril was reconstructed using cryo-EM. **C:** NMR atomic-resolution structure of the fibril showing the core structure of each filament (the β-sheet stack lying perpendicular to the fibril axis, forming a cross β-sheet array). Modified from Fitzpatrick *et al.*, (2013).

It is broadly accepted that both forms of protein aggregation occur via a nucleation-dependent mechanism involving well-defined phases (Figure 1.3) (Makin *et al.*, 2005, Markossian *et al.*, 2009). With regards to fibril formation, misfolded proteins mutually associate to form a nucleus, the rate limiting step in the process and determinant of the lag

phase of the reaction. Continuous attachment of monomers to this nucleus leads to the formation of assemblies referred to as protofibrils (Markossian and Kurganov, 2004, Markossian *et al.*, 2009, Wilson *et al.*, 2008). Protofibrils then recruit other misfolded monomeric units, leading to an elongation phase in which the fibrils grow at a rapid rate (Dobson, 2003, Markossian and Kurganov, 2004, Wilson *et al.*, 2008). Upon reaching a point where fibril recruitment is maximal (high fibril concentration, low monomer concentration), a plateau phase in the reaction is reached. This is characterised by the lateral association of fibril filaments and the formation of mature amyloid fibrils (Figure 1.3) (Chiti and Dobson, 2006, Wilson *et al.*, 2008).

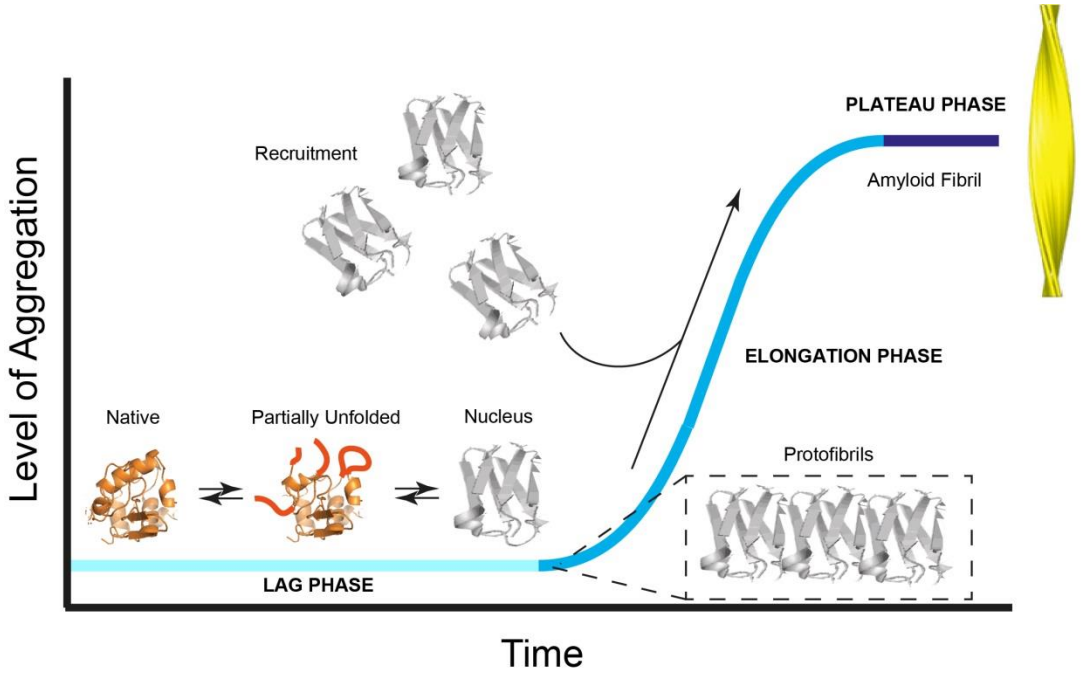

Figure 1.3 The nucleation-dependent mechanism of amyloid fibril formation
Amyloid fibril formation consists of three phases. The lag (nucleation) phase (*light blue*) is the time in which a nucleus and protofibrils are produced. The elongation phase (*blue*) involves protofibrils recruiting other non-native monomeric proteins to their ends causing rapid fibril growth. The plateau phase (*dark blue*) is a point where protofibrils laterally associate and a mature amyloid fibril is formed. Modified from Chiti and Dobson, (2006), Fitzpatrick *et al.*, (2013), Wilson *et al.*, (2008).

1.2 Protein Quality Control (PQC)

The formation of ordered and disordered protein aggregates is an indicator of a failure in the pathways that normally act to maintain protein homeostasis (proteostasis) in the cell. One super family of proteins that are crucial in preventing protein aggregation (and therefore maintaining proteostasis) are the heat shock proteins (Hsps), a large family of molecular chaperone proteins that were initially categorised based on their apparent monomeric molecular mass.

1.2.1 ATP-dependent heat shock proteins

Members of the Hsp family in which the chaperone activity is dependent on ATP hydrolysis include Hsp40, Hsp60, Hsp70 and Hsp90. Both Hsp70 and Hsp90 are cytosolic ATP-dependent chaperones that fold synthesised polypeptides into their native conformation, whereas Hsp60 aids in providing further stability of native structures (Langer *et al.*, 1992a).

As the growing polypeptide emerges from the ribosome, it is presented to monomeric Hsp70 which recognises short hydrophobic motifs along the polypeptide. Hsp70 shields this exposed hydrophobicity from interacting with other regions within the polypeptide as well as other non-native cellular proteins (Landry *et al.*, 1992b). The folding function of Hsp70 is ATP-dependent and is also regulated by its co-chaperone Hsp40. This co-chaperone recognises and binds to newly synthesised polypeptides from the ribosome, and in doing so, recruits Hsp70 for folding (Beckmann *et al.*, 1990). Once partially folded, co-factors and ATP-hydrolysis act to release the polypeptide from Hsp70. The polypeptide may then complete the process of folding into its native state or may require further stabilisation by Hsp60 folding machinery or undergo another round of interaction with Hsp70 (Langer *et al.*, 1992a, Thulasiraman *et al.*, 1999).

Hsp60 helps to stabilise and fold partially folded polypeptides formed following interaction with Hsp70. Hsp60 essentially forms a chamber, with Hsp10 acting as a 'lid' for this chamber. When inside the Hsp60-Hsp10 chamber, the polypeptide is shielded from the external environment, which enables folding to occur (Cheng *et al.*, 1989, Fenton *et al.*, 1994, Hartl *et al.*, 1992, Langer *et al.*, 1992b). The folding and stabilisation of the polypeptide is also mediated by shielding of hydrophobic patches; inside the chamber the polypeptide undergoes a series of conformational changes which drive correct folding (Martin *et al.*, 1993). Once the polypeptide has folded, Hsp10 dissociates from Hsp60 to release the protein into solution (Mayhew *et al.*, 1996). If, following one round of folding within the Hsp60-Hsp10 chamber, the polypeptides are still in a non-native conformation, the polypeptide may re-enter the chamber and repeat the above processes until a native conformation is achieved.

1.3 Small heat-shock proteins (sHsps)

The small heat-shock proteins (sHsps) are a family of ATP-independent chaperones that also play a key role in proteostasis. The expression of sHsps is up-regulated under a wide range of cellular and physiological stresses (Jakob *et al.*, 1993). Mammalian sHsps are typically large, polydisperse and dynamic oligomers that undergo constant subunit-exchange *in vivo.* The sHsps are dynamic proteins; they have a relatively low monomeric mass, ranging from 10-42 kDa, but typically exists as large multimeric assemblies which undergo constant subunit-exchange (Jakob *et al.*, 1993). For example, the ubiquitously expressed and most studied mammalian sHsps, Hsp27 and αB-crystallin (αB-c), form large polydisperse assemblies built from monomeric (in the case of αB-c) or non-reduced disulfide-bonded dimeric (in the case of Hsp27) subunits. The sHsp family members are defined by the

presence of a conserved central α-crystallin domain (αCD). This central domain is flanked by an N-terminal domain and a C-terminal domain (which includes a C-terminal extension), both of which vary in sequence and length between sHsp members (Figure 1.4) (Bloemendal, 1977, de Jong *et al.*, 1974). The αCD of numerous members of the sHsp family has been intensively studied, with numerous crystal structures resolved (Figure 1.5) (Bagneris *et al.*, 2009). A key feature of most sHsps is a C-terminal IXI motif (Ile159-Pro160-Ile161 in αB-c) (Figure 1.5, blue sticks), which is absent in Hsp20 and Hsp22 (Figure 1.4). In αB-c this motif has been shown to bind into a hydrophobic groove in the αCD and this leads to dimer-dimer assembly into a triangular array (Clark *et al.*, 2011, Jehle *et al.*, 2010). This motif in αB-c allows the formation of higher order assemblies, through the assembly of hexameric units to form large oligomers, as proposed by a model based on NMR data (Jehle *et al.*, 2011).

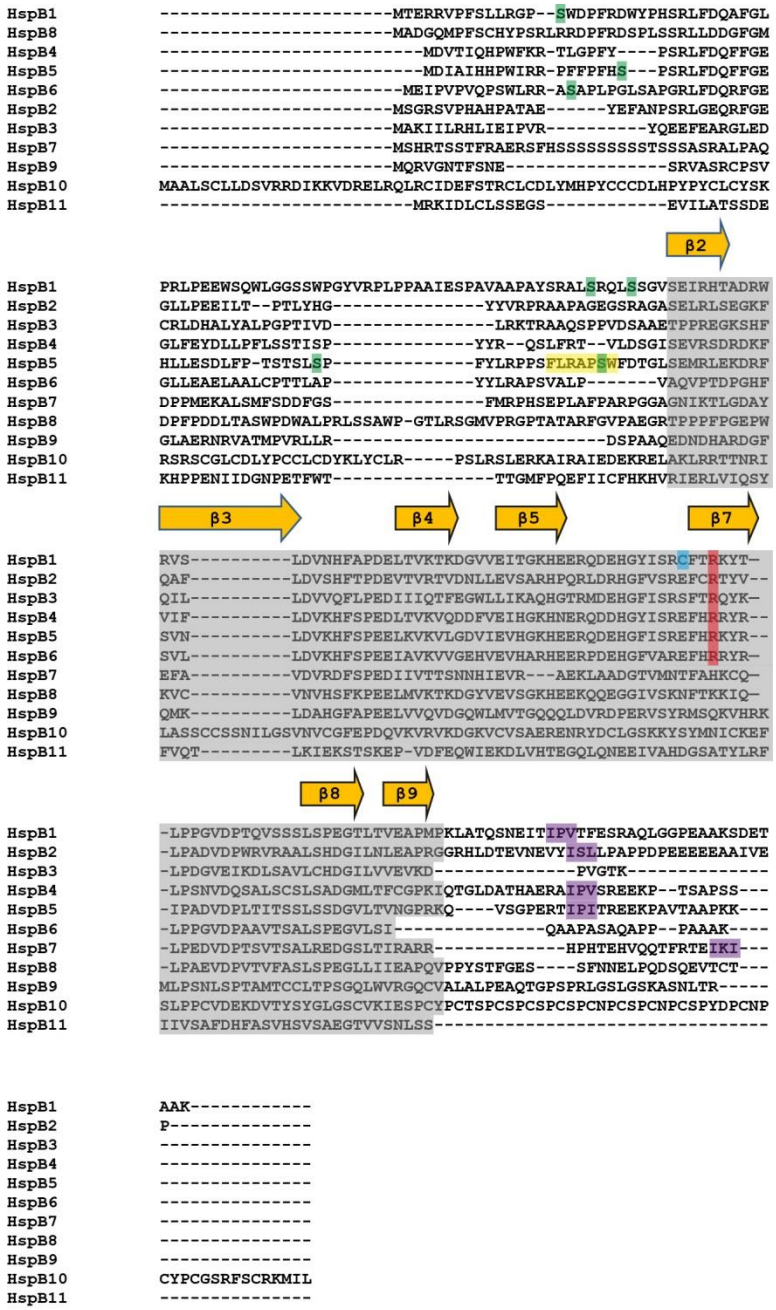

Figure 1.4: Primary sequence alignment of members of the human sHsp family

The αCD (*grey*) is flanked by the N-terminal domain and a C-terminal domain. The αCD is composed of 8 β-sheets (numbered β2-β9, *orange arrows*); β4-β5-β7-sheets are involved in charged interactions with neighbouring monomers to form the dimer interface (see Figure 1.7). Serine residues in the N-terminal region that undergo phosphorylation *in vivo* are highlighted (*green*). The C-terminal IXI/V motif (*magenta*) is involved in higher- order oligomerisation [note the absence of this motif in HspB3 (HspL27), HspB6 (Hsp20) and HspB8 (Hsp22)]. A dimer interface arginine (R120 of αB-c and R140 of Hsp27), mutations of which are associated with numerous congenital diseases (detailed in Table 1.1) is shown in red. The cysteine (C137) involved in forming Hsp27 disulfide-linked dimers is shown in cyan. The site of point mutations and an inversion mutation of the N-terminal region of αB-c (residues 54-60) that were the subject of work described in this thesis (Chapter 5) are highlighted in yellow. Sequences were aligned using ClustalW multiple sequence alignment software (Thompson *et al.*, 1994).

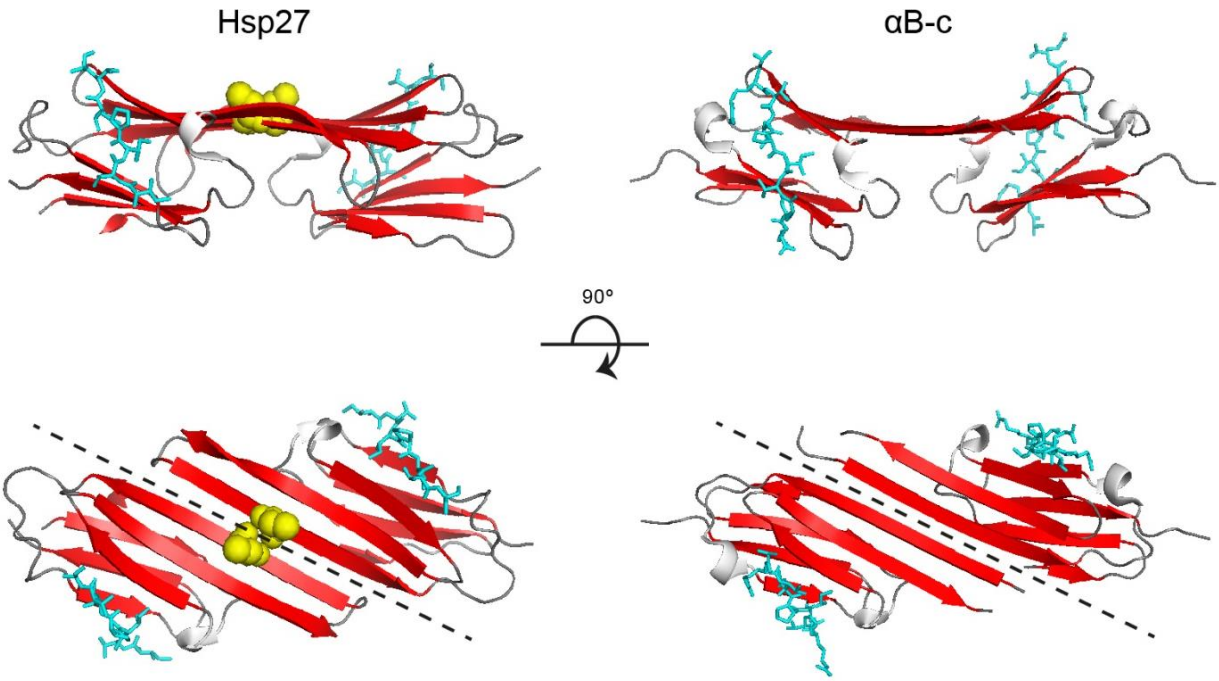

Figure 1.5: Core domain crystal structures of Hsp27 and αB-crystallin
The core domains of Hsp27 (pdb entry 4MJH) and αB-c (pdb entry 45MT) are similar and have a curved β-sheet sandwich structure. The Hsp27 core domain exhibits more curvature along the β-sheet network near the dimer interface (*dashed line*) compared to αB-c and has an intermolecular disulfide-bond via Cys137 of the β7-sheet of each monomer (*yellow spheres*). A region in the C-terminal domain, which contains the IXI/V motif (*blue sticks*), can anchor into the β4-β8 groove and this is thought to stabilise the oligomer. Crystal structures modified from Hochberg *et al.*,(2014).

The large, dynamic and polydisperse behaviour of mammalian sHsps prevents their crystallisation, the most common and high resolution technique used for determining protein structure. The formation of large sHsp oligomers is thought to arise from the association of monomeric and/or dimeric 'building blocks' (Baldwin *et al.*, 2011b, Baldwin *et al.*, 2011c, Braun *et al.*, 2011, Jehle *et al.*, 2011). The polydispersity of sHsps is attributed to the equilibrium between associated and dissociated forms of these building blocks (e.g. Hsp27 and αB-c), which undergo constant subunit-exchange where the stoichiometries of the oligomers ranges extensively. Numerous studies have suggested that this dissociated (monomeric and/or dimeric) form of these sHsps is believed to be the 'chaperone-active' unit (Figure 1.6) (Hochberg *et al.*, 2014, Jovcevski *et al.*, 2015, McDonald *et al.*, 2012).

However, it has not been conclusively shown that the dimer is solely responsible for chaperone activity. Thus, more work is needed to explore the structure-function relationship of sHsps. In order to define the structure-function relationship of sHsps, the focus of this work described in this thesis was on the archetypal human sHsps, Hsp27 and αB-c.

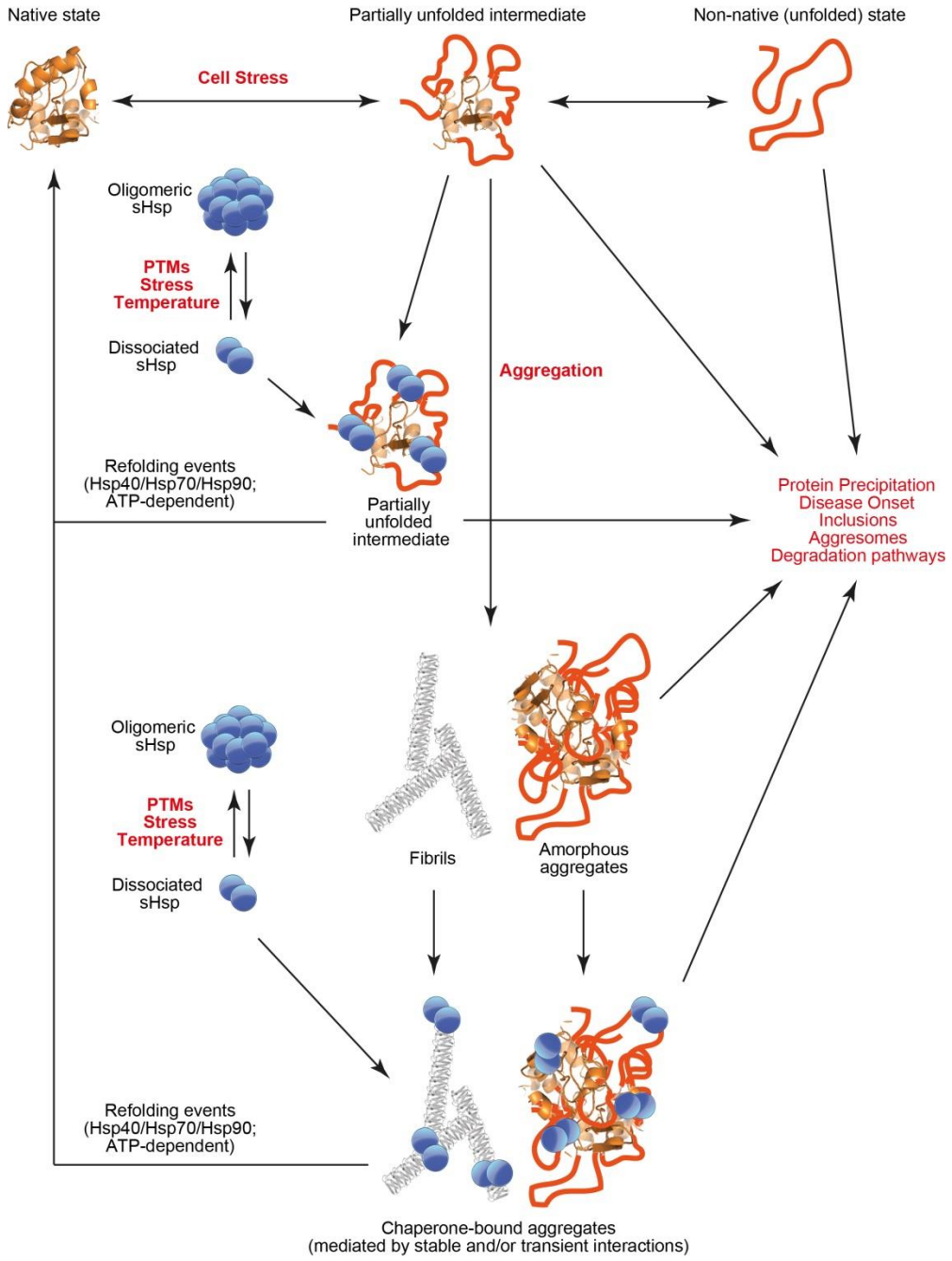

Figure 1.6: The role of sHsps in maintaining proteostasis
The unfolding and/or misfolding of proteins can lead to their association and subsequent formation of amorphous or fibrillar aggregates. The sHsps (e.g. Hsp27 and αB-c) interact with partially unfolded intermediates and mature aggregates, via either stable or transient interactions, to prevent further aggregation. These complexes can subsequently be shuttled into other proteostasis pathways (e.g. proteasome degradation) or refolding pathways, which are driven by ATP-dependent chaperones (Hsp40/Hsp70/Hsp90). The quaternary structure of sHsps is modulated by an association and dissociation equilibrium between smaller and larger oligomers. This equilibrium is controlled by numerous factors, including cell stress (e.g. oxidative stress, pH, temperature) and post-translational modifications (PTMs), all of which increase the amount of dissociated Hsp27 or αB-c (via enhanced oligomer dissociation or increased subunit-exchange rate) able to interact with a range of client proteins. Modified from Ecroyd and Carver, (2009).

1.1 Hsp27 (*HspB1*)

1.1.1 Structure

Hsp27 is a 205 amino acid sHsp that is constitutively expressed in epidermal, muscle and cancer cells (Garrido *et al.*, 1997, Jonak *et al.*, 2011). Hsp27 undergoes stress-induced phosphorylation at three key serine residues (S15, S78 and S82), which is thought to regulate its structure and chaperone function (Arrigo, 2011, Landry *et al.*, 1992a). When studied *in vitro* Hsp27 has been reported to form large polydisperse oligomers with an average molecular mass of 530 - 800 kDa, corresponding to oligomers containing between 24 – 35 monomeric units (Garrido, 2002, Rogalla *et al.*, 1999). The presence of these large oligomers in cells has also been demonstrated by fractionating HeLa cell lysates by size-exclusion chromatography (SEC) and probing for fractions containing Hsp27 by western blotting (Arrigo, 2011). However, the large oligomers observed by SEC and western blotting potentially show that Hsp27 is forming complexes with cellular proteins and not exclusively forming large oligomers. Interestingly, Hsp27 is one of the few sHsps (the others being αA-crystallin and Hsp20) to contain a cysteine residue (Cys137). In Hsp27 this single cysteine is located within the β7 sheet of the αCD and has been shown by non-reducing SDS-PAGE (Almeida-Souza *et al.*, 2010, Baranova *et al.*, 2011) and MS (Jovcevski *et al.*, 2015) to form a disulfide bond with an adjacent Hsp27 monomer. This covalent interaction, coupled with the ionic/electrostatic interactions along the dimer interface of the αCD, provides further structural stability to the Hsp27 dimer.

Recently, the oligomeric state of Hsp27 has been shown to be influenced by its concentration in solution (Lelj-Garolla and Mauk, 2006), such that dilution (to the low μM range) results in the dissociation of the large oligomer into dimers (McDonald *et al.*, 2012).

This suggests that the oligomeric assembly of Hsp27 is stable at high concentrations (> 15 μM). The concentration-dependent dissociation of Hsp27 oligomers is further enhanced by PTM (primarily phosphorylation). Interestingly, this concentration-dependent dissociation of large oligomers is not observed for αB-c and Hsp20 at a similar range of concentrations (Bukach *et al.*, 2004). This indicates that the associative forces that maintain the oligomeric assembly of αB-c and Hsp20 are much stronger compared to Hsp27. A possible reason why Hsp27 oligomers dissociate from the large oligomer so readily is that the structural motifs responsible for maintaining inter-dimer contacts (primarily the N-terminal domain and the C-terminal domain) within an oligomer are significantly different to those that do so in αB-c or Hsp20. One way in which the dimeric building block is maintained in Hsp27 is the inter-molecular disulfide-bond at Cys137 that is present on the β7 sheet along the dimer interface (Figure 1.5).

Serine phosphorylation of Hsp27 primarily occurs in the N-terminal domain and the majority of these post-translational changes are performed by MAPKAPK kinases (Landry *et al.*, 1992a). Hsp27 phosphorylation can occur at three serines (S15, S78 and S82) in response to cellular stress (Arrigo, 2011, Landry *et al.*, 1992a). Previous work has suggested that phosphorylation of Hsp27 at two serines (S15 and S78 in this instance) dissociates the large oligomer and leads to the formation of smaller oligomers, possibly tetramers (Doshi *et al.*, 2010, Jonak *et al.*, 2011). This dissociation was observed by analytical-SEC; however, this technique is unable to discern the exact stoichiometries of these dissociated oligomers, which could potentially range from monomers to hexamers. Using analytical-SEC and analytical ultracentrifugation, the triple phosphorylation mimic of Hsp27 (i.e. Hsp27-S15/78/82D) was reported to also predominantly forms small oligomers ranging from

dimers or tetramers (Jovcevski *et al.*, 2015, McDonald *et al.*, 2012, Rogalla *et al.*, 1999). However, these low resolution approaches are unable to determine the exact size of the oligomers present or the relative abundance in solution. This ambiguity is compounded by the polydispersity of Hsp27, such that neither analytical-SEC nor analytical ultracentrifugation can accurately resolve each of the oligomers present in solution.

The site-specific and precise mechanism by which phosphorylation of these serine residues prevents the oligomerisation of Hsp27 has yet to be determined. The location of these sites may be a key factor as these phosphorylated residues appear not to be directly involved in the cross β-sheet interactions that mediate dimer formation by the αCDs in respective monomers where numerous models have indicated that the N-terminal domain is either buried within an oligomer (Jehle model) (Jehle *et al.*, 2011, Peschek *et al.*, 2009) or on the surface of an oligomer (Braun model) (Braun *et al.*, 2011). Comparisons between the proposed models have been extensively reviewed previously (Delbecq and Klevit, 2013). The negative charges introduced by phosphorylation at S15, S78 and S82 may cluster in the quaternary structure of the oligomer such that they lead to charge repulsion between neighbouring dimers preventing them from forming larger oligomers. This would favour the Jehle model where such a model implies that the unstructured N-terminal domain is responsible for maintaining oligomeric assembly and that phosphorylation modulates the quaternary dynamics of Hsp27 oligomers.

1.1.2 **Function**

Under stress conditions, Hsp27 has been shown to inhibit protein aggregation of numerous client proteins (Aquilina *et al.*, 2013, Bukach *et al.*, 2009, Hochberg *et al.*, 2014, Kampinga *et al.*, 1994, Ojha *et al.*, 2011, Rogalla *et al.*, 1999). For example, previous work has shown that

Hsp27 is capable of abrogating the aggregation of toxic amyloid-β (Aβ) peptides *in vitro* (Ojha *et al.*, 2011). Due to the dynamic nature of Hsp27 oligomerisation, these previous studies could not identify the species responsible for chaperone activity (i.e. it remains to be established whether the dissociated species or larger oligomers interact with client proteins). Previous work has also highlighted that Hsp27 plays a role in various other cellular functions, e.g. enhancing stability of the cytoskeleton (Pivovarova *et al.*, 2007, Pivovarova *et al.*, 2005) and inhibiting apoptosis (Doshi *et al.*, 2010, Pivovarova *et al.*, 2007). Wildtype (WT) Hsp27 binds to the barbed end of filamentous-actin resulting in the inhibition of filamentous-actin polymerisation *in vitro* (Doshi *et al.*, 2010). It is postulated that this acts to stabilise the actin cytoskeleton, however, there is no conclusive evidence *in vivo* that Hsp27 binds directly to actin ends (Doshi *et al.*, 2010, Graceffa, 2011). There is also no conclusive evidence to indicate whether dimers or oligomers (or both) are responsible for actin stabilisation in this study. Moreover, the phosphorylation state of Hsp27 that potentially interact with actin filaments in the cells was not established.

Hsp27 has been reported to associate with numerous cell death signalling molecules during multiple stages of apoptosis, such as the serine-threonine kinase Akt and the FAS death receptor (Garrido *et al.*, 1999, Wu *et al.*, 2007). For example, Hsp27 prevents caspase activation (and hence apoptosis) by inhibiting the interaction of cytochrome C with procaspase-9 (Garrido *et al.*, 1999), such that the apoptosome complex fails to form (Garrido *et al.*, 1999). Hsp27 also suppresses signalling in the mitochondria by forming a complex with p38 mitogen-activated protein kinase and MAPKAPK-2. By suppressing mitochondrial signalling, serine-threonine kinases are activated which phosphorylate Hsp27, inhibiting apoptosis (Rane *et al.*, 2001, Rane *et al.*, 2003, Wu *et al.*, 2007). Overall, the

various roles that Hsp27 plays in the cell share a common theme with respect to its function. All these properties essentially show that Hsp27 acts as a stabilising protein, i.e. Hsp27 binds to a wide variety of proteins in order to stabilise them. The anti-apoptotic properties of Hsp27 have also been thought to play a role in numerous cancers. Hsp27 expression is increased substantially in cancer cells where it acts to inhibit apoptosis, thus increasing cancer cell viability (Arts *et al.*, 1999, Cornford *et al.*, 2000, Parcellier *et al.*, 2005). As a result, therapeutic approaches to decrease the levels (e.g. by siRNA) or activity (by drugs) of Hsp27 in cancer cells have been explored recently (Rocchi *et al.*, 2006, Schepers *et al.*, 2005, Xia *et al.*, 2009).

1.2 αB-crystallin (*HspB5*)

1.2.1 Structure

α-crystallin is a sub-family of sHsps originally isolated from the vertebrate eye lens (Bloemendal, 1977). Initially, the isolation of these proteins proved to be intriguing, as these proteins were isolated as a large water-soluble assembly with a mass range from 200 kDa to > 1 MDa (Haley *et al.*, 1998). It was found that α-crystallin is made up of two protein subunits, αA-crystallin (αA-c, *HSPB4*) and αB-crystallin (αB-c) (Siezen *et al.*, 1978). These two proteins share 57% sequence similarity and are present in the vertebrate lens at a ratio of ~3:1 (αA-c:αB-c) (Horwitz *et al.*, 1999). αB-c is also constitutively expressed in brain, liver, lung and muscle tissue (Kato *et al.*, 1991) and its level of expression is dramatically regulated in response to stress and certain pathological states (Clark and Muchowski, 2000, Sun and MacRae, 2005). The polydisperse homo-oligomeric forms of αB-c range from 10-mers to 40-mers (Aquilina *et al.*, 2003) with an average molecular mass of approximately 600 kDa (corresponding to a 30-mer) as assessed by analytical-SEC (Aquilina *et al.*, 2003).

Phosphorylation of αB-c also primarily occurs at three serine residues (S19, S45 and S59) (Kato *et al.*, 2001) and this increases its polydispersity, reduces the size of the oligomers and increases the rate of subunit-exchange (Aquilina *et al.*, 2004, Ecroyd *et al.*, 2007, Rogalla *et al.*, 1999). The polydispersity of the α-crystallins (as well as Hsp27 and Hsp20) is abolished by extensive deletion (~50%) of the N- and C-terminal domains (Bagneris *et al.*, 2009, Laganowsky *et al.*, 2010). Jehle *et al.* (2010) showed, using a combination of solid state-NMR and small-angle X-ray scattering (SAXS), that human αB-c is a curved dimer with a ~121° angle between the series of β-sheets (β4-β5-β6+7) present in the αCD (Jehle *et al.*, 2010). Both sides of the dimer have regions of ionic interaction, leading to the hypothesis that specific residue pairs (e.g. G99-H119 and G117-H101) form pH-dependent electrostatic interactions on both sides of the dimer, resulting in its curvature and increased stability (Jehle *et al.*, 2010). Later structures of the human αB-c core domain confirmed that the dimer is curved and indicated that the dimer interface can adopt three different elongated antiparallel interaction (AP) registries (termed API, APII, APIII), which result in a shift of two residues in the β6+7 sheet (Bagneris *et al.*, 2009, Hochberg *et al.*, 2014, Laganowsky *et al.*, 2010) (Figure 1.7). These subtle variations in the register may play a role in determining chaperone efficacy.

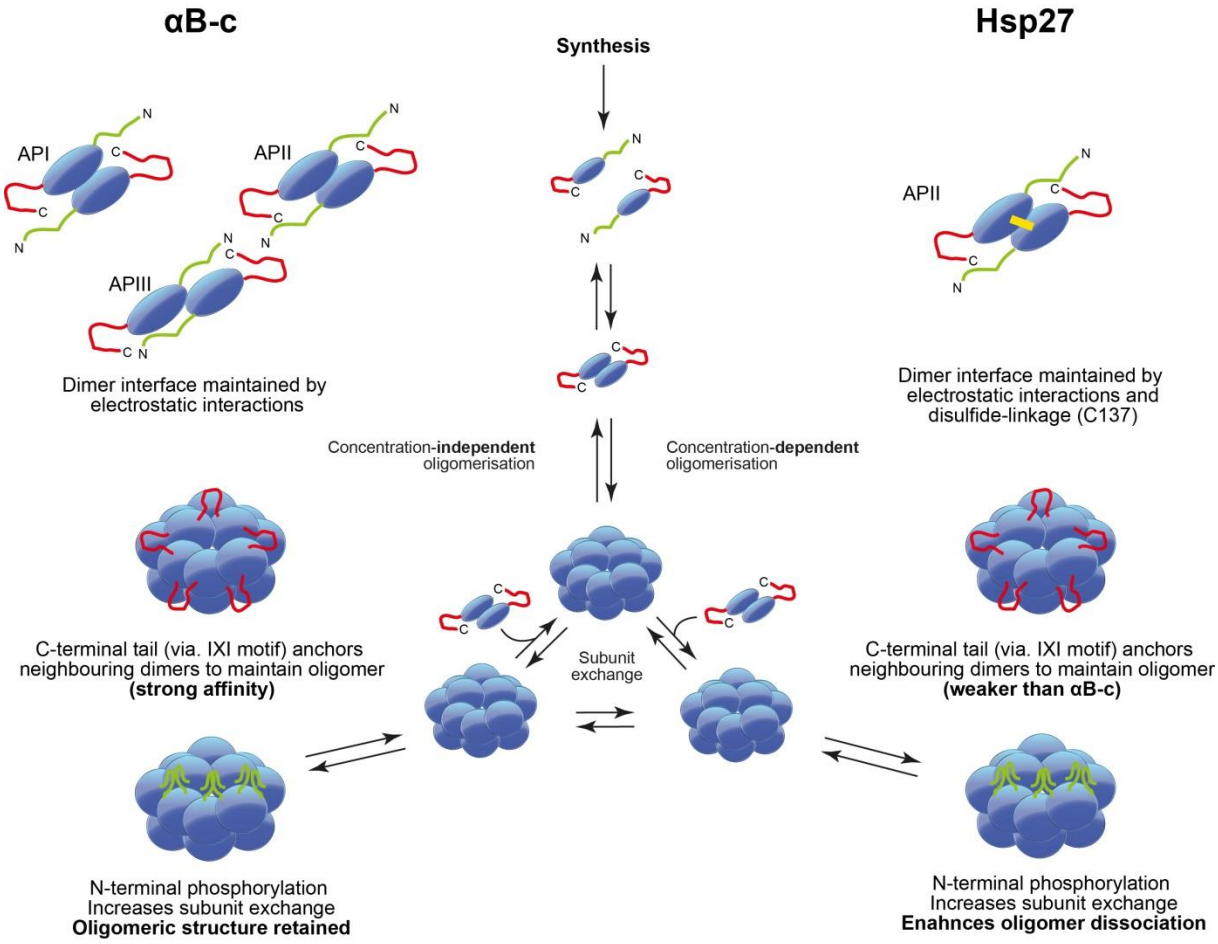

Figure 1.7: Oligomerisation dynamics of Hsp27 differ to that of αB-c

Oligomerisation of Hsp27 and αB-c is primarily mediated by a combination of N-terminal (charged/hydrophobic interactions; *green*) and C-terminal (IXI motif mediated interactions; *red*) interactions between monomers and dimers. After synthesis and folding, sHsp monomers associate to form dimers, which are stabilised by electrostatic interactions (αB-c and Hsp27) and disulfide bonds (Hsp27; *yellow*) (refer to Figure 1.5 for crystal structures). Dimers of αB-c can adopt a range of elongated antiparallel interaction (AP) registries (termed API, APII, APIII) along the dimer interface, whereas Hsp27 only adopts an APII conformation (Bagneris *et al.*, 2009, Hochberg *et al.*, 2014). The concentration-dependent oligomerisation is unique to Hsp27, demonstrating that the strength of the N-terminal and C-terminal interactions that maintain the oligomeric structure are weaker in Hsp27 than in αB-c. Phosphorylation of the N-terminal domain of both sHsps leads to an increase in subunit-exchange rate, which enhances chaperone activity (Aquilina *et al.*, 2013, Ecroyd *et al.*, 2007, Jovcevski *et al.*, 2015, Morris and Aquilina, 2010). However, phosphorylation of Hsp27 also leads to oligomer dissociation, with phosphorylation at three serines leading to complete dissociation of the oligomer (Jovcevski *et al.*, 2015, McDonald *et al.*, 2012, Rogalla *et al.*, 1999).

The implementation of a 'hybrid' approach (i.e. using a variety of biophysical techniques such as cryo-EM, NMR and structural homology modelling) helped to address and extensively study the structural heterogeneity of αB-c. These hybrid studies have also highlighted another facet of the oligomerisation dynamics of αB-c; the N-terminal region, in particular residues 54 – 70, of one αB-c dimer appears to interact with a neighbouring αB-c dimer through a yet to be determined process (Figure 1.8) (Jehle *et al.*, 2011). This same N-terminal region of αB-c is thought to play a key role in binding to partially folded clients, as determined by limited proteolysis-MS (Aquilina and Watt, 2007, Sreelakshmi and Sharma, 2005). Structural and functional studies of point mutations (including those that mimic phosphorylation, i.e. serine to aspartic acid or glutamic acid) and inversion/deletions within this region, have in general, resulted in a decrease the polydispersity of αB-c oligomers (Aquilina *et al.*, 2004, Biswas *et al.*, 2007, Ecroyd *et al.*, 2007, Numoto *et al.*, 2012, Santhoshkumar *et al.*, 2009). A notable example is a mutant isoform of αB-c in which residues 54 – 60 were inverted (Santhoshkumar *et al.*, 2009, Sreelakshmi and Sharma, 2006). When this mutant was analysed by SEC coupled to multi-angle light scattering (SEC-MALS) it appeared to exist as a near monodisperse population of αB-c oligomers with an average molecular mass of 356 kDa (17-mer) (Santhoshkumar *et al.*, 2009, Sreelakshmi and Sharma, 2006). Deletion of these residues (i.e. 54 – 60) from αB-c also decreased the polydispersity of αB-c, but not to the same extent as the inversion mutation (Sreelakshmi and Sharma, 2005, Sreelakshmi and Sharma, 2006). Moreover, intrinsic tryptophan fluorescence of the inversion mutant was significantly lower compared to the WT protein, suggesting that the N-terminal domain was less exposed to solution (Sreelakshmi and Sharma, 2006). The rate of subunit-exchange (with αA-c WT) of the 54 – 60 inversion mutant of αB-c was also decreased compared to αB-c WT, suggesting that the structure and

dynamics of this mutant isoform is significantly different to that of the WT protein (Sreelakshmi and Sharma, 2006).

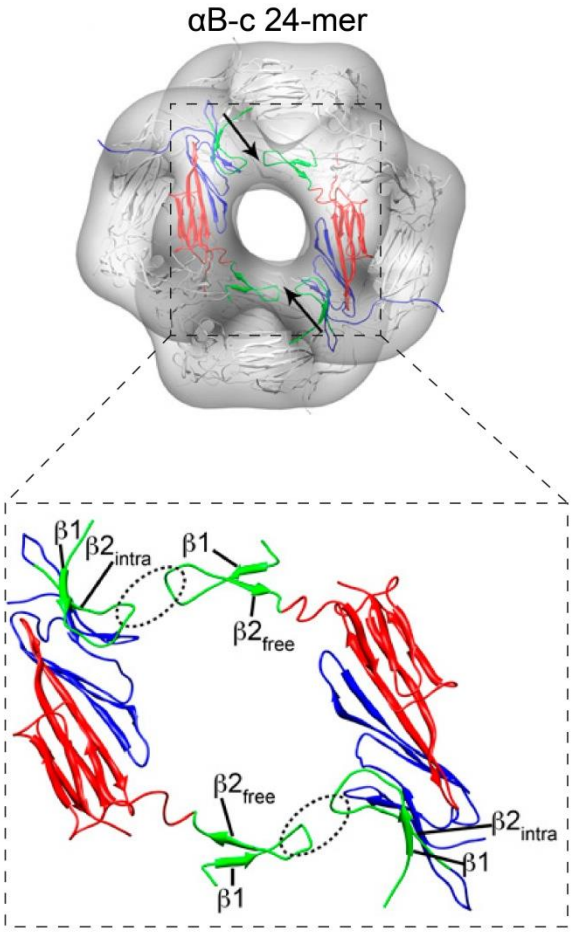

Figure 1.8 Potential inter-dimer interactions of oligomeric αB-crystallin based on a hybrid model
A proposed model of an αB-c 24-mer derived from cryo-EM, NMR and structure prediction modelling. The model depicts the predicted tertiary structure of full-length αB-c dimers interacting with neighbouring dimers in the higher-order oligomer (*zoomed inset*). The specific regions in the loop region between β1 and β2 sheets (residues 54-70) which are predicted to interact with neighbouring dimers to help maintain the oligomeric assembly of the 24-mer are highlighted in the *dotted circles*. Modified from Jehle *et al.*, (2011).

Previous work, again using SEC-MALS, has also indicated that deletion of residue A57 decreases the oligomeric polydispersity of αB-c compared to αB-c WT, however it does not significantly affect the intrinsic tryptophan fluorescence of the protein, nor chaperone

activity (Biswas *et al.*, 2007). Overall, the drastic changes in structure and function of αB-c that result from deletion or mutation in residues 54-70 warrants further examination as to the key residues that modulate αB-c oligomerisation in the N-terminal domain.

1.2.2 **Function**

Initially, the function of αB-c was to primarily aid in lens transparency and the refractive index of the lens (Delaye and Tardieu, 1983). With time, the chaperone function of αB-c was key in maintaining lens transparency and shown to be an effective chaperone when thoroughly examined across a range of amorphous and fibrillar client proteins (Ahmad *et al.*, 2008, Cox *et al.*, 2016, Kulig and Ecroyd, 2012, Mainz *et al.*, 2015, Muchowski *et al.*, 1997). Numerous papers have investigated the effect of post-translational modifications on αB-c, with a particular focus on the effects phosphorylation has on chaperone activity, polydispersity and oligomeric state (Aquilina *et al.*, 2004, Ecroyd *et al.*, 2007, Rogalla *et al.*, 1999). Mutations that mimic phosphorylation (MMP) of αB-c (S19D, S19/45D and S19/45/59D) have been shown to either increase or decrease its chaperone activity compared to the WT protein (Ahmad *et al.*, 2008, Aquilina *et al.*, 2004, Ecroyd *et al.*, 2007). The overall effect of phosphorylation on the chaperone function of αB-c remains highly controversial; a number of studies have reported conflicting data with regards to the effect phosphorylation has on the chaperone activity of αB-c. For example, previous studies have demonstrated that phosphorylation enhances (Ahmad *et al.*, 2008, Ecroyd *et al.*, 2007, Peschek *et al.*, 2013) or reduces (Aquilina *et al.*, 2004, Ito *et al.*, 1997) chaperone activity. However, the variation in the results from different studies was later explained by work demonstrating that the effect of phosphorylation on the chaperone activity of αB-c is specific to the client protein being used to assess the activity and dependent on the number

of sites of phosphorylation (Ecroyd *et al.*, 2007). Client proteins possess different tertiary and quaternary structures and it is thought that the binding affinity of αB-c for client proteins is, in general, higher when the client proteins are more destabilised, resulting in an increase in chaperone activity (Ecroyd *et al.*, 2007, Koteiche and McHaourab, 2003).

More recently, focus has shifted towards the mechanisms involved in abrogating protein aggregation, as *in vitro* assay conditions (e.g. buffer components, pH, temperature and oxidative state) can influence not only the aggregation of the client protein, but also the interaction between chaperone and client (e.g. stable versus transient interactions). The choice of client protein, the type of aggregation (amorphous versus fibrillar) and buffer conditions all influence the relative chaperone activity of sHsps (Ecroyd *et al.*, 2007). For example, substrate proteins such as BSA and insulin are commonly used in *in vitro* chaperone assays to assess chaperone activity since they are capable of forming amorphous or fibrillar aggregates depending on the solution conditions under which they are incubated. However, in the case of insulin, harsh conditions, including high temperatures (> 50°C) and low pH (< 3.0), are required to induce the formation of fibrillar aggregates *in vitro*. Thus, the physiological relevance of the ability of chaperones to prevent insulin aggregation into fibrils under these conditions is questionable. Recently, the acidic calcium-binding milk protein α-lactalbumin has been shown to be a suitable substrate protein for assessing the chaperone activity of sHsps as it can be induced to form amorphous or fibrillar aggregates in near-physiological (and very similar) buffer conditions *in vitro* (37°C, pH 7.0 -7.4) (Carver *et al.*, 2002, Kulig and Ecroyd, 2012, Lindner *et al.*, 1997). Moreover, it has been shown that αB-c abrogates both the amorphous and fibrillar aggregation of α-lactalbumin (Kulig and Ecroyd, 2012). More recent work has identified regions of αB-c that are responsible for the

recognition and binding to client proteins (Mainz *et al.*, 2015). NMR chemical shift analyses showed that the disordered N-terminal domain of αB-c was responsible for stably binding to lysozyme to prevent amorphous aggregation of this protein, whereas the β3, β4, and β8 sheets of the core domain were involved in transient interactions with the $A\beta^{1-42}$ peptide to prevent the formation of fibrils (Mainz *et al.*, 2015).

1.3 Diseases associated with protein aggregation in which sHsps are implicated

Proteins are often required to undergo a series of unfolding and refolding events as part of their normal life-cycle, for example when crossing membranes or during cellular stress. In situations where sHsps and folding chaperones (Hsp60, Hsp70) are unable to function optimally, proteins have the potential to form amyloid fibrils and/or amorphous aggregates, leading to the onset of numerous protein misfolding/conformational diseases (Figure 1.6) (Dobson, 1999). Moreover, mutations in Hsp27 and αB-c have been shown to cause disease. For example, congenital conditions such as desmin-related cardiomyopathy and nuclear cataract have been associated with mutations in αB-c (R120G and D140N, respectively) (Liu *et al.*, 2006, Vicart *et al.*, 1998) (Table 1.1). Mutations in Hsp27 have been associated with the neurological disorders Charcot-Marie-Tooth disease (S135F and R136W), a hereditary neuropathy resulting in peripheral nerve degeneration, and distal hereditary motor neuropathy (R127W, S135F, T151I and P182L) (Evgrafov *et al.*, 2004). A summary of the disease-related mutations in Hsp27 and αB-c is given in Table 1.1.

Table 1.1: Known disease-related mutations of Hsp27 and αB-c.
Numerous point mutations as well as deletions and truncations, have been associated with congenital diseases. Highlighted are the location of these mutations with regards to the N-terminal (*cyan*), αCD (*red*) and C-terminal (*green*) regions of sHsps.

sHsp	Mutation(s)	Associated Disease	Ref.
HspB1 (Hsp27)	P39L G48R	Distal hereditary motor neuropathy	(Evgrafov *et al.*, 2004, Houlden *et al.*, 2008, Ikeda *et al.*, 2009, James *et al.*, 2008, Kijima *et al.*, 2005)
	L99M R127W S135F R140G K141Q T151I		
	T180I P182S P182L		
	R127W S135F R136W	Charcot-Marie-Tooth disease type 2	(Luigetti *et al.*, 2010, Tang *et al.*, 2005)
	T180I		
HspB5 (αB-crystallin)	R11H R56W	Various forms of cataracts	(Berry *et al.*, 2001, Chen *et al.*, 2009, Devi *et al.*, 2008, Khan *et al.*, 2010, Liu *et al.*, 2006)
	R120G D140N		
	A171T 450delA		
	R120G	Dilated cardiomyopathy	(Inagaki *et al.*, 2006, Pilotto *et al.*, 2006)
	G154S R157H		
	S21AfsX24	Myofibrillar myopathy and desmin-related cardiomyopathy	(Selcen and Engel, 2003, Vicart *et al.*, 1998)
	R120G		
	Q151X G154S 464delCT		

In addition to mutations in sHsps causing disease, immunohistochemical studies have repeatedly shown that sHsps co-localise with protein aggregates that are associated with disease. For example, Hsp20, Hsp27 and αB-c are found in amyloid plaques in post-mortem Alzheimer's disease brain tissues (Clark and Muchowski, 2000, Iwaki *et al.*, 1992, Renkawek *et al.*, 1994a, Renkawek *et al.*, 1994b). The presence of these chaperones in senile plaques is thought to be due to them having a protective role by inhibiting further aggregation and reducing toxicity (Binger *et al.*, 2013, Renkawek *et al.*, 1994a, Renkawek *et al.*, 1994b, Shammas *et al.*, 2011, Waudby *et al.*, 2010). The presence of molecular chaperones in

protein aggregates can also be considered as a toxic 'loss of function' since the chaperones are sequestered into the aggregate and therefore are not available in the cell to perform other critical functions. Moreover, mutations in sHsps may contribute to aggregation due to the mutations destabilising the dimer interface (resulting in more monomer compared to dimer) or enhancing subunit-exchange (increasing the amount of dissociated species) to such an extent that the chaperone becomes 'hyperactive', contributing to disease onset. The presence of an excess of these dissociated 'active' species may also interfere with other proteostasis pathways, thereby overloading the PQC network, leading to disease. The overall message coming from this previous work is that, when chaperones fail to prevent protein aggregation this can lead to their deposition and co-localisation into aggregates and plaques. As a result of the ability of sHsps to inhibit aggregation and stabilise proteins in general, these chaperones have been targeted for the development of therapeutics to combat neurodegenerative diseases, an area that has been the subject of recent reviews (Basha *et al.*, 2012, Boncoraglio *et al.*, 2012, Edwards *et al.*, 2011, Garrido *et al.*, 2012).

1.4 Delineating the structure of sHsps

Structural characterisation of proteins is crucial in defining their function. Characterising the structure of proteins allows researchers to identify residues and/or domains of functional importance. Techniques that are commonly used to structurally characterise proteins include X-ray crystallography, solid-state and solution-state nuclear magnetic resonance (NMR), nanoelectrospray ionisation MS (nanoESI-MS) and matrix assisted laser desorption/ionisation MS (MALDI-MS) (Aquilina *et al.*, 2003, Aquilina *et al.*, 2005, Bagneris *et al.*, 2009, Baldwin *et al.*, 2011a, Jehle *et al.*, 2010, Liu *et al.*, 2015). Other techniques, such

as analytical-SEC and native gel electrophoresis (native-PAGE), can provide additional information on protein structure.

1.4.1 **Native MS overcomes structural heterogeneity**

A complete view of the tertiary and quaternary structure of the full-length human sHsps that form polydisperse oligomers has long been a goal of structural biologists that study these sHsps. The partially disordered and polydisperse nature of sHsps hinder traditional approaches to characterise the tertiary and quaternary structures of these proteins. To date, the vast majority of work has involved low-resolution techniques such as SEC-MALS, analytical ultracentrifugation and native-PAGE (Bukach *et al.*, 2009, Bukach *et al.*, 2004, Datskevich *et al.*, 2012). In light of this, alternate high-resolution approaches have been used to further investigate the structure and dynamics of these polydisperse assemblies.

Native mass spectrometry (MS) is one technique that offers great potential for the study of multimeric protein assemblies and has been successfully used to study the quaternary structure of sHsps, including αB-c (Aquilina *et al.*, 2003, Aquilina *et al.*, 2004, Aquilina *et al.*, 2005, Benesch *et al.*, 2006, Benesch *et al.*, 2008, Hochberg *et al.*, 2014) and Hsp27 (Aquilina *et al.*, 2013, Heirbaut *et al.*, 2016, Hochberg *et al.*, 2014, Jovcevski *et al.*, 2015). In doing so, data from native MS has shed new light on the structure and dynamics of these proteins (Hilton and Benesch, 2012). In native MS the protein of interest is placed into a volatile buffer (commonly ammonium acetate), and is then transferred from this solution-phase into the gas-phase via ionisation of the solution into droplets (achieved by the application of electrical potential to the sample), which undergo subsequent desolvation and fission, resulting in multiply charged protein ions that maintain a ‘native-like’ state (Figure 1.8). The multiply charged ions observed from nanoESI-MS are the result of differential ionisation of

exposed basic amino acid residues (lysine, arginine, histidine and the peptide backbone). Following the above processes, proteins are subsequently separated based on their mass to charge ratio (*m/z*) (Figure 1.9). The resolving power of native MS enables a wide range of structural features to be measured, such as oligomeric distribution and polydispersity (using collision-induced dissociation-MS; CID-MS), unfolded/unstructured states (tertiary structure), assembly stability (using collision-induced unfolding-MS) and quaternary conformation of proteins (the latter two via. ion-mobility – MS) (Figure 1.9).

To determine the oligomeric distribution of a polydisperse protein such as the sHsps (e.g. αB-c) by MS, a CID approach was previously used, whereby the ionised protein is subjected to collisions with an inert gas (nitrogen or argon) in the collision cell of a mass spectrometer (Benesch, 2009, Shukla and Futrell, 2000). The CID process results in asymmetric dissociation of oligomers with increased collision energy, such that the fundamental unit (usually a monomer) that dissociates from a complex carries a large proportion of charge relative to its mass. CID is capable of removing up to three monomers from any mammalian sHsp oligomeric assembly; regions of the spectrum corresponding to 'stripped' oligomers are therefore commonly referred to as the *n*-1, *n*-2 and *n*-3 regions, where *n* is the number of subunits that constitute any sized oligomer (Aquilina *et al.*, 2003).

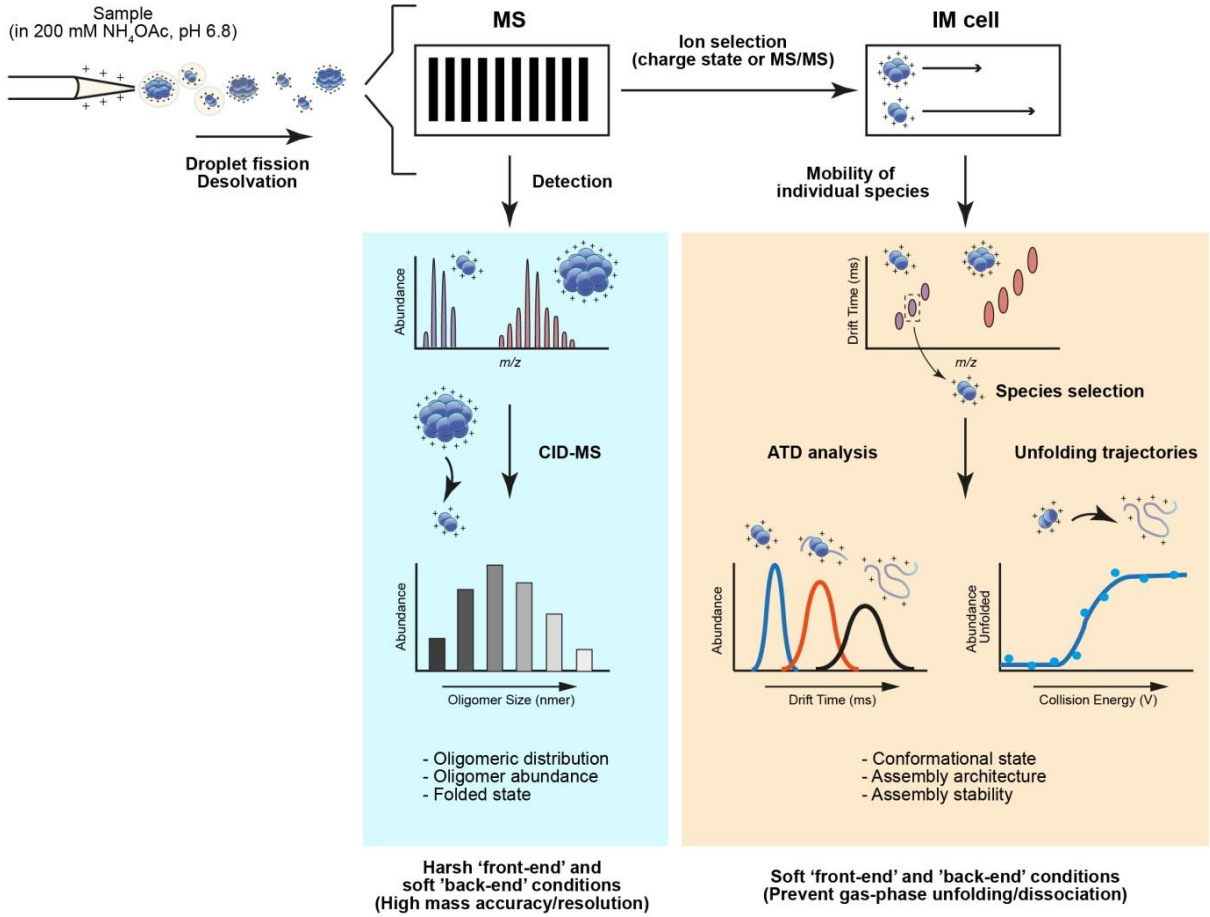

Figure 1.9: Workflow diagram outlining how native MS can be used to investigate the structure and dynamics of large multimeric proteins such as the sHsps
Proteins are prepared in a volatile buffer (200 mM NH_4OAc) and, during desolvation and droplet fission, the proteins transfer from the solution-phase to the gas-phase. Basic amino acid residues that are exposed become ionised and the resultant multiply charged protein ions are transferred through the mass spectrometer, which detects various species based on their mass to charge ratio (*m/z*). Collision-induced dissociation (CID), whereby an accelerating potential in the presence of an inert gas (such as argon or nitrogen) is used to remove ('strip') subunits from the large assemblies, allows quantification of oligomeric distribution and abundance (*blue box*). Ion mobility (IM) – MS can provide information of the conformational state of protein assemblies by comparing the arrival time distribution (ATD) of different species. The stability of individual protein species can also be analysed by IM-MS by observing their unfolding dynamics as a result of collision-induced unfolding (CIU) (*orange box*).

1.4.2 Native MS of the α-crystallin core domain of sHsps

Native MS of the αCD (residues 68 – 153) of αB-c has revealed that, rather than being exclusively dimeric, the αCD exists in equilibrium between monomers and dimers (Hochberg *et al.*, 2014). The proportion of dimer increases with concentration, which indicates that

even these stable αB-c core domains are in a state of oligomeric equilibrium. Moreover, using a mixture of unlabelled and ^{13}C-labelled constructs and native MS, the αB-c WT core domain constructs were also found to undergo rapid subunit-exchange (Hochberg *et al.*, 2014). Under non-reducing conditions, an E117C mutant (Glu117 is equivalent to Cys137 in Hsp27) of the αB-c core domain was found to be exclusively dimeric due to disulfide bond formation across the interface (Hochberg *et al.*, 2014).

1.4.3 **Oligomerisation and polydispersity of sHsps**

The extent of the polydispersity of sHsps was first quantified in detail by a MS study that investigated the oligomeric distribution of bovine αB-c (isolated from eye lenses) (Aquilina *et al.*, 2003). It was found that αB-c primarily forms oligomers of 24-33 subunits (Aquilina *et al.*, 2003), however, oligomers as small as 10-mers and up to 40-mers were also detected. This was the first detailed description of the range of oligomeric species (stoichiometries) present in this polydisperse system. Similar distributions were observed in human αB-c and C-terminally truncated forms of recombinant human αA-c (Aquilina *et al.*, 2005).

Oligomerisation and polydispersity of the sHsps is both temperature and pH dependent (Aquilina *et al.*, 2005, Baldwin *et al.*, 2011c, Ecroyd *et al.*, 2007). Thermodynamic and kinetic MS studies have demonstrated that the strength of the intra-dimer interfaces of αB-c oligomers is pH dependent. Thus, the preference for even-sized oligomers is reduced with acidification (Baldwin *et al.*, 2011a, Baldwin *et al.*, 2011c). A recent comprehensive structural model of αB-c oligomers postulated that the oligomerisation of αB-c is the result of two key components; the intra-dimer interface (site of dimerization) and the inter-dimer ‘edge’ (dimer-dimer contact regions) (the Baldwin model) whereby αB-c is a symmetrical oligomer and proposes that all monomers are equivalent to one another (i.e. tertiary

structure of the monomer is identical within the oligomer) (Baldwin *et al.*, 2011c). Based on the respective free energies, the relative strength of these components influences the distribution of oligomers. This work also proposed that it is the exchange of monomers, not dimers, between different sized oligomers that contribute to the polydispersity of sHsps (Baldwin *et al.*, 2011c). By combining MS and NMR data, it has also been proposed that subunit-exchange is limited by the interactions of the C-terminal domain, in particular the canonical IXI motif, with the β4+β8 groove of the αCD. These interactions are responsible for anchoring monomers within an oligomeric assembly (Baldwin *et al.*, 2011a, Hilton *et al.*, 2013, Jehle *et al.*, 2011) (Figure 1.5). Evidence that the C-terminal domain aids in maintaining oligomer assembly (Pasta *et al.*, 2004) was further supported by work showing that the IXI motif binds to the hydrophobic β4+β8 groove (Delbecq *et al.*, 2012, Jehle *et al.*, 2011, Laganowsky *et al.*, 2010). Overall, the interaction between the C-terminal domain with the β4+β8 groove appears to be transient, consistent with the observation of rapid binding kinetics (in the millisecond scale) (Baldwin *et al.*, 2011a, Hochberg and Benesch, 2014). Moreover, monomers within a αB-c oligomer were found to exist in a single conformation indicating that they do not undergo any distinct change in tertiary structure when bound within an oligomer compared to when they are 'free' in solution (Baldwin *et al.*, 2011a). However, little work has been done to investigate the tertiary and quaternary structure of full-length sHsp dimers.

Other models of the αB-c oligomer (24-mer) have been proposed by other groups which differ from the Baldwin model. Both the Braun (based on solid state NMR, cryo-EM and structural homology modelling experiments) (Braun *et al.*, 2011) and Jehle (based on solid state NMR, SAXS and negative-stain EM experiments) (Jehle *et al.*, 2011) models depict the

24-mer as an asymmetrical oligomer whereby each monomer is not equivalent (i.e. tertiary structure of the monomer is not identical within the oligomer) and that the C-terminal domains are exposed on the surface of the oligomer. Where the two models differ significantly is in the position of the N-terminal domain. The Jehle model shows that the N-terminal domain is buried within an oligomer (Jehle *et al.*, 2011, Peschek *et al.*, 2009) whilst the Braun model is on the surface of an oligomer (Braun *et al.*, 2011). Both of these models also postulate that the formation of the 24-mer must occur with a formation of a hexameric ring, which is stabilised by inter-dimer interactions between the αCD and the C-terminal domain (Braun *et al.*, 2011, Jehle *et al.*, 2011, Peschek *et al.*, 2009). Following the formation of this hexameric ring, the 24-mer is formed from four hexamers, and are stabilised via interactions of the N-terminal domain (Braun *et al.*, 2011, Jehle *et al.*, 2011, Peschek *et al.*, 2009). Overall, all the models presented do not account for the role of the N-terminal domain in αB-c oligomerisation experimentally and is based on assumptions and structural prediction/homology modelling. This is a major pitfall in these proposed models as the N-terminal domain of αB-c is readily modified by PTMs, and these modifications have been shown to alter the quaternary structure/dynamics, in turn, altering its functions as a chaperone. In the context of αB-c, the Baldwin model is more accurate whereby each monomer is equivalent to one another and accounts for the strengths between the intra-dimer interface (site of dimerization) and the inter-dimer 'edge' (dimer-dimer contact regions) under various conditions/states (i.e. pH and phosphorylation). These interfaces ultimately govern oligomerisation, and consequently, subunit-exchange rates, irrespective of stoichiometry (i.e. the interactions that maintain a 24-mer would be the same as those that maintain any other sized oligomer). Also, there may be significant differences in the model when applied to Hsp27, especially as the interfaces involved appear to be

significantly weaker than αB-c as Hsp27 oligomerisation is heavily regulated by both concentrations and N-terminal PTMs (Rogalla *et al.,* 1999; Theriault *et al.,* 2004). Overall, the differences between each model demonstrate the complexity of this system which is confounded by the partially disordered state of αB-c oligomers.

Whilst it well established that αB-c is a polydisperse oligomer in solution, the precise nature of the architecture and conformation of these oligomers remained elusive until recently. The rapid advances in attaining high resolution data from MS and other approaches (IM-MS, NMR, cryo-EM and X-ray crystallography) has recently been exploited in order to define the three-dimensional shape of the polydisperse oligomers of αB-c (Baldwin *et al.*, 2011b). Determining these features helped rationalise the polydispersity of αB-c *in vitro*. For example, by combining data from both tandem-MS and ion-mobility MS, numerous polyhedral architectures were identified for 24-, 26- and 28-mers of αB-c, all of which readily interconvert (via dissociation and association of dimers/monomers) without drastic changes in the overall architecture (Baldwin *et al.*, 2011b). It should be noted that the gas-phase (i.e. MS) data on sHsp structure and dynamics correlate well with solution-phase (NMR, SEC, cryo-EM) data, demonstrating that the data obtained from MS based approaches is relevant when studying αB-c and sHsp structure (Baldwin *et al.*, 2011b, Benesch *et al.*, 2010). Overall, these models have helped define the shape and dynamics of the polydisperse assemblies formed by αB-c and provide a platform for the study of other sHsps, as well as other large oligomeric polydisperse proteins.

Another key feature of the sHsps is their ability to interact with other family members to form heterogeneous oligomers. A well-known *in vivo* example of this is the formation of α-crystallin, a hetero-oligomer of αA-c and αB-c (at a ratio of 3:1 αA-c:αB-c). Understanding

the subunit-exchange dynamics of these assemblies is crucial in relation to their chaperone activity. Previous work that investigated subunit-exchange of the α-crystallins used fluorescence resonance energy transfer (FRET) based experiments, which required labelling of the protein prior to measuring the rate of subunit-exchange (Bova *et al.*, 1997, Bova *et al.*, 2000). The labelling of proteins with fluorophores can be overcome through the use of MS to monitor subunit-exchange between sHsp oligomers. However, there have been instances where MS based approaches require labelling (^{15}N or ^{13}C) of the sHsp to attain baseline resolution between peaks, particularly when investigating homo-oligomeric subunit-exchange of Hsp26 from yeast by MS (Benesch *et al.*, 2010). The first instance in which α-crystallin subunit-exchange was observed and quantified by MS showed that complete exchange of αA-c and αB-c subunits occurred in ~30 min (Aquilina *et al.*, 2005). Further work using MS to monitor α-crystallin subunit-exchange demonstrated that αB-c subunits more readily dissociated from the larger α-crystallin assemblies that αA-c subunits (Morris and Aquilina, 2010). This led to the proposal that the αB-c subunits are more solvent exposed and have fewer inter-dimer contacts in the hetero-oligomer than αA-c subunits (Morris and Aquilina, 2010). Thus, the associative forces that maintain contacts between subunits in the α-crystallin oligomer are weaker for αB-c subunits than those formed by αA-c subunits.

Recent work using deuteration-assisted small-angle neutron scattering and native MS has led to an alternative model of subunit-exchange whereby 'travelling subunits' are responsible for exchange, a process that is strongly temperature dependent (Inoue *et al.*, 2016). This work proposed that the abundance of small species (i.e. monomer, dimer and trimer) increased with temperature. However, it was concluded that from this work that

there was no loss in the abundance of the larger oligomers, despite the increased abundance of smaller species. The observed increase in the abundance of smaller species may be attributed to enhanced ionisation efficiency and/or partial unfolding induced by temperature during the native MS (Inoue *et al.*, 2016).

Native MS of mixtures of Hsp27 and αB-c, which hetero-oligomerise *in vivo* (Arrigo *et al.*, 2007, Kato *et al.*, 1992, Sakuma *et al.*, 1998), showed that αB-c and Hsp27 undergo complete subunit-exchange to form a heterogeneous species and the rate of subunit-exchange increases with temperature (Aquilina *et al.*, 2013). The rates of subunit-exchange determined by MS were comparable to those attained from FRET studies of Hsp27/αA-c and αA-c/αB-c hetero-oligomers (Bova *et al.*, 2000), however there was no need to label the sHsps in the MS-based experiment. This is critical as recombinant forms of αA-c and Hsp27 can form disulfide-linked dimers post-purification, which can modulate the quaternary dynamics of these assemblies. Taken together, it is clear that studying sHsp oligomers is a crucial first step in understanding their dynamic behaviour (Figure 1.9).

1.5 Use of MS to study the structure-function relationship of sHsps

Recent structural data on human sHsps have helped provide clues as to the molecular mechanism of their chaperone function. MS has also played a key role in these experiments. For example, by using a limited proteolysis and MS approach, it was found that the N-terminal domain of αB-c bound to aggregation-prone α-lactalbumin is more resistant to proteolytic cleavage than αB-c 'free' in solution (Aquilina and Watt, 2007). In this work a phenylalanine-rich region, residues 17-28, of the N-terminal domain of αB-c was identified as mediating substrate binding. In this same study, the C-terminal domain of αB-c (in particular residues R157 – R163) was also somewhat resistant to proteolytic cleavage and

therefore implicated in substrate binding (Aquilina and Watt, 2007). The key advantage of using MS over other techniques to determine key regions involved in chaperone and substrate interactions is that it accurately identifies peptides released via proteolytic cleavage.

MS has also been used to show that *in vitro* refolding of urea-denatured α-crystallin changes the quaternary structure of the protein compared to protein that has not been denatured (Benesch *et al.*, 2008). In particular, when compared to the control (non-denatured), the oligomeric distribution of the refolded α-crystallin demonstrated a loss in dimeric substructure. This correlated with a decrease in the chaperone activity of refolded α-crystallin compared to non-denatured α-crystallin (Benesch *et al.*, 2008). Moreover, the results of this work suggest that the ratio of monomeric to dimeric units in the substructure of the α-crystallin oligomers may regulate the chaperone activity of the protein.

The effects of PTMs have on the oligomeric structure of sHsps have also been examined by MS. For example, phosphorylation of αB-c at three serines (S19, S45 and S59) does not result in the complete dissociation of oligomers, nor reduce its polydispersity (Ecroyd *et al.*, 2007, Peschek *et al.*, 2009, Peschek *et al.*, 2013). The increased levels of phosphorylation of αB-c results in an increase in the rate of subunit-exchange, which leads to an increase in the abundance of dissociated species, enhancing its interaction with destabilised substrate proteins (Ecroyd *et al.*, 2007, Peschek *et al.*, 2013). In the case of Hsp27, upon phosphorylation at three serines (S15, S78 and S82) almost complete dissociation of oligomers was observed by MS (Jovcevski *et al.*, 2015). This dissociation also correlated with enhanced chaperone activity (Hayes *et al.*, 2009, Jovcevski *et al.*, 2015). Generally, phosphorylation of sHsps has been regarded as a molecular switch, which activates

oligomeric dissociation and/or enhances subunit-exchange (by destabilisation of inter-dimer contacts), such that more chaperone-active species are present. The large sHsp oligomers act as storage forms of the chaperone-active species (Figure 1.9 and 1.10). It is quite possible that both non-phosphorylated and phosphorylated forms of sHsps are able to oligomerise together and undergo subunit-exchange, which adds yet another level of complexity to the structure-function relationship of these dynamic proteins.

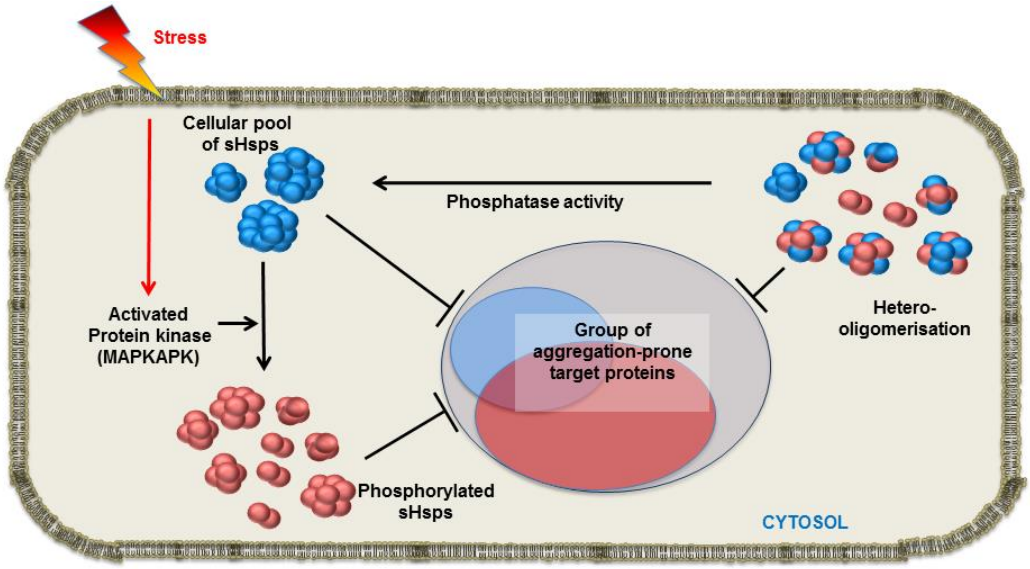

Figure 1.10: The role of phosphorylation of intracellular sHsps
Phosphorylation of Hsp27 and αB-c is mediated by MAPKAPK-2, -3 and -5 during periods of cell stress (e.g. temperature, pH). The production of the phosphorylated forms of these sHsps results in a range of structural changes, such as an increase in subunit-exchange rate and oligomer dissociation. Due to the dynamic nature of sHsps, both non- and phosphorylated forms may undergo subunit-exchange with each other to form a wide range of heterogeneous species. All populations are capable of interacting with a range of client proteins to prevent their aggregation, however, phosphorylation may act to change and broaden the range of client proteins that these sHsps are capable of interacting with in cells. Modified from Treweek *et al.*, (2015).

1.6 Aims

The sHsps are a very crucial part of the proteostasis network in cells. It is critical that the molecular mechanisms by which they acts as molecular chaperones is well understood. The overall aims of this work were to use MS-based techniques to interrogate the structure-function relationship of these dynamic and polydisperse proteins. In order to investigate the structure, function and interactions of the human sHsps Hsp27 and αB-c, this work had three specific aims:

(i) To examine the site-specific effect that phosphorylation has on the structure and chaperone function of Hsp27.

(ii) To probe the roles post-translational modification (i.e. phosphorylation and disulfide-linkage) have on the structure and dynamics of Hsp27.

(iii) To investigate the role of the region encompassing residues 54-60 in the N-terminal domain in the structure and chaperone function of αB-crystallin.

Chapter 2:

Materials and Methods

Chapter 2: Materials and Methods

2.1 Materials

Unless otherwise stated, all reagents used were obtained from Amresco (Ohio, USA) or Sigma-Aldrich (St. Louis, USA) and all were of analytical grade.

Hsp27 phosphomimics (S15D, S78D, S82D, S15/78D, S15/82D, S78/82D and S15/78/82D) were kind gifts from Dr. Megan Kelly and Assoc. Prof. Heath Ecroyd (both from the University of Wollongong, Australia). The amorphous and fibrillar aggregation assays (section 2.7.1) and cell lysate aggregation assays (section 2.7.2) using the Hsp27 phosphomimics were performed by Dr. Megan Kelly.

2.2 Gel electrophoresis

2.2.1 SDS-PAGE

Protein samples were visualised by SDS-PAGE, consisting of a 4% (v/v) stacking gel and 15 % (v/v) resolving gel. Electrophoresis was performed using a Mini Protean 3 system (BioRad, California, U.S.A), which was powered by a Bio-Rad power pack 300 power supply (BioRad, California, U.S.A). Protein samples were combined with a SDS-PAGE loading buffer (25 mM Tris-HCl, 1% w/v bromophenol blue, 30% w/v glycerol, 10% w/v SDS, 5% v/v β-mercaptoethanol, pH 6.5) at a ratio of 1:1, followed by incubation at 90°C for 5 min prior to loading into wells of the gel. Each gel was loaded with 5 µL of unstained SDS-PAGE broad range molecular mass standards (BioRad, California, U.S.A) to determine protein molecular mass. Separation was achieved at 150 V until the dye reached the bottom of the gel. Gels were stained with Coomassie blue stain solution (10% v/v methanol, 40% v/v acetic acid, 0.02% w/v brilliant blue) for 1 h, followed by destaining in Coomassie blue destain solution

(10% v/v methanol, 40% v/v acetic acid) until proteins were visible. Imaging of proteins was performed using a Gel Logic 2200 PRO imaging system (Carestream, New York, U.S.A).

2.2.2 Native-PAGE

Native-PAGE was performed as described previously (Cassiman *et al.*, 1981). Essentially, gels consisted of a 4% (v/v) stacking and 6% (v/v) resolving gel. 50 µM of each protein was mixed with an equal volume of native-PAGE loading buffer (20 µL) (0.5 M Tris-HCl pH 6.8; 30% w/v glycerol; 1% w/v bromophenol blue) and loaded into wells. Separation was performed at 150 V using a Mini Protean 3 system (BioRad, California, U.S.A) for 2.5 h. Staining and imaging was performed as described previously (section 2.1.1).

2.3 Expression and purification of Hsp27 and αB-c isoforms

The gene encoding human Hsp27 (*HSPB1;* UniProt accession number P04792) was expressed in *E. coli* BL21(DE3) using a plasmid kindly gifted by Dr. W. C. Boelens and Dr. W. W. de Jong (University of Nijmegen, The Netherlands), in which *HSPB1* was cloned into the *Bam*HI and *Nde*I restriction sites of pET3a (Novagen, Darmstadt, Germany). The Hsp27 phosphomimic-encoding constructs (S15D, S78D, S82D, S15/78D, S15/82D, S78/82D and S15/78/82D) were generated by site-directed mutagenesis of the wild-type gene by GenScript (New Jersey, U.S.A). Protein expression was induced at OD_{600} ~0.6-0.8 with 0.5 mM IPTG and cells were cultured at 37°C for 4 h with shaking. Cells were pelleted at 5,000 x *g*, 4°C for 15 min and stored at -20°C ready for extraction.

The gene encoding human αB-c (*HSPB5;* UniProt accession number P02511) was expressed in *E. coli* BL21(DE3) using a plasmid kindly gifted by Dr. W. C. Boelens and Dr. W. W. de Jong, in which *HSPB5* was cloned into pET24d(+) (Novagen, Darmstadt, Germany). The N-terminal mutants of αB-c (P58A, S59A, S59K, R56S/S59R and Invert 54-60) were generated by site-

directed mutagenesis of the WT gene by GenScript (New Jersey, USA). Expression and harvesting was performed as described above.

2.3.1 **Extraction**

Cell lysis and protein purification was performed as previously described (Horwitz *et al.*, 1998b) with minor changes. Briefly, cell pellets were resuspended in ice-cold lysis buffer (50 mM Tris-HCl, 100 mM NaCl, pH 8.0) (3 mL buffer per gram of pellet) on ice. To the cell lysate, an EDTA free protease inhibitor cocktail (1:100 v/v) and lysozyme (50 µM per gram of pellet) was added and lysates were kept on ice for 30 min with occasional stirring. Deoxycholic acid (10 mM per gram of pellet) was added and lysates were incubated for 30 min at 37°C with shaking. DNase I (10 µM per gram of pellet; Roche Diagnostics Basel, Switzerland) was added and the lysates incubated at room temperature until no longer viscous. Lysates were centrifuged at 17,000 x *g* for 15 min at 4°C (Sorvall RC6 centrifuge, F21-8x50Y rotor). Supernatant was retained and ultracentrifuged at 100,000 x *g* for 30 min at 4°C. The supernatant was treated with DTT (10 mM), PEI (0.12% v/v) and EDTA (1 mM) and incubated at room temperature for 10 min followed by centrifugation at 17,000 x *g* for 10 min. The supernatants were then syringe filtered through a 0.22 µm PES membrane filter prior to anion-exchange chromatography.

2.3.2 **Purification**

All chromatography was performed using either an AKTA FPLC system (Amersham Biosciences, Amersham, U.K) or Next Generation Chromatography (NGC) FPLC system (BioRad, California, U.S.A). Filtered supernatants were loaded onto a HiPrep 16/60 DEAE FastFlow anion-exchange column (Amersham Biosciences, Amersham, U.K) equilibrated in 20 mM Tris-HCl, 1 mM EDTA, 0.02% NaN_3, 0.1 mM PMSF, pH 8.5. Protein was eluted at 2.0 mL/min using a stepwise elution (10%, 20% and 100%) of the same buffer but containing

1 M NaCl. Fractions containing Hsp27 or αB-c, as determined by 15% SDS-PAGE, were pooled and concentrated to ~3 mL using a Vivaspin 20 (GE Healthcare, Illinois, U.S.A.), with molecular weight cut-off of 30,000 Da, by centrifugation at 2,900 x *g* at 4°C. Concentrated samples were syringe filtered through a 0.22 µm PES membrane before loading samples onto a HiPrep 26/60 Sephacryl S-300 HR SEC (GE Healthcare, Illinois, U.S.A.) equilibrated in either 200 mM NH_4OAc (pH 6.8) or 50 mM phosphate buffer (pH 7.4). Proteins were eluted from the column at 1.0 mL/min using the same buffer. Fractions containing Hsp27 or αB-c, as determined by 15% SDS-PAGE, were pooled and concentrated using a Vivaspin 20 as described above. Concentrated samples were stored at -20°C until use. Protein concentration was determined by using an extinction coefficient ($\varepsilon^{0.1\%}$) of 1.65 for Hsp27 and 0.85 for αB-c (Shashidharamurthy *et al.*, 2005).

2.4 Expression and purification of monomeric α-synuclein

Expression and purification of monomeric α-synuclein (αS) (*SNCA;* UniProt accession number P37840) was performed as previously described (Buell *et al.*, 2014). Briefly, αS was expressed in *E. coli* BL21 (DE3) using a plasmid gifted by Mr James Brown (University of Cambridge, UK), in which *SNCA* was cloned into the *NdeI* and *HindIII* restriction sites of the pT7-7 plasmid (Addgene, Massachusetts, USA). This sequence contained a TAC to TAT mutation at codon 136 to prevent cysteine misinsertion and subsequent dimerization (Masuda *et al.*, 2006). Protein expression was induced at OD_{600} ~0.6-0.8 and cells were harvested at 37°C for 4 h with shaking. Cells were pelleted at 6,000 x *g*, 4°C for 15 min and stored at -20°C ready for extraction.

2.4.1 Extraction

Cell pellets were resuspended in cell lysis buffer (20 mL/litre of culture) containing 100 mM Tris-HCl (pH 8.0), 10 mM EDTA and an appropriate amount of protease inhibitor cocktail.

Cells were lysed by three cycles of freeze-thaw followed by sonication (30% amplitude for 15 s on and 30 s off for a total of 5 cycles). Lysates were incubated in a water bath at 95°C for 20 min and centrifuged at 22,000 x *g* at 4°C for 20 min. Supernatants were subsequently treated with streptomycin sulfate (100 µM) at 4°C for 20 min with stirring and then centrifugation at 22,000 x *g* at 4°C for 20 min. The supernatant was collected and streptomycin sulfate addition and centrifugation repeated once more. The supernatant was treated with 0.4 g/mL ammonium sulfate at 4°C for 30 min with stirring to precipitate αS, which was collected by centrifugation at 22,000 x *g* at 4°C for 20 min. The pellet was resuspended in a ~10 mL of 25 mM Tris-HCl (pH 7.7) prior to dialysis overnight at 4°C against a buffer consisting of 20 mM Tris-HCl, 1 mM EDTA, 0.02% NaN_3 (pH 8.5).

2.4.2 **Purification**

Filtered extract was loaded onto a MonoQ 5/50 GL anion-exchange column (GE Healthcare) equilibrated in 20 mM Tris-HCl, 1 mM EDTA, 0.02% NaN_3 (pH 8.5). Protein was eluted at 0.5 mL/min using a gradient elution (0 - 50%) of the same buffer but containing 2 M NaCl. Fractions (2 mL) containing αS, as determined by 15% SDS-PAGE, were pooled and concentrated using a Vivaspin 20 with molecular weight cut-off of 10,000 Da by centrifugation at 8,000 x *g* at 4°C. Samples were syringe filtered through a 0.22 µm PES membrane before loading (3 mL) onto a HiLoad 16/600 Superdex 75 Prep Grade SEC (GE Healthcare) equilibrated in 50 mM phosphate buffer (pH 7.4). Proteins were eluted at 1.0 mL/min using the same buffer. Fractions containing purified αS, as determined by 15% SDS-PAGE, were pooled and concentrated to 100 – 200 µM (to prevent oligomerisation and aggregation) and snap frozen for storage at -80°C. Protein concentration was determined by using the theoretical extinction coefficient ($\varepsilon^{0.1\%}$) of 0.4, based on the amino acid sequence (Gasteiger E., 2005).

2.4.3 **Preparation of α-synuclein seed fibrils**

After purification, monomeric αS (150 µM in 50 mM phosphate buffer, pH 7.4) was heated and stirred at 45°C for 24 h prior to sonication (30% amplitude for 15 s on and 30 s off for a total of 3 cycles). This process was repeated once more prior to snap freezing the seeds with liquid nitrogen, which were then stored at -80°C.

2.5 General biophysical studies

2.5.1 **Analytical size-exclusion chromatography (SEC)**

The average oligomeric size of Hsp27 and αB-c isoforms was determined by analytical-SEC. Samples (approximately 50 µM) were loaded onto either a Superdex 75 10/300 GL or Superose 6 10/300 GL analytical-SEC (both from GE Healthcare), which had been equilibrated in 50 mM phosphate buffer and 100 mM NaCl (pH 7.4), at a flow rate of 0.3 mL/min at room temperature. The size exclusion columns were calibrated using standards (Bio-Rad) containing bovine thyroglobulin (670 kDa), bovine γ-globulin (158 kDa), chicken ovalbumin (44 kDa) and horse myoglobin (17 kDa).

2.5.2 **Intrinsic tryptophan and bis-ANS fluorescence**

Intrinsic tryptophan fluorescence was used to examine changes in the tertiary and quaternary structure of Hsp27 (Hsp27 contains the following tryptophan residues; W16, W22, W42, W45, W51 and W95) and αB-c (αB-c contains the following tryptophan residues; W9 and W60) (see alignment Figure 1.5). bis-ANS fluorescence was used to determine the relative amount of exposed regions of hydrophobicity. Tryptophan fluorescence and bis-ANS fluorescence spectra were attained using a Cary Eclipse fluorescence spectrophotometer (Varian, USA). Proteins were prepared to a final concentration of 10 µM in 50 mM phosphate buffer (pH 7.4). Proteins were incubated at room temperature for 15 min prior to tryptophan fluorescence analysis. bis-ANS (final concentration 20 µM) was then added and

the samples incubated for 3 min at room temperature prior to measurement of the bis-ANS fluorescence. The excitation wavelength was set at 295 nm and 350 nm and emission wavelength was recorded from 300-400 nm and 400-600 nm for tryptophan fluorescence and bis-ANS studies, respectively. The slit widths for excitation and emission spectra were both set at 5 nm.

2.5.3 **Far-UV CD Spectroscopy**

Far UV-CD was utilised to determine secondary structure motifs of Hsp27 and αB-c isoforms. Spectra were acquired using a Jasco Far UV spectropolarimeter (Jasco, Japan). All proteins were measured at room temperature using a 1 mm quartz cuvette (Hellma Analytics, Germany). Acquisition settings were as follows: 100 nm/min continuous scanning, 1 nm bandwidth, 0.2 data pitch, 6 scans were acquired and averaged with Savotsky-Golay smoothing (25 convolutions). All proteins were prepared to a final concentration of 10 µM in 10 mM phosphate buffer (pH 7.4). Far UV-CD spectra were buffer corrected and subsequently deconvoluted using BeStSel deconvolution software (Micsonai *et al.*, 2015).

2.5.4 **Dynamic light scattering (DLS)**

To determine the mean particle size (Z-average) and relative thermal stability of the sHsps in solution, DLS was performed. Proteins were prepared in 50 mM phosphate buffer (pH 7.4) at 50 µM and incubated at 37°C for 1 h prior to measurement. Samples were plated (100 µL) into 96-well microwell plates and analysed using a Zetasizer Auto Plate Sampler system (Malvern, Malvern, U.K.). Thermal stability was assessed by using an inbuilt temperature gradient with 2.5°C for 10 min increments ranging from 25°C to 95°C. The melting temperature of each isoform was defined as a 2-fold increase in hydrodynamic diameter from the measurement taken at 25°C. Experiments were repeated twice and data shown are representative from these two experiments.

2.5.5 Bulk - Fluorescence resonance energy transfer (Bulk-FRET) experiments to measure subunit-exchange

Bulk-FRET was used to determine whether Hsp27-WT and Hsp27-3D were capable of subunit-exchange. Hsp27-WT was labelled with Alexa Fluor-488 and Alexa Fluor-647 (both lysine labelled) dyes (Thermo Fisher Scientific; Massachusetts, USA) and Hsp27-3D was labelled with Alexa Fluor-488. Individual stocks of labelled proteins were made up to 25 µM in 50 mM phosphate buffer (pH 7.4). Samples were equilibrated by incubation at 37°C for 1 h and placed on ice for 20 min to halt subunit-exchange (Bova *et al.*, 1997). Subunit-exchange was monitored using a POLARstar plate reader (BMG Lab Technologies) based on the change in FRET over time. Equimolar ratios of the putative subunit-exchange pairs (i.e. Hsp27-WT-488 + Hsp27-3D-647; Hsp27-WT-488 + Hsp27-WT-647) were plated into a black 384-microwell plate and FRET monitored for 90 min at 37°C by measuring the levels of fluorescence with a 490/650 nm excitation/emission filter set. The ratio of fluorescence intensity at any point in time (F(t)) to fluorescence intensity at time zero (F(0)) (i.e. F(t)/F(0)) was calculated. An increase in this fluorescence ratio was indicative of subunit-exchange. Subsequent reaction curves were fitted with a one-phase association (exponential) curve to determine the subunit-exchange rate constant (k). Subunit-exchange was also confirmed by analytical-SEC (section 2.5.1) whereby samples were taken directly from the 384-well microplates and loaded onto a Superdex 200 10/300 GL column pre-equilibrated with 50 mM phosphate buffer (pH 7.4) with multi-wavelength detection set at 280, 495 and 650 nm at a flow rate of 0.4 mL/min.

2.6 Mass Spectrometry-based studies

2.6.1 Denatured mass spectrometry (MS)

Denatured MS was performed on a Synapt G1 HDMS (Waters) using a nanoelectrospray ionisation source. Proteins were denatured using formic acid (1 % v/v final concentration)

and acetonitrile (40% v/v final concentration) and samples were incubated overnight at room temperature to ensure complete denaturation. Instrument conditions were set as previously described (Aquilina *et al.*, 2003). Key instrument parameters were as follows: capillary voltage (kV): 1.5; sampling cone (V): 50; extraction cone (V): 4; trap/transfer collision energy (V/V): 6/4; trap gas (L/hr): 2.5; backing gas (mbar): ~2.0. Each protein was electrosprayed from gold-coated borosilicate glass capillaries (Harvard Apparatus; Massachusetts, USA) prepared in-house. The mass spectrometer was calibrated using caesium iodide (10 mg/mL) and all spectra were analysed using MassLynx V4.1 software with minimal smoothing applied to raw spectra.

2.6.2 **Native MS**

Native MS was performed on a quadrupole time-of-flight (Q-ToF) 2 MS and Synapt G1 HDMS (Waters) using a nanoelectrospray ionisation source. Instrument conditions were set as previously described which have been optimised to maintain native structure of large protein assemblies (Aquilina *et al.*, 2013). Key instrument parameters on both mass spectrometers were as follows: capillary voltage (kV): 1.60-1.65; sampling cone (V): 150-200; extraction cone (V): 7-10; trap/transfer collision energy (V/V): 25/15; trap gas (L/hr): 6.5; backing gas (mbar): ~5.0-7.0. For CID experiments, the voltages in the collision cell were increased in 20 V increments (from 20 - 200 V). Prior to native MS, all sHsp isoforms were buffer-exchanged into 200 mM NH_4OAc (pH 6.8) using a Superdex 200 10/300 GL column. Oligomeric distribution spectra were acquired at a concentration of 40 µM, due to the concentration-dependence of the oligomeric state of Hsp27 (Theriault *et al.*, 2004), whilst the dilution MS experiments were performed at range of concentrations from 0.7 to 47 µM. Each protein was nanoelectrosprayed and respective spectra were analysed as described previously (section 2.6.1).

2.6.3 **Ion-Mobility MS (IM-MS)**

Ion mobility-MS was performed on a Synapt G1 HDMS (Waters) using a nanoelectrospray ionisation source. To investigate the quaternary architecture of Hsp27 assemblies, softer front end conditions on the MS were required to minimise gas-phase compaction and unfolding prior to detection. Key instrument parameters were as follows: capillary voltage (kV): 1.60-1.65; sampling cone (V): 40; extraction cone (V): 2.0; trap/transfer collision energy (V/V): 15/10; trap gas (L/hr): 6.0; backing gas (mbar): ~6.5. The parameters for the IM were as follows: IM cell wave height (V): 8-10; IM cell wave velocity (m/s): 300; transfer t-wave height (V): 8; transfer t-wave velocity (m/s): 200. Proteins were buffer exchanged and prepared as described earlier (section 2.4.5). Cytochrome C and myoglobin (both equine; Sigma-Aldrich) were used as IM calibrants for small oligomeric assemblies (monomers to tetramers) as previously described (Ruotolo *et al.*, 2008).

To investigate the collision-induced unfolding (CIU) dynamics of Hsp27 dimers, given that all the single phosphomimic isoforms were structurally and functionally similar (as were all the double phosphomimic isoforms), the S15D, S15/82D and S15/78/82D mutants were selected as representatives of the 1D, 2D and 3D isoforms, respectively (and are referred to as Hsp27-1D, Hsp27-2D and Hsp27-3D). Hsp27-WT was excluded from this analysis as the population of free dimer at the concentrations used (50 µM) was too low to be detected by IM-MS. In these experiments the dimer^{13+} was selected to ensure no overlap from other charged species, and IM spectra was acquired under the conditions stated above such that the trap and transfer collision energy was increased in 5 V increments from 15 – 60 V. Ion mobility heat maps and CIU difference plots were generated using CIUsuite with default settings (Eschweiler *et al.*, 2015). To determine the relative proportion of unfolded dimer with increasing activation energy, unfolding curves were produced. The IM chromatograms

at each activation energy increment were measured and normalised to the highest intensity. The relative abundance of unfolded dimer was determined by the intensity of any unfolded species present (i.e. any observed intensity that is not attributable to the folded dimer).

The IM data for the large oligomer (12-mer^{31+}) were calibrated using egg white avidin and human transthyretin (both Sigma-Aldrich) and acquired as described previously (Baldwin *et al.*, 2011b, Ruotolo *et al.*, 2008). Key instrument parameters were as follows: capillary voltage (kV): 1.60-1.65; sampling cone (V): 40; extraction cone (V): 2.0; trap/transfer collision energy (V/V): 15/10; trap gas (L/hr): 6.0; backing gas (mbar): ~6.5. IM parameters were as follows: IM cell wave height (V): 10-14.5; IM cell wave velocity (m/s): 300; transfer wave height (V): 8; transfer wave velocity (m/s): 200. Arrival time distribution (ATD) and drift time data was acquired and calculated using Driftscope 2.1 (Waters) as described previously (Ruotolo *et al.*, 2008).

2.6.4 **Oligomeric dissociation MS**

The oligomeric dissociation of Hsp27-WT, 1D and 2D mutants was observed by MS as described previously (Rose *et al.*, 2011). The peak areas corresponding to Hsp27 dimers (A_D) and oligomers (ranging from tetramers to 24-mers; A_O) were summed to determine the total peak area of each spectrum (A_T):

$$A_D + A_O = A_T$$

The relative proportion of dimer relative to oligomer (P_D) was determined by dividing the dimer peak area (A_D) by the total peak area of the whole spectrum (A_T):

$$A_D/A_T = P_D$$

The dissociation curves were fitted using the one phase decay function. For each protein, at least 5 data points were plotted and this experiment was repeated 3 times. All curve fitting analyses was performed using Prism 5.0 (GraphPad) software.

2.6.5 **Limited proteolysis – MS**

Purified proteins were subjected to proteolysis by trypsin (Roche Diagnostics; Basel, Switzerland) at a molar ratio of 1000:1 (Hsp27:protease) in 50 mM phosphate buffer (pH 7.4) at 37°C. At designated time points (0, 10, 20, 30 and 60 min) 10 µL aliquots of the digestion reaction were removed and digestion was quenched by addition of SDS-PAGE loading buffer (for analysis by SDS-PAGE). Samples for SDS-PAGE were analysed and imaged as described earlier (section 2.2.1). In some experiments proteolysis of Hsp27 by trypsin at the above stated molar ratio, which was analysed by MS, was performed in 200 mM NH4OAc (pH 6.8) and digestion was quenched by addition of formic acid and DTT (to final concentrations of 10% v/v and 1 mM, respectively) and sprayed under denatured MS conditions (section 2.6.1). Peptides from digestion were identified by the peaks in each spectrum and compared to the theoretical digestion of Hsp27-WT and Hsp27-3D (performed using BioLynx Protein/Peptide editor V4.1). Peptide identification was based on the charge of the peptide (± 1 Da) when compared to the theoretical size of the peptide.

2.6.6 **Reduction and thiol-blocking**

Hsp27-WT (100 µM) was incubated with 1 mM tris(2-carboxyethyl)phosphine (TCEP) for 30 min at room temperature prior to the addition of 100 mM iodoacetamide (IA). Samples were incubated on ice for 15 min prior to buffer-exchanging by running the sample over a Superdex 200 10/300 GL column (GE Healthcare), which had been pre-equilibrated in 200 mM NH_4OAc (pH 6.8), at a flow rate of 0.4 mL/min at room temperature.

2.7 Functional studies

2.7.1 Aggregation assays

The aggregation and precipitation of target proteins, reported via either ThT fluorescence (amyloid fibril) or light-scattering (amorphous aggregation) assays, was monitored by using sealed 96-microwell plates and a FLUOstar Optima plate reader (BMG Lab Technologies). To assess the protective effects of Hsp27 phosphomimics against aggregation the amorphous aggregation of insulin (100 μM), incubated at 37°C in 50 mM phosphate buffer (pH 7.4), or BSA (50 μM), incubated in PBS, was initiated by the addition of DTT (20 mM). Chaperones were added at molar ratios of 8:1 (insulin:Hsp27) or 2:1 (BSA:Hsp27). Aggregation was monitored by measuring the change in apparent absorbance due to light scattering at 340 nm, which was negligible in the absence of insulin or BSA. The formation of amyloid fibrils by κ-casein was monitored using an *in situ* ThT-binding assay (Ecroyd *et al.*, 2008). Chaperones were added at a molar ratio of 1:1 to κ-casein (25 μM) in 50 mM phosphate buffer (pH 7.0). Samples were incubated with 10 μM ThT at 37°C and fluorescence levels measured with a 440/490 nm excitation/emission filter set. The change in ThT fluorescence in the absence of κ-casein was negligible in this assay.

The chaperone activity of the N-terminal αB-c mutants was also assessed via ThT fluorescence (amyloid fibril) or light-scattering (amorphous aggregation) assays, using sealed 384-microwell plates and a FLUOstar Optima plate reader (BMG Lab Technologies). Amorphous aggregation of insulin (100 μM), incubated at 37°C in 50 mM phosphate buffer (pH 7.4), was initiated by addition of DTT (20 mM). The αB-c isoforms were added at molar ratios of 1:1 and 1:0.75 (insulin:αB-c). Aggregation was monitored by measuring the change in apparent absorbance due to light scattering at 340 nm.

To examine the ability of the N-terminal αB-c mutants to prevent amyloid fibril formation an αS elongation assay was performed (Buell *et al.*, 2014). Essentially, this assay measures the ability of chaperones to inhibit the elongation of αS fibrils using short preformed αS seed fibrils (section 2.4.3). Fibril elongation was monitored using an *in situ* ThT-binding assay. Chaperones were added at a molar ratio of 2:1 and 4:1 (αS:αB-c) to the monomeric pool of αS (50 µM) in 50 mM phosphate buffer (pH 7.4) with 10% w/w αS seed fibrils. Samples were incubated with 50 µM ThT at 37°C and fluorescence levels measured with a 440/490 nm excitation/emission filter set.

In all protein aggregation assays, the relative ability of each chaperone to prevent aggregation was evaluated by comparing the change in light scatter at 340 nm or ThT fluorescence at the conclusion of each assay, as previously described (Ecroyd and Carver, 2008). The change in light scatter at 340 nm or ThT fluorescence in each sample was used to calculate the relative efficacy of the Hsp27 or αB-c isoforms compared to the WT counterparts. All assays were performed at least three times and data are reported as mean ± SEM of these independent assays. Data were analysed by one-way ANOVA and Dunnett's multiple comparisons post-hoc test using Prism 5.0 (GraphPad) software.

2.7.2 **Cell lysate aggregation assays**

The cell lysate aggregation experiments were based on a previous method with minor modifications (Peschek *et al.*, 2013). Briefly, Neuro-2a cells were collected and washed in PBS and stored at -20°C until required. Cells were resuspended in ice cold hypotonic buffer (40 mM phosphate buffer, pH 7.4) containing protease inhibitors (Pierce, Massachusetts, USA) and placed on ice for 15 min. The cell suspension was then repeatedly passed through a gel-loading pipette tip to disrupt the cells before being placed at -20°C for 30 min. The

sample was thawed, the lysate cleared by centrifugation, and a 20 × stock of PBS used to adjust the salt concentration to physiological levels. The concentration of proteins in each sample was adjusted with PBS so that the A280 nm was 2.0, prior to the addition of Hsp27 (or an equivalent volume of buffer or concentration of BSA). Samples were heated at 45°C for 1 h, centrifuged (12,000 × *g*, 10 min, 4 °C), the pellet washed with an equivalent volume of PBS then resuspended again with the same volume of PBS. Protein aggregation was assessed by 15% SDS-PAGE, performed as described above. The intensity of selected bands was quantified using GelAnalyzer2010 (www.gelanalyzer.com). These experiments were performed at least three times and data are reported as mean ± SEM of these independent assays. Data were analysed by unpaired t-test using Prism 5.0 (GraphPad) software.

Chapter 3: Results -

Phosphomimics destabilise Hsp27 oligomeric assemblies and enhance chaperone activity

Disclaimer and Author Contributions

The data presented in this chapter has been peer reviewed and published in the journal *Chemistry and Biology* (now known as *Cell Chemical Biology*).

Jovcevski, B., Kelly M. A., Rote A. P., Berg T., Gastall H. Y., Benesch J. L., Aquilina J. A. and Ecroyd H. (2015). "Phosphomimics Destabilize Hsp27 Oligomeric Assemblies and Enhance Chaperone Activity." *Chem. Biol.* **22**(2): 186-195.

All the Hsp27 isoforms used in this work were expressed and purified by Kelly M. A., Rote A. P. and Ecroyd, H. (University of Wollongong). Experiments involved in collecting and analysing the data presented in Figure 3.1A-D were performed by Kelly M. A., Rote A. P. and Ecroyd, H. The aggregation assay experiments presented in Figure 3.5A-B were performed by Kelly M. A.

Chapter 3: Phosphomimics destabilises Hsp27 oligomeric assemblies and enhance chaperone activity

3.1 Introduction

Hsp27 is a systemically expressed mammalian small heat-shock protein (sHsp) which typically exists as large, polydisperse assemblies (Hickey *et al.*, 1986, Sun and MacRae, 2005). In conjunction with the two other dominant non-lenticular sHsps, αB-c and Hsp20, Hsp27 is a key component of the cell's proteostasis network where it acts as a molecular chaperone. Overall, the association between Hsp27 and neurodegenerative diseases demonstrates that its chaperone function is critical to proteostasis.

Hsp27 is unique amongst the sHsps in that it can form covalent disulfide-bonded homodimers, whereas the dimers of the other sHsps are linked by a charged network along the β6+7 sheets (Bagneris *et al.*, 2009, Hochberg *et al.*, 2014). Previous work has shown that under conditions of cellular stress (Almeida-Souza *et al.*, 2010), disulfide-bonded dimers of Hsp27 can form in the cell. Under such conditions, the quaternary dynamics of Hsp27 may differ significantly to αB-c since the exchanging unit of Hsp27 is a covalently-linked dimer as opposed to the more facile, non-covalent exchange of monomers for αB-c (Baldwin *et al.*, 2011c). The N-terminal region of Hsp27 undergoes phosphorylation *in vivo* at numerous serine residues (Arrigo, 2011, Ito *et al.*, 1997, Lambert *et al.*, 1999, Miesbauer *et al.*, 1994), with serines 15, 78 and 82 being those most predominantly modified, in a process mediated by MAPKAPK-2 and MAPKAPK-3 kinases (Arrigo, 2011, Landry *et al.*, 1992a). Phosphorylation at these sites is induced by cellular stress and leads to alterations to the quaternary structure and dynamics of Hsp27, such that, when it is phosphorylated at all three of these serine residues, or at two serines in rodent Hsp27 (Lambert *et al.*, 1999),

there is a decrease in the size of the Hsp27 oligomer (Hayes *et al.*, 2009, McDonald *et al.*, 2012, Rogalla *et al.*, 1999).

Initial studies into the impact of phosphorylation on Hsp27 structure and function indicated that phosphorylated Hsp27 is less effective than WT protein at inhibiting citrate synthase and insulin aggregation (Rogalla *et al.*, 1999), although later studies reported that phosphorylation corresponded with an increase in substrate binding affinity and ability to inhibit the amorphous aggregation of insulin (Hayes *et al.*, 2009). Phosphomimicking forms of Hsp27 show a decrease in oligomer size (Lambert *et al.*, 1999), enhanced chaperone activity and an increased ability to bind to destabilised forms of T4L lysozyme (Hayes *et al.*, 2009, McDonald *et al.*, 2012, Rogalla *et al.*, 1999, Shashidharamurthy *et al.*, 2005). However, to-date there has not been a comprehensive survey performed on the specific effects of phosphorylation at each of these three serine residues on Hsp27 oligomer size, oligomer distribution and chaperone function.

Native MS provides a method to gain a detailed insight into the tertiary and quaternary features of dynamic proteins (Benesch and Ruotolo, 2011). This approach has enabled the determination of oligomeric distributions of polydisperse ensembles of sHsps (Aquilina *et al.*, 2003, Aquilina *et al.*, 2013, Baldwin *et al.*, 2011c), and to define the stoichiometries of plant sHsp and substrate complexes (Stengel *et al.*, 2010). More recently, native MS was used to quantify the dissociation of modified and unmodified superoxide dismutase 1 dimers, a process thought to be critical to the aggregation of this protein in association with ALS (McAlary *et al.*, 2013). Thus, MS is an ideal technique for the study of the dynamic and polydisperse Hsp27 oligomers.

This study explores in detail the potential impact phosphorylation at each of these three serine residues has on the quaternary structure and chaperone function of Hsp27. It does this through the use of mutations that mimic phosphorylation (MMP), i.e. phosphorylatable serine residues were mutated to aspartic acids; which are commonly used to study sHsp phosphorylation (Aquilina *et al.*, 2004, Ecroyd *et al.*, 2007, Hayes *et al.*, 2009, McDonald *et al.*, 2012, Rogalla *et al.*, 1999) and allows the site-specific effects to be studied *in vitro*. A previous study demonstrated that Hsp27 MMPs exhibit similar structural and functional properties compared to the phosphorylated form (Hayes *et al.*, 2009).

3.2 Methods

Human Hsp27-WT and serine to aspartic acid mutations at residues 15, 78 and/or 82 (to mimic phosphorylation) were generated. These represent each of the seven possible Hsp27 isoforms ($Hsp27_M$) produced by phosphorylation at one, two or three serines. All the Hsp27 isoforms were expressed and purified as described previously (section 2.3). Native-PAGE (section 2.2.2), analytical-SEC (section 2.5.1), CD-spectroscopy (section 2.5.3) and native MS (section 2.6.2) were used to examine the structure of Hsp27-WT and $Hsp27_M$. The concentration-dependent propensity of Hsp27 oligomeric assemblies to dissociate were also examined using a MS approach (section 2.6.4). The chaperone activity of these Hsp27 isoforms against amorphous and fibril aggregation was assessed using *in vitro* aggregation assays (section 2.7.1). The ability of Hsp27 to prevent protein aggregation in whole cell lysates was also examined (section 2.7.2).

3.3 Results

3.3.1 Oligomeric size and polydispersity is decreased with mutations that mimic phosphorylation

Previous studies have indicated that specific kinase-mediated phosphorylation of Hsp27 can occur at three serine residues (S15, S78 and S82) and that levels of phosphorylation and disulfide-bonding are up-regulated by conditions of cellular stress (Almeida-Souza *et al.*, 2010, Gaestel *et al.*, 1991, Landry *et al.*, 1992a). We sought to confirm the increase in Hsp27 phosphorylation upon stress using HeLa cells subjected to heat (45 °C for 2 h). Blotting with phosphoserine-specific antibodies demonstrated that S78 and S82 were phosphorylated under basal conditions and that phosphorylation of S15 is dramatically increased in response to heat stress (Figure 3.1A, left panel). In order to elucidate the impact of this modification to the structure and function of Hsp27, we expressed recombinant Hsp27 with serine to aspartic acid mutations at residues 15, 78 and 82 to mimic phosphorylation and generated each of the seven possible Hsp27 isoforms ($Hsp27_M$).

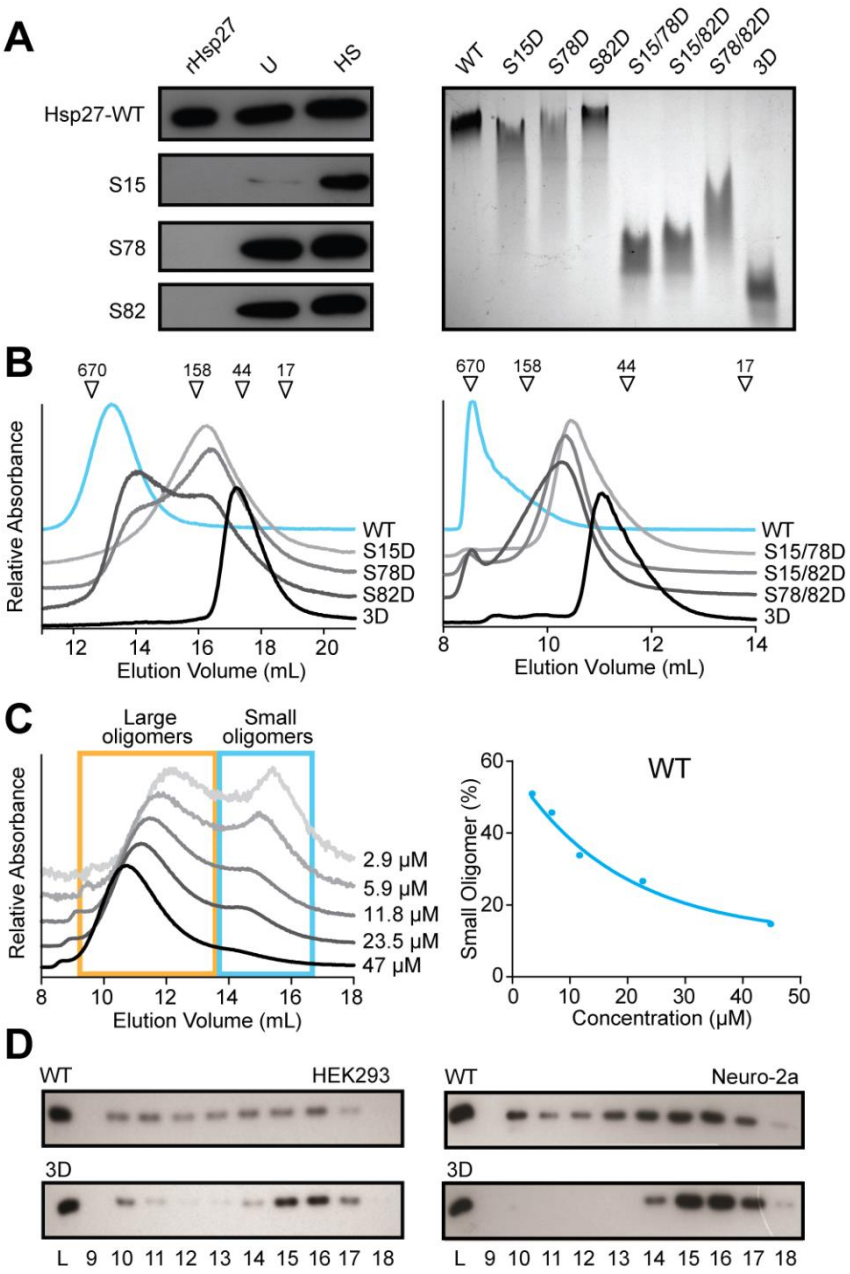

Figure 3.1: Mutations that mimic phosphorylation decrease the size of Hsp27 oligomers
A*:** Western blotting of HeLa cell extracts (*left panel*) under non-stressed (U) and heat-stressed (HS, 45°C for 2 h) conditions indicating that phosphorylation of Hsp27 occurs at serine residues 15, 78 and 82 (rHsp27: recombinant Hsp27). Discontinuous native-PAGE (*right panel*) of Hsp27-WT (50 µM) and its phosphomimic variants reveals a decrease in oligomer size as the number of MMP increases. ***B*:** Analytical-SEC demonstrates a decrease in oligomer size of Hsp27-1D (*left panel, Superose 6*) and Hsp27-2D (*right panel, Superdex 75*) compared to WT. Hsp27-WT and $Hsp27_M$ were loaded at equal concentrations (50 µM). The elution volumes at which molecular weight standards eluted are indicated above. ***C: The dissociation of large oligomers of Hsp27-WT (orange box) into smaller oligomers (blue box) upon dilution was also observed using analytical-SEC (*left panel*); the increasing abundance of small oligomers upon dilution (dilution was performed prior to loading) was used to determine the propensity of oligomeric dissociation (*right panel*). ***D:*** Western blotting of cell lysates (L) fractionated by analytical-SEC showing the decrease in average oligomer size between Hsp27-WT and Hsp27-3D when expressed in HEK293 (*left panel*) or Neuro-2a (*right panel*) cell lines (elution fractions indicated by numbering below).

Analytical-SEC revealed that Hsp27-WT eluted early from the column as a broad peak, corresponding to an average molecular mass of ~590 kDa (Figure 3.1B). The MMP caused substantial reductions in the size of Hsp27, where the single $Hsp27_M$ isoforms eluted as very broad peaks corresponding to molecular masses between 100-420 kDa (Figure 3.1B, left panel), whilst the broad eluent peak of the double $Hsp27_M$ isoforms had an average mass of 90 kDa (Figure 3.1B, right panel). Significantly, Hsp27-S15/78/82D (Hsp27-3D) eluted as a single peak at a volume (Superose 6: 11.2 mL and Superdex 75: 17.4 mL) corresponding to that of a protein of size ~45 kDa, concordant with a Hsp27 dimer (Figure 3.1B). Native gel electrophoresis also confirmed that MMP at one residue did not greatly affect the average size of Hsp27 oligomers (Figure 3.1A, right panel), whereas when present on two or three residues they substantially decreased the average size of the Hsp27 oligomer, as evidenced by their significantly increased migration compared to WT. Previously, SEC was used to show that Hsp27-WT undergoes concentration-dependent dissociation *in vitro* (Rogalla *et al.*, 1999, Theriault *et al.*, 2004). This attribute was therefore exploited to observe the propensity of Hsp27 oligomers dissociating into their constitutive units by SEC via the relative abundance of large and small oligomers across a range of concentrations (Figure 3.1C, left panel).

We also investigated whether the differences observed in the oligomeric size and distribution between Hsp27-WT and Hsp27-3D were detectable in cells. Human embryonic kidney (HEK293) and mouse neuroblastoma (Neuro-2a) cells were transiently transfected in order to express either Hsp27-WT or Hsp27-3D, prior to fractionation of cell lysates by SEC and probing with Hsp27-specific antibodies (Figure 3.1D). In both cell lines, Hsp27-WT was detected in a broad range of fractions, indicating its presence as polydisperse oligomers in cells. By contrast, the majority of the Hsp27-3D was detected in fractions that eluted later

from the column, indicating that it predominately exists as smaller oligomers, in the range of 45–90 kDa (Figure 3.1D).

Whilst SEC demonstrated that MMP decrease oligomer size and polydispersity, in order to more fully elucidate the oligomeric distribution of $Hsp27_M$, MS analyses of these proteins were performed using conditions which preserve their native state upon transfer from solution into the gas phase (low collision energy, 30 V) (Figure 3.2) (Aquilina *et al.*, 2003). Collision-induced dissociation was also used to exploit the phenomenon of asymmetric partitioning, which occurs when one or more highly-charged subunits (unfolded dimer) are dissociated from an oligomeric assembly (high collision energy, 200 V) (Figure 3.2). This technique is therefore extremely effective for the analysis of polydisperse assemblies, such as the sHsps, since the spectrum is greatly simplified when overall charge is reduced (Aquilina *et al.*, 2003, Benesch *et al.*, 2008).

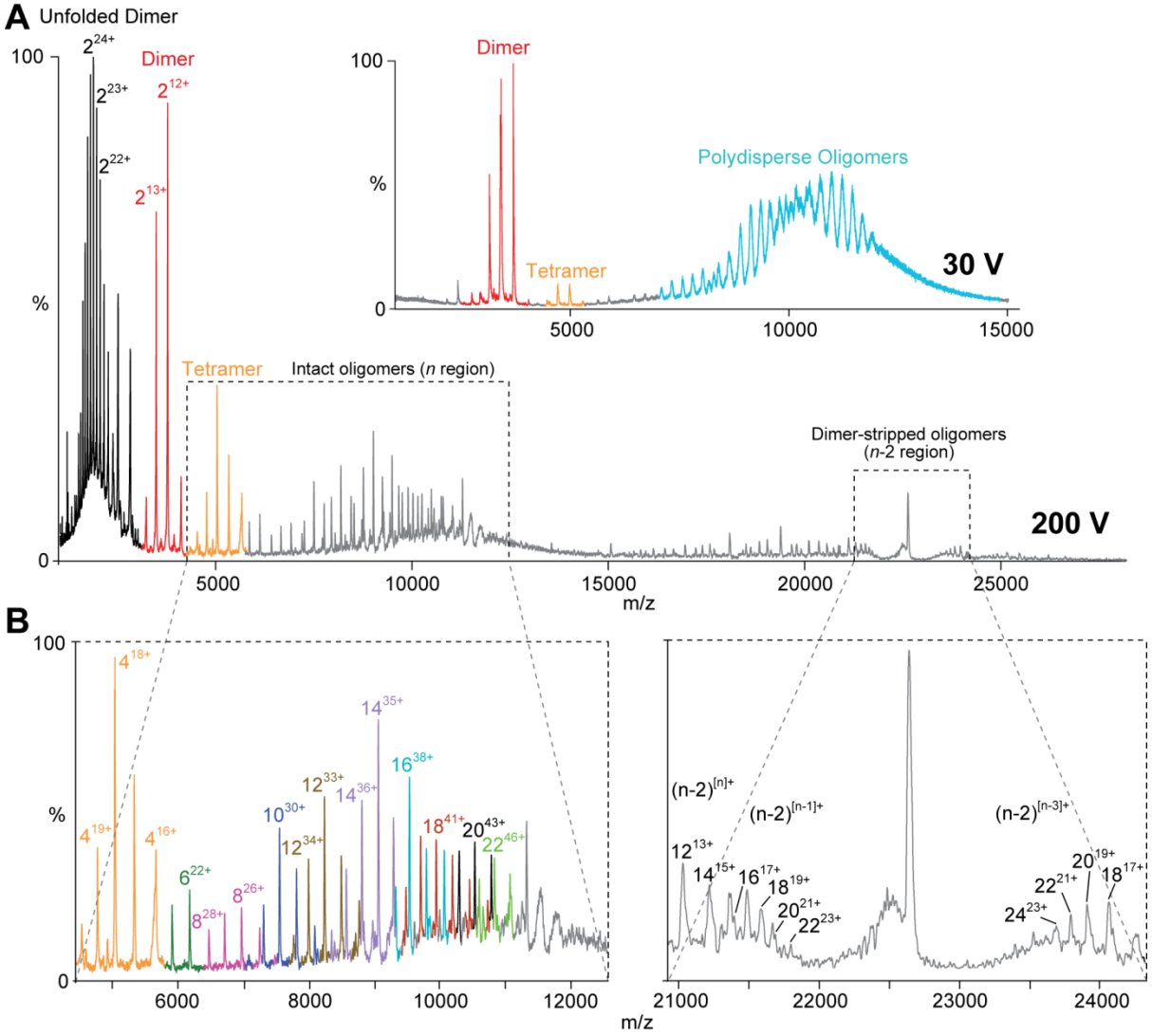

Figure 3.2: Collision-induced dissociation mass spectrometry of Hsp27 phosphomimics
A: The spectrum acquired at low collision energy (30 V) illustrates the polydisperse nature of $Hsp27_M$, in this case Hsp27-S15D, with a large unresolved peak envelope observed between 7,000 and 14,000 *m/z* (blue), as well as signals from dimer (red) and tetramer (orange). At higher accelerating voltage (200 V) signal in the *n*-2 region became apparent and the *n* region resolved substantially. ***B:*** The unambiguous charge state distributions in the *n* region were used to comprehensively identify and assign the abundance of oligomers present, ranging from dimers to 24-mers (charge state in superscript; *left panel*). The *n*-2 region (*right panel*) was of limited use in describing the distribution of $Hsp27_M$ as the strictly dimeric nature gave rise to considerable charge state overlap ($[n]^+$ and $[n-1]^+$) when compared to previously studied mammalian sHsps.

Typically in other polydisperse assemblies (e.g. αB-c and Hsp27 under reducing conditions), signal from the monomer-stripped (*n*-1) and dimer-stripped (*n-2*) oligomer regions are unambiguously resolved, with the latter being used to determine oligomer distribution and abundance (Aquilina *et al.*, 2013). However, due to the disulfide-bonded dimeric substructure of Hsp27 in these experiments, its spectra under non-reducing conditions showed significant charge state overlap in the *n*-2 region (Figure 3.2B, right panel) as well as the absence of an *n*-1 region (Figure 3.2A). Surprisingly, the intact oligomer (*n*) region was completely resolved by collisional cleaning and thus the size and abundance of all oligomers present could be identified from this region (Figure 3.2B, left panel).

Previous MS data demonstrated that Hsp27-WT (under DTT-induced reduced conditions) exists as a polydisperse assembly of even-sized oligomers, ranging from 16- to 30-mers, with the 20-mer being the most abundant (Aquilina *et al.*, 2013). Much like Hsp27-WT, the $Hsp27_M$ isoforms were comprised of even-sized oligomers; however, they were significantly shifted to a smaller range of assemblies. In the case of the single $Hsp27_M$ forms, oligomers ranged from dimers to 24-mers, and up to 22-mers for the double $Hsp27_M$ isoforms (Figure 3.3A) (Appendix I; Figure 8.1). This region also showed that the 14-mer was the most abundant large oligomer (≥ 6-mers) present in each of the $Hsp27_M$ analysed in this study, except for Hsp27-S78/82D, where the 8-mer was the most abundant (Figure 3.3A).

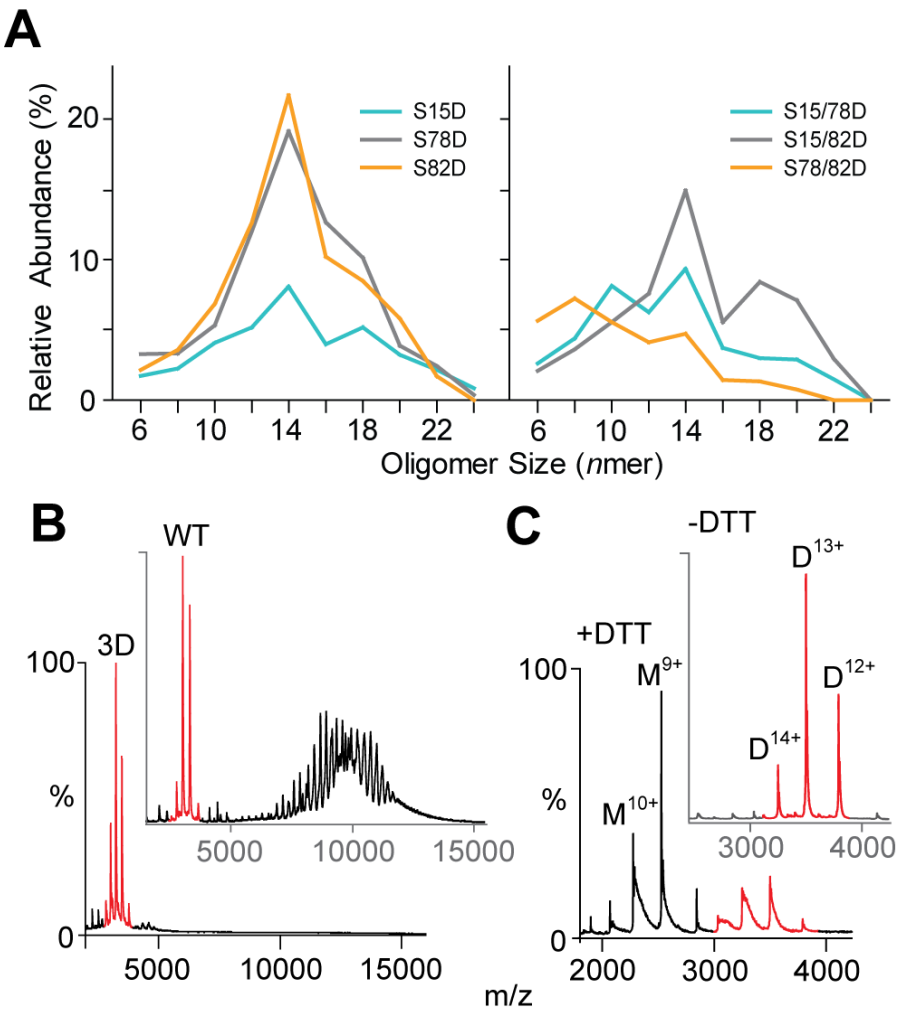

Figure 3.3: Oligomeric distribution of Hsp27 phosphomimics by MS
***A*:** Oligomeric distributions of $Hsp27_M$ were determined by collision-induced dissociation mass spectrometry, with large oligomers ranging from hexamers to 24-mers. ***B*:** Native mass spectrometry of Hsp27-WT, present as a mixture of dimers (red) and large polydisperse oligomers (~10,000 *m/z*), and Hsp27-3D, which is predominantly dimeric. ***C*:** DTT-induced reduction of Hsp27-3D shows that the majority of the dimers (D; red) fall apart into monomers (M; black).

Using relatively low-resolution biophysical approaches, the oligomeric state of Hsp27-3D has previously been reported to range from small oligomers to dimers (Hayes *et al.*, 2009, Lambert *et al.*, 1999, Rogalla *et al.*, 1999, Shashidharamurthy *et al.*, 2005). Significantly, our MS data conclusively demonstrates that for Hsp27-3D the equilibrium between large oligomers and dissociated species is significantly shifted, such that it exists predominately as a monodisperse dimer at concentrations of up to 50 µM (Figure 3.3B). This dimer is

covalently linked through a disulfide bond, as the addition of DTT resulted in a sizeable proportion of these dimers dissociating into monomers (Figure 3.3C).

3.3.2 **Oligomeric plasticity of Hsp27 phosphomimics**

Work, including our own (Figure 3.1C), has indicated that at low concentrations in solution, Hsp27-WT dissociates into its constituent subunits (McDonald *et al.*, 2012, Rogalla *et al.*, 1999, Theriault *et al.*, 2004). However, due to the dynamic nature of these assemblies, it has proved difficult to investigate this process in a quantitative manner. The ability of MS to quantify the relative abundance of individual species within a heterogeneous mixture provided a powerful tool to study the concentration-dependent dissociation of Hsp27. Under identical instrument conditions, the relative intensities of ions above 4,000 *m/z* (arising from all oligomers with $n \geq 4$) were diminished with successive dilution for each $Hsp27_M$ form. Moreover, at the higher concentration of 25 µM, the abundance of dimer was observed to be approximately commensurate with the degree of serine substitution; ranging from 15% for WT to 38% for Hsp27-2D (Figures 3.4A-C). Based on the concentration-dependent ratio of dimers to oligomers, we observed that the propensity of Hsp27 dissociation increased with the number of MMPs. Only intermediate oligomers were observed for Hsp27-2D (6-mers and 8-mers) during the dilution MS experiments and no monomer was observed across all Hsp27 isoforms. Our data therefore suggest that upon phosphorylation, the Hsp27 assemblies are less constrained by associative forces inherent to the quaternary structure of WT, permitting the more facile detachment of sub-oligomeric species, in particular the dissociation of dimers from an oligomeric assembly.

We reasoned that this shift in oligomeric dissociation propensity may have arisen from variations in the secondary structure of Hsp27-WT and its phosphomimics. Far-UV CD

spectroscopy shows alterations of Hsp27 secondary structure with successive serine substitutions (Figure 3.4D). A negative ellipticity minimum was observed at 218 nm, consistent with antiparallel β-sheet structure. A positive maximum at 230 nm was also apparent, corresponding to random coil secondary structure. The amount of random coil became markedly more pronounced with increased modification and appears to be absent in Hsp27-WT (Figure 3.4D). The observed maximum for $Hsp27_M$ is indicative of the dissociated state of Hsp27, in which the structural elements are accessible to the polarised light, giving rise to the enhanced signal across all wavelengths.

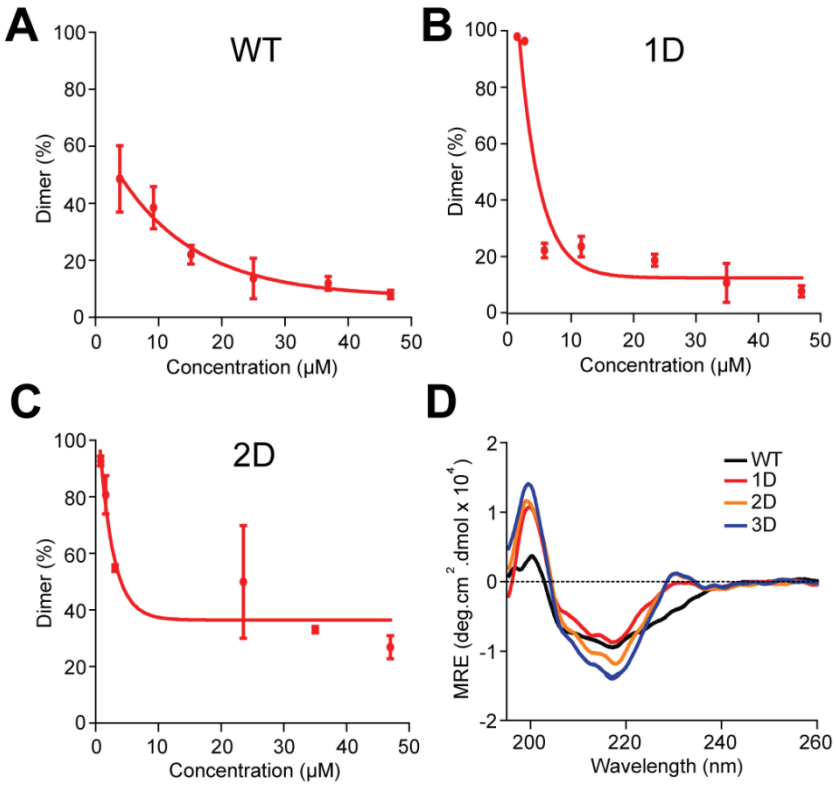

Figure 3.4: MS-derived dissociation curves and far-UV CD spectroscopy of Hsp27-WT and its phosphomimics

Increased dissociation of large oligomers to dimers was observed upon dilution. ***A-C:*** Hsp27-WT (*A*), Hsp27-1D (S15D; *B*) and Hsp27-2D (S15/82D; *C*) were representative of each degree of phosphomimicry. Increasing the number of MMP led to an increase in oligomeric dissociation propensity (n = 3; mean ± SD). ***D:*** Far-UV CD spectroscopy of $Hsp27_M$: the spectra of the Hsp27-1D (red) and Hsp27-2D (orange) forms were of sufficient similarity to be represented by single traces. The spectrum of Hsp27-3D (blue) showed greater negative ellipticity than Hsp27-1D and Hsp27-2D, however all $Hsp27_M$ isoforms exhibited increased random coil (~235 nm) compared to Hsp27-WT (black).

3.3.3 Mutations that mimic phosphorylation enhance Hsp27 chaperone activity

Having established that significant structural changes occur to Hsp27 as a result of MMP, we sought to observe its functional consequences on Hsp27 chaperone activity. Protein aggregation assays in the presence of Hsp27-WT and $Hsp27_M$ isoforms were conducted such that the concentration of Hsp27 was well above the concentration where Hsp27 oligomers completely dissociate (i.e. final concentration was 12.5 μM or higher). Insulin and bovine serum albumin (BSA) were used to assess the efficacy of $Hsp27_M$ isoforms in preventing amorphous aggregation, and κ-casein fibrillar aggregation of target proteins. In the absence of chaperone, amorphous aggregation of insulin commenced after 4 min and increased rapidly, until ~20 min at which point it plateaued (Figure 3.5A, inset). Neither a change in light scatter (insulin or BSA) nor ThT fluorescence (κ-casein) was detected when the sHsps or buffer were incubated alone in these experiments. Overall, an increase in the number of MMPs was accompanied by an enhanced ability of Hsp27 to prevent both amorphous and fibrillar aggregation of target proteins (Figure 3.5A). The single $Hsp27_M$ isoforms showed mixed chaperone effectiveness, with S78D and S82D in the insulin assay and S82D in the BSA assay better able to protect against aggregation compared to Hsp27-WT (Figure 3.5A) (Appendix I; Figure 8.2). Each of the double $Hsp27_M$ mutants and Hsp27-3D was significantly more effective at inhibiting amorphous and fibrillar aggregation of the target proteins than Hsp27-WT (Figure 3.5A).

The capacity of Hsp27-WT and 3D to prevent the heat-induced precipitation of proteins from cell lysates was also examined (Figure 3.5B-C). In the absence of chaperone, Neuro-2a lysate proteins precipitated from solution to form an insoluble pellet (Figure 3.5B, lane H). Addition of Hsp27-WT or Hsp27-3D, at concentrations ranging from 2.5-10 μM, inhibited the

heat-induced precipitation of the lysate proteins, whilst BSA afforded no protection (Figure 3.5B). Densitometry analysis of the most intense protein band (Figure 3.5B, red box) evident in the precipitate by SDS-PAGE revealed that significant protection of lysate proteins was afforded by Hsp27-3D at 5 µM and 10 µM compared to WT (Figure 3.5C). Interestingly, Hsp27-WT afforded the same level of protection as Hsp27-3D at 2.5 µM (Figure 3.5C). This finding is consistent with the dimer abundance data, which demonstrates that at this concentration ~ 50 % of Hsp27-WT also exists as a dimer. Therefore, the abundance of dimer appears central to the protection of target proteins under heat stress conditions.

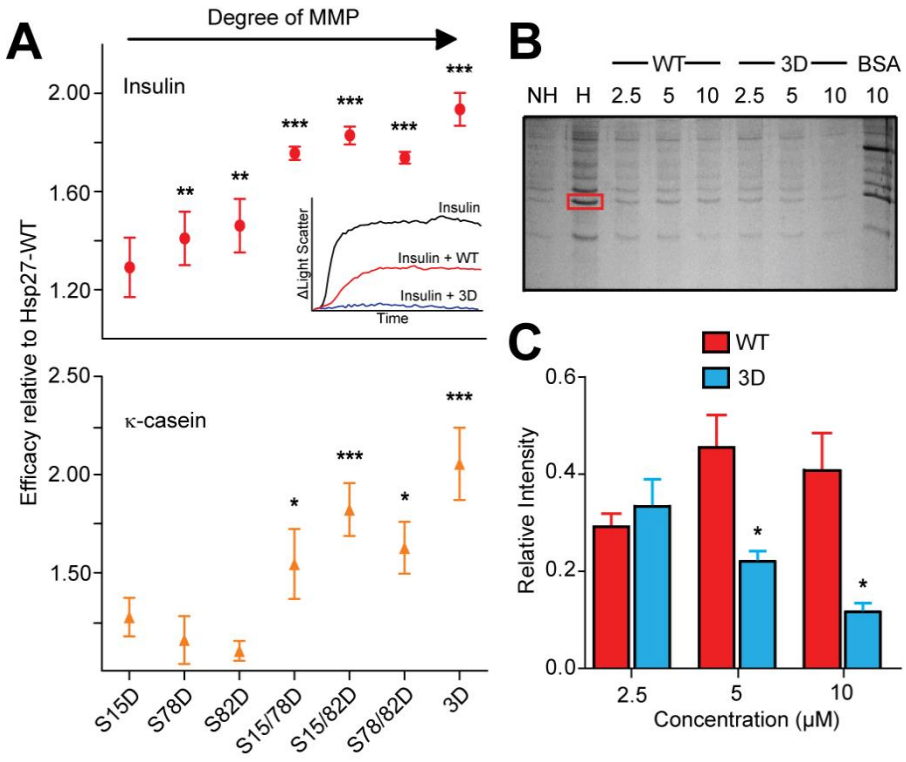

Figure 3.5: MMP of Hsp27 enhances its chaperone activity
A: Chaperone efficacy was determined relative to Hsp27-WT for each target protein. Inhibition of amorphous insulin aggregation was monitored by the change in light scatter at 340 nm, whilst fibrillar κ-casein aggregation was monitored by the change in ThT fluorescence emission at 490 nm. Variants that showed a significant increase in activity compared to Hsp27-WT are indicated (*= $p < 0.05$; **= $p < 0.01$; ***= $p < 0.001$) (n = 3 – 5; mean ± SEM). ***B:*** Precipitates from non-heated (NH) and heated (H) Neuro-2a cell lysates in the presence and absence of Hsp27-WT, Hsp27-3D or BSA at various concentrations (above in μM) were observed by SDS-PAGE. Chaperones and/or controls were added to the cell lysates and heated to 45°C for 1 h; a specific band (red box) was chosen for quantitative analyses. ***C:*** The selected band was analysed to determine the protection afforded by Hsp27-WT and Hsp27-3D on heated Neuro-2a cell lysates. Significant increases in protection compared to Hsp27-WT are indicated (*= $p < 0.05$) (n = 3; mean ± SEM).

3.4 Discussion

The primary aim of this work was to produce the first systematic explication of the site-specific effects of Hsp27 phosphorylation. To achieve this, we constructed phosphomimics using aspartic acid substitutions at the three known phosphorylation sites (S15, S78 and S82), to obtain seven distinct variants which likely occur *in vivo*. Our examination of the proteins' quaternary organisation and chaperone function revealed that two serine substitutions substantially reduced the average size of Hsp27 oligomers, while Hsp27-3D

was observed to be predominantly dimeric. In this state, the chaperone activity was demonstrably enhanced, conforming to a model in which the dimer is a more efficient chaperone than the polydisperse assemblies. This finding hints at a mechanism for Hsp27 activity in which the dimer-dimer contacts maintained in multimeric Hsp27 are disrupted by phosphorylation, and when exposed, contribute to the stress response with exceptional efficiency (Gaestel *et al.*, 1991, Landry *et al.*, 1992a).

We therefore employed MS to definitively resolve the structural variations induced by MMPs. Using a MMP approach does present some limitations in that this modification only introduces a single negative charge whereas a phosphoserine adds two. Phosphorylation of Hsp27 *in vitro* results in a complex mixture of unphosphorylated as well as singly and doubly phosphorylated isoforms (Hayes *et al.*, 2009). Therefore using MMPs allows a systematic approach to study the effect of phosphorylation at each serine residue. The MS data is in agreement with previous analytical-SEC work, showing that Hsp27-S15D and Hsp27-S78/82D form large, polydisperse species (Rogalla *et al.*, 1999), compared to Hsp27-WT. We observed a shift towards smaller oligomeric species across all single and double $Hsp27_M$ isoforms, which has also been observed in rodent Hsp27 (Lambert *et al.*, 1999). The majority of the published literature which has investigated the effects of phosphorylation on Hsp27 structure and function has focused on the Hsp27-3D isoform. Debate has risen with regards to its oligomeric state, claims ranging from dimers, as determined by analytical ultracentrifugation, to tetramers, observed using SEC (Hayes *et al.*, 2009, Rogalla *et al.*, 1999, Shashidharamurthy *et al.*, 2005). Our combination of SEC and MS data definitively shows that Hsp27-3D predominantly exists as disulfide-linked dimers under non-reducing conditions, which dissociate into monomers upon reduction. Overall, the shift in distribution and presence of smaller oligomers in each of the single and double $Hsp27_M$ isoforms, and

the dimeric preference of Hsp27-3D, indicates that phosphorylation at any of the three serine residues significantly alters the dimer ⇌ oligomer equilibrium compared to WT.

Hsp27 undergoes concentration-dependent dissociation in the μM range (Figure 3.4). Similar behaviour was observed with Hsp26 from yeast where the oligomeric equilibrium is concentration and temperature-dependent, shifting towards monomers and dimers, leading to enhanced chaperone activity (Benesch *et al.*, 2010). As a result, we reason that the strength of the dimer-dimer interface of Hsp27 oligomers are significantly weaker compared to the oligomer-forming interfaces of other sHsps, such as αA-c and αB-c (Baldwin *et al.*, 2011c, Hilton *et al.*, 2013). We observed Hsp27-WT as a broad distribution of oligomers in both transfected HEK293 and Neuro-2a cell lysates. This phenomenon may also have other implications in the cell, where Hsp27 may be compartmentalised intracellularly at concentrations that manipulate its oligomeric state, independent of phosphorylation. Kinase activation and subsequent phosphorylation of Hsp27 would enable higher concentrations of Hsp27 to exist at cellular locales in a dissociated state in response to cellular stress.

As our MS approach enables us to identify and quantify individual oligomers within the heterogeneous ensemble, we have used it to observe the dissociation propensity of these large oligomers (≥ 6-mers) into dimers. This process could equally be applied to identify and quantify the abundance of any sized Hsp27 oligomer (and indeed other oligomeric assemblages) with concentration. Similar dissociation propensities were observed for Hsp27-WT via MS to those obtained by analytical-SEC, however, MS accurately resolves the concentration-dependent ratio of dimers to oligomers as SEC is unable to distinguish between small oligomers (dimers to 6-mers) in solution (small oligomers, Figure 3.1C). This confirms that MS is a suitable tool for observing the dissociation of these large polydisperse

proteins. Overall, the increased dissociation propensity of Hsp27 with MMP is consistent with the hypothesis that multiple phosphorylation events act cumulatively to reduce the barrier to dissociation.

MS and SEC data indicates that the double and triple $Hsp27_M$ variants exhibit a significant shift towards the presence of dimers. We believe that the location of these modified serines is clustered in close proximity within the N-terminal domain, to a point where phosphorylation at any of the three serine residues results in similar changes to the secondary and quaternary structure. The far-UV CD spectroscopy data supports this as there was no major change in secondary structure observed amongst all the single or double $Hsp27_M$ isoforms. The observed increase in random coil, with increasing MMPs, indicates that these modifications are attributed to either differences in secondary structure of Hsp27 dimers or that the secondary structure of free dimers is able to be resolved more readily than large oligomers. The structural alterations that are caused by phosphorylation-induced destabilisation of Hsp27 have been difficult to elucidate due to the dynamic nature of this sHsp. Since three serine phosphorylation sites are located in the unstructured N-terminal region of Hsp27, we hypothesise that these residues may be clustered in the tertiary structure of the protein and are more solvent exposed, inhibiting oligomerisation through negatively charged inter-dimer repulsions. This is in stark contrast to αB-c, another sHsp that is phosphorylated in the N-terminal domain, in which increasing the number of MMP does not result in such a dramatic change in oligomer size, but does lead to enhanced chaperone activity (via increased subunit-exchange, thus increasing the abundance of dimers) (Ecroyd *et al.*, 2007, Peschek *et al.*, 2013). Both mechanisms however are consistent with a model in which phosphorylation enhances chaperone function by increasing the amount of dissociated species able to interact with target proteins. Conversely, class II

cytosolic sHsps, found in plants, have been shown to be active when highly assembled (Basha *et al.*, 2010). It should be noted that these plant sHsps do not have phosphorylation sites compared to mammalian sHsps, which may indicate that a combination of charged and hydrophobic interactions may potentially be involved in recognition and binding of destabilised client proteins.

Our functional studies demonstrate that the ability of Hsp27 to prevent both amorphous and fibrillar protein aggregation increases with the number of MMP. Also, in conjunction with data on oligomer dissociation, we observed a strong correlation between enhanced chaperone activity and increased dimer abundance. Since the chaperone function of all the single $Hsp27_M$ isoforms was equivalent in these assays (as was the case for the double $Hsp27_M$ isoforms) we suggest that no single serine residue has a dominant role in regulating the chaperone efficacy of Hsp27. Rather, the number of phosphoserine residues is the critical factor and this regulates the chaperone activity by promoting oligomeric dissociation into dimers. Such a model is supported by our data showing that Hsp27-WT was equally effective as Hsp27-3D at preventing the heat-induced precipitation of cell lysate proteins at concentrations (i.e. 2.5 µM) at which approximately half of the Hsp27-WT exists as free dimers. At higher concentrations the proportion of Hsp27-WT dimer was decreased and it was less effective than Hsp27-3D in this assay. Overall, we propose that phosphorylation at two or three serine residues would liberate the disordered N-terminal domain of Hsp27 dimers, making them more accessible for interaction with destabilised target proteins, thereby enhancing chaperone activity.

Interrogation of the suite of Hsp27 isoforms with MMP proved a valuable approach in studying the impact phosphorylation has on the structure and function of Hsp27. Our results

are consistent with a model in which phosphorylation destabilises Hsp27 oligomers leading to an increase in the abundance of efficacious dimers, which correlates with enhanced activity. It appears that the large oligomers act as reservoirs of these chaperone-active dimers. Phosphorylation can therefore be regarded as a molecular switch, activating Hsp27 during periods of cellular stress and helping to maintain intracellular proteostasis.

Chapter 4: Results - Post-translational modifications alter the structure and dynamics of Hsp27 dimers and oligomers

Chapter 4: Post-translational modifications alter the structure and dynamics of Hsp27 dimers and oligomers

4.1 Introduction

It is generally accepted that the quaternary structure and dynamics of sHsps underlie their molecular chaperone function. This has previously been shown extensively for αB-c, but is less clear for Hsp27. This thesis has previously established the structure-function relationship of phosphorylated Hsp27 using MMP (section 3.1), whereby the dissociation of oligomers and chaperone activity was enhanced with an increasing number of MMP. As a result, it is proposed that the dimer is the chaperone-active unit of Hsp27. However, it is unclear whether the dissociation of oligomers into dimers (i.e. changes in quaternary structure) or phosphorylation-induced changes in the conformation and/or dynamics of the dimer itself (i.e. changes in tertiary structure), or both, are responsible for the enhanced chaperone activity of phosphorylated Hsp27. Moreover, there has been little work conducted to date exploring the structural dynamics of Hsp27 at the tertiary and quaternary level.

The aim of the work presented in this Chapter was to explore the impact that post-translational modifications (PTMs), primarily phosphorylation and disulfide-bonding, have on the tertiary and quaternary structure and dynamics of Hsp27. To do so, isoforms of Hsp27 with MMP (as described in Chapter 3) were exploited. Isoforms of Hsp27 with an increasing number of MMP were examined using ion mobility – mass spectrometry (IM-MS) to ascertain the conformational state(s) of two oligomeric forms (dimers and 12-mers). In addition, the unfolding dynamics of Hsp27 dimers was examined via collision-induced unfolding (CIU) in order to observe any differences with MMP.

It has previously been reported that disease-associated mutations in Hsp27 result in increased amounts of Hsp27 monomer as a result of an increased susceptibility of the disulfide-bond (formed at Cys137), which covalently links monomers into dimers along the dimer interface, to be reduced. (Almeida-Souza *et al.*, 2010, Evgrafov *et al.*, 2004). It was proposed that this increased monomerisation makes Hsp27 'hyperactive' resulting in aberrant interactions with cellular proteins, leading to disease (Almeida-Souza *et al.*, 2010). However, the effect(s) reduction of the disulfide-bond involving Cys137 has on Hsp27 quaternary structure has not been thoroughly investigated. Thus, this study also compared the quaternary structure of oxidised Hsp27 with Hsp27 following reduction and thiol-blocking of Cys137.

4.2 Methods

Human Hsp27-WT and $Hsp27_M$ were expressed and purified as described previously (section 2.2). Intrinsic tryptophan fluorescence (section 2.5.2), analytical-SEC (section 2.5.1) and limited proteolysis (section 2.6.5) provided solution-phase information on the tertiary and quaternary structure of the Hsp27 isoforms. The unfolding dynamics of Hsp27 dimers was investigated by using a combination of native MS (section 2.6.2) and IM-MS (section 2.6.3). The rate of subunit-exchange between Hsp27-WT and Hsp27-3D was determined by bulk-FRET analysis (section 2.5.5). The effects of disulfide-bonding on Hsp27 quaternary structure was assessed by reducing and thiol-blocking (with iodoacetamide, section 2.6.6) Cys137. The reduction and blocking efficiency was determined by denatured MS (section 2.6.1). The quaternary structure of the non-reduced and reduced and thiol-blocked Hsp27 forms were subsequently analysed by native MS (section 2.6.2).

4.3 Results

4.3.1 Bulk measurement techniques show minor changes in Hsp27 tertiary and quaternary structure with serine substitutions that mimic phosphorylation

The work described in Chapter 3 outlined the structural changes that occur to Hsp27 upon introduction of site-specific serine substitutions that mimic phosphorylation. This work showed that successive MMP result in an increased propensity for Hsp27 oligomers to dissociate into dimers. This increased abundance of dimers with MMP strongly correlates with enhanced chaperone activity. To determine whether other changes occur to the tertiary and quaternary structure of Hsp27 upon introduction of MMP further biophysical studies were conducted on these isoforms. Intrinsic tryptophan fluorescence studies revealed that Hsp27 isoforms with one and two MMP had an enhanced tryptophan fluorescence compared to Hsp27-WT, however, this was not accompanied by a shift in the emission maximum (Figure 4.1A-B). There was a further increase in tryptophan fluorescence for Hsp27-3D over that observed for the single and double $Hsp27_M$ isoforms, indicating that tryptophan residues become more exposed with three MMP (Figure 4.1A-B). Overall, the subtle changes in tryptophan fluorescence observed for MMP can be attributed to increased rates of subunit-exchange, rather than changes in tertiary structure, with increasing number of MMP.

Analytical-SEC of $Hsp27_M$ in ammonium acetate (NH_4OAc) (i.e. the buffer used for all the MS experiments) in general parallels that observed when phosphate buffer is used (see Chapter 3, Figure 3.1B); an increase in the number of MMP reduces the size of Hsp27 oligomers (Figure 4.1C-D). Single $Hsp27_M$ isoforms eluted at an elution volume identical to that of Hsp27-WT (~670 kDa) (Figure 4.1C). A peak corresponding to oligomers with an average mass of 158 kDa species was also present for the S15/78D and S15/82D isoform smaller

oligomers (Figure 4.1D). Hsp27-S78/82D eluted as a single peak that was smaller than Hsp27-WT, but with no distinct 158 kDa species (Figure 4.1D). Interestingly, Hsp27-3D co-eluted as two very broad peaks from 40 – 158 kDa (Figure 4.1C-D), in contrast to what was observed previously (see Chapter 3, Figure 3.1B) in which Hsp27-3D was found to elute as a single peak corresponding to a dimer. A potential reason for this discrepancy may be the differences in both pH and buffer systems (phosphate and ammonium acetate buffers; pH 7.4 compared to pH 6.8 respectively). Previous studies have shown that differences in pH (± 1 pH) alter quaternary structure and subunit-exchange dynamics in αB-c (Baldwin *et al.*, 2011c).

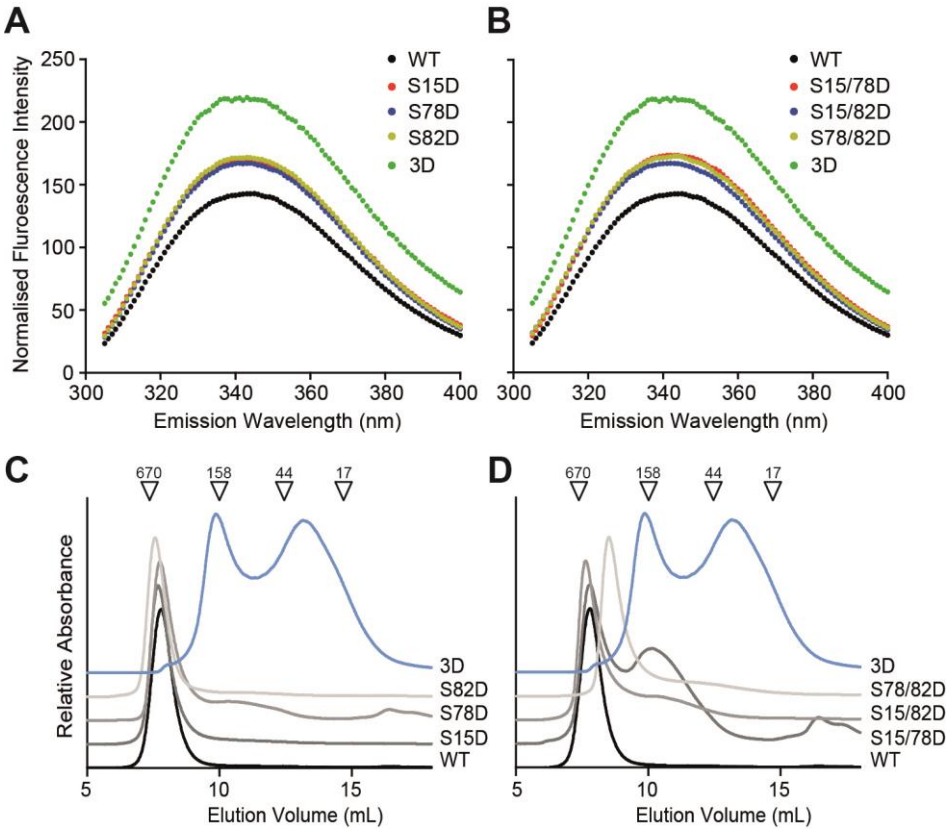

Figure 4.1: Analytical size-exclusion chromatography and intrinsic tryptophan fluorescence of $Hsp27_M$

A-B*:** Intrinsic tryptophan fluorescence of single $Hsp27_M$ (A***) and double $Hsp27_M$ isoforms (***B***) (50 µM) in 50 mM phosphate buffer (pH 7.4) showing an increase in tryptophan exposure with successive serine substitutions ***C-D:*** Analytical-SEC of single $Hsp27_M$ (***C***) and double $Hsp27_M$ (***D***) (50 µM) in 200 mM NH_4OAc (pH 6.8) where successive serine substitutions enhance oligomer dissociation. Both Hsp27-WT and Hsp27-3D are also included for relative comparison.

4.3.2 Increased serine substitutions alter the conformation and unfolding dynamics of Hsp27 dimers

Characterising the secondary, tertiary and quaternary structure of partially disordered proteins by classical techniques (e.g. intrinsic tryptophan fluorescence, bis-ANS fluorescence and far-UV CD spectroscopy) only provides relatively low resolution, bulk-averaged measurements. As a result, alternate approaches are required to probe the structure of these assemblies with greater resolution. IM-MS is an extremely useful tool to analyse the size, shape and conformation of proteins (Ruotolo *et al.*, 2008). By isolating a particular species of interest, in this case the dimer^{13+} (~3,510 *m/z*) or the 12-mer^{31+} (~8,800 *m/z*), both unique mass/charge state species (i.e. this charge-state ion does not overlap with other species), differences in the oligomeric forms can be probed (in terms of shape and conformation) with increasing numbers of MMP (Figure 4.2A). To preserve the native-like state of these oligomeric forms, low activation energy (i.e. low sample and extraction cone voltages) in the mass spectrometer was utilised prior to IM separation and detection (Figure 4.2). When this is achieved, an arrival time distribution (ATD) of a particular species (dimer^{13+} and 12-mer^{31+}) is generated, which can be used to calculate a collisional cross-sectional (CCS) area (Figure 4.2B). Changes in ATD (if any) can then be observed with increasing activation (collision) energy, which results in an increase in the drift time of the dimer. An increase in CCS area is indicative of unfolding and is referred to as collision-induced unfolding (CIU). The unfolding process can be visualised to determine distinct conformations that a dimer may adopt during unfolding (i.e. folded, compaction, unfolded intermediate and unfolded), as well as the relative stability of a species as a function of activation energy (Figure 4.2B). By performing these IM-MS analyses at a set wave velocity (the velocity at which a species is pushed along the IM chamber of the mass spectrometer)

and at a range of wave heights (WH in V), differences in the mobility of that species as it travels through the IM chamber can be interrogated.

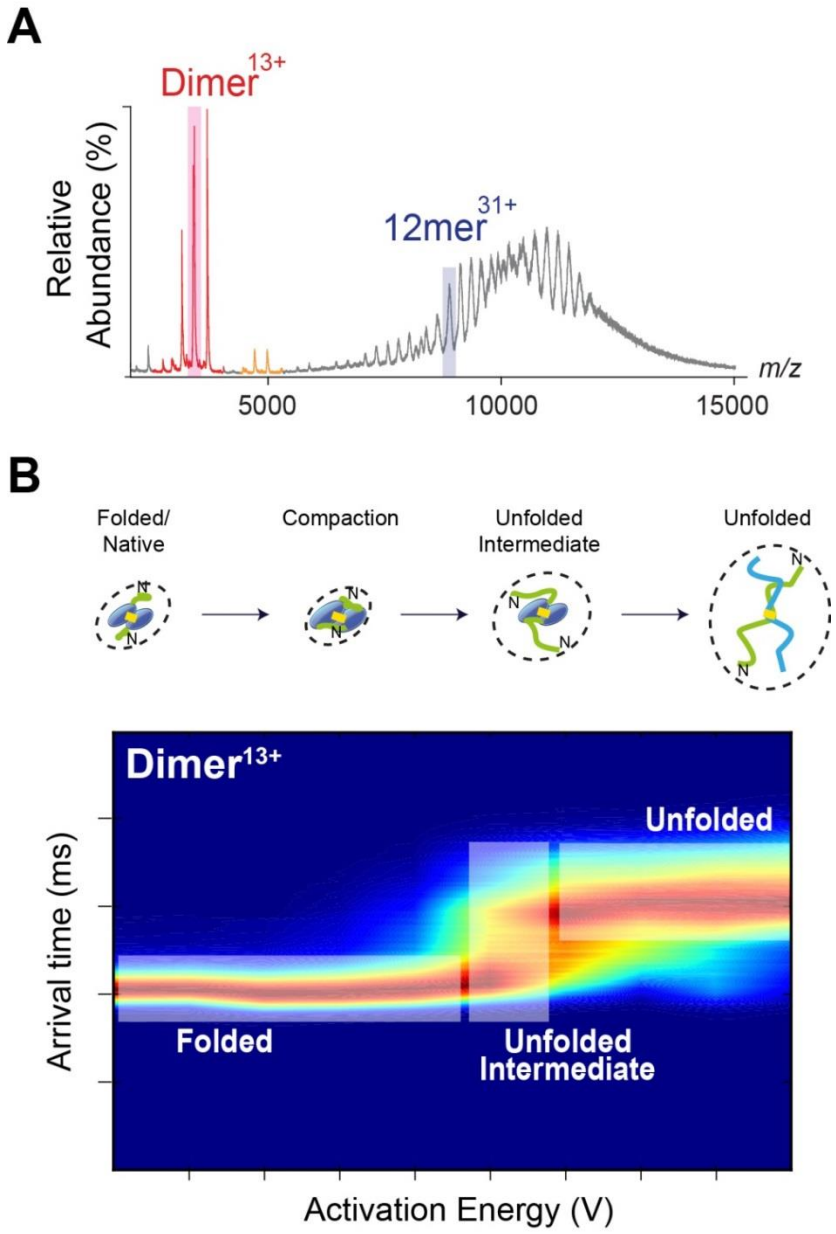

Figure 4.2: Arrival time distribution analysis and collision-induced unfolding trajectories of Hsp27 using ion mobility – mass spectrometry
***A*:** Native MS of Hsp27-S15D, as a representative, demonstrating the approach used to observe the conformation and unfolding dynamics of Hsp27 dimers. The 13+ charge state of dimers (3,510 *m/z*; *red box*) and the 31+ charge state of the 12-mer (8,800 *m/z*, *blue box*) were selected for analysis. ***B*:** Heat map analysis shows the various conformations that Hsp27 dimers take up in the gas-phase under low activation energy. The increase in activation (collision) energy results in the initial compaction of dimers, which then unfold with further increases in activation energy. The unfolding intermediates can be observed prior to complete unfolding of the dimer (generic collision-induced unfolding, CIU, pathway illustrated above the heat map).

Figure 4.3A shows the arrival time distribution (ATD, i.e. drift time) of the Hsp27 dimer^{13+} with successive MMPs at a set wave height (WH, in V) under low activation energy and gentle source conditions (i.e. native-like/folded state; Figure 4.2B). The increase in drift time (observed at WH8) and/or a broadening of the ATD peak at all WHs with an increasing number of MMP indicates that the Hsp27 dimer has a greater CCS area with successive MMP (Figure 4.3A) (Appendix II; Table 8.1). Hsp27-WT was not able to be included in this analysis as the proportion of free dimer in solution at the concentrations required for this experiment (50 µM) was too low to be detected under the instrument settings used in these experiments. In any case, the data with the Hsp27$_M$ isoforms demonstrates that with successive MMP the tertiary structure of Hsp27 dimers changes such that they have a larger CCS area (Figure 4.3A) (Appendix II; Table 8.1). The data is consistent with a slight increase in both flexibility and unstructured state of Hsp27 dimers with MMP. In contrast, there was no distinct shift in either the drift time nor ATD peak broadness (and hence the CCS area) observed for the 12-mer^{31+} between the Hsp27$_M$ and Hsp27-WT isoforms indicating that there is no observable difference in the structure of this oligomer with MMP compared to Hsp27-WT (Figure 4.3B).

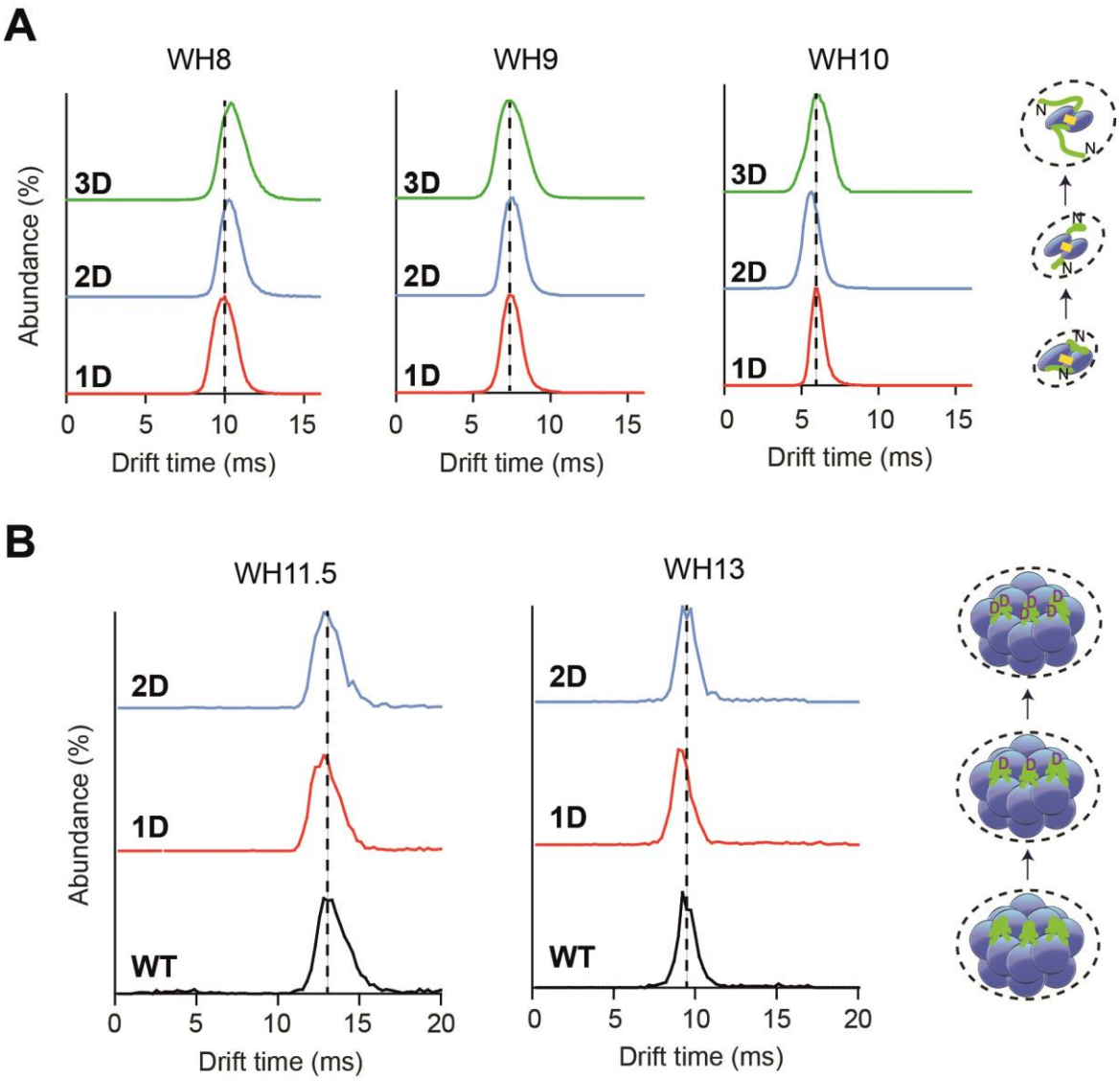

Figure 4.3: ATD analysis of $Hsp27_M$ dimers and 12-mers by IM-MS
***A*:** ATD analysis of $Hsp27_M$ dimers^{13+} at low activation energy (15 V) showing that the dimer becomes more unstructured (increasing drift time and/or peak width) with an increasing number of MMP. ***B*:** ATD analysis of Hsp27-WT and $Hsp27_M$ 12-mers^{31+} at low activation energy (15 V) which shows that the drift time and peak width (and hence conformation) of the 12mer does not vary significantly with increasing numbers of MMP. In A and B, each Hsp27 isoform was analysed at a range of wave heights (WH in V).

To further assess the differences in the quaternary structure and increased flexibility of Hsp27 dimers upon phosphorylation, IM-MS was used to visualise the unfolding dynamics of these dimers at different WHs using CIU in the gas-phase. By applying increasing voltage in the collision cell of the mass spectrometer, whilst maintaining low activation energy in the

source, the unfolding of Hsp27 dimers with increased collision energy was observed (Figure 4.4). In addition, dissociation (symmetric/asymmetric) of the dimer was not observed by IM-MS as no other species were observed during these experiments. Across all isoforms, it appears that the (disulfide-linked) dimer unfolds in a similar manner and without any preference of one monomer unfolding prior to the other evidenced by only a single conformation/species being observed after 40 V (i.e. non-asymmetrical unfolding where two species/unfolding events would be observed with increasing activation energy, indicative of one monomer unfolding prior to the other) (Figure 4.3-4.4). Also, compaction of the dimer in Hsp27-2D and Hsp27-3D was observed at 30 V at WH8 and WH10, prior to unfolding (Figure 4.4B-C and H-I). However, the amount of activation energy required to unfold the dimer increases with successive MMP, such that Hsp27-3D is the most resistant to unfolding of all the Hsp27 isoforms (45 V at WH8 and WH9, compared to 40 V for Hsp27-1D and 2D at these wave heights) (Figure 4.4C and F; Figure 4.6). In order to determine the differences in the unfolding dynamics of Hsp27 dimers, unfolding maps of the pair-wise comparison of $Hsp27_M$ isoforms (i.e. Hsp27-1D versus 2D and Hsp27-1D versus 3D etc.) were generated. These enabled quantitative differences in the ATD of the unfolding dimer with increasing activation energy to be measured (Figure 4.5). Interestingly, the folded and unfolded states of Hsp27-3D differ when compared to Hsp27-1D and -2D across multiple wave heights; more activation energy is required for the unfolding of the Hsp27-3D dimer compared to the Hsp27-1D or -2D dimers (Figure 4.6). The unfolding trajectories of Hsp27-1D and Hsp27-2D compared to Hsp27-3D at the 9 V wave height resulted in a RMSD value of 11.62 % and 13.52 %, respectively (internal RMSD 5.44 %; Appendix II; Figure 8.4) (Figure 4.5E-F). This indicates that the unfolding dynamics of Hsp27-3D differ substantially to that of Hsp27-1D and Hsp27-2D. Overall, these data suggest that successive MMP induce changes

in the quaternary structure of Hsp27 dimers, including an increase in stability and flexibility. These changes may facilitate the enhanced chaperone activity of phosphorylated Hsp27 compared to Hsp27-WT.

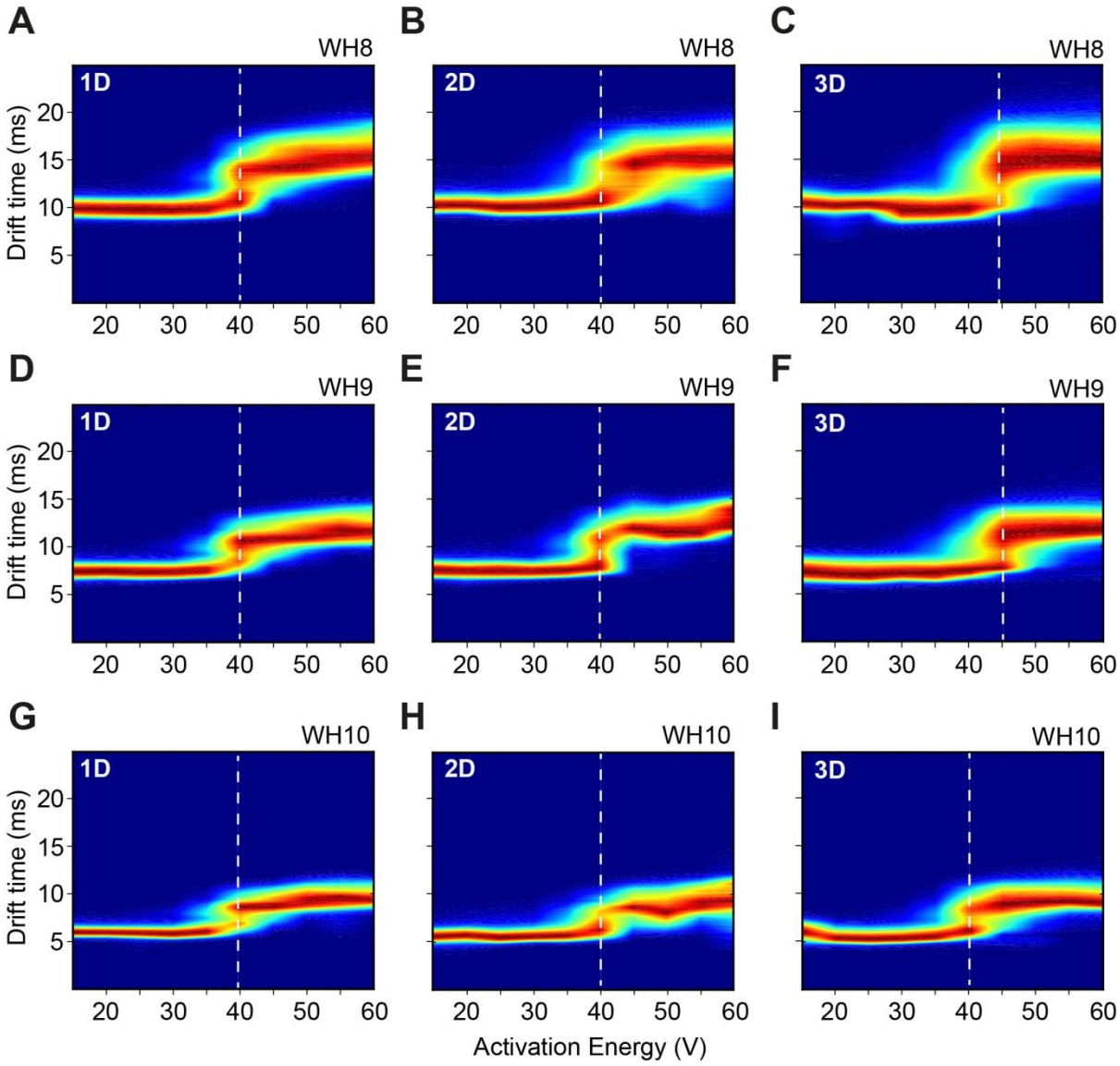

Figure 4.4: Observing the collision-induced unfolding of $Hsp27_M$ dimers by IM-MS
The CIU of the $Hsp27_M$ $dimer^{13+}$ (monitored via changes in the drift time of species in the IM chamber) was examined with increasing activation energy (V). The heat maps indicate that no distinct intermediates between folded and unfolded states are present as the dimer unfolds in the gas-phase as a function of activation energy at the same wave height (WH in V) (WH8: ***A-C***; WH9: ***D-F***; WH10: ***G-I***). Across all wave heights, only a single unfolding transition is observed (*white dashed line*), indicating that both monomers (which are disulfide-linked via Cys137) unfold simultaneously in the gas-phase. CIU heat maps were generated using CIUsuite with default settings (Eschweiler *et al.*, 2015).

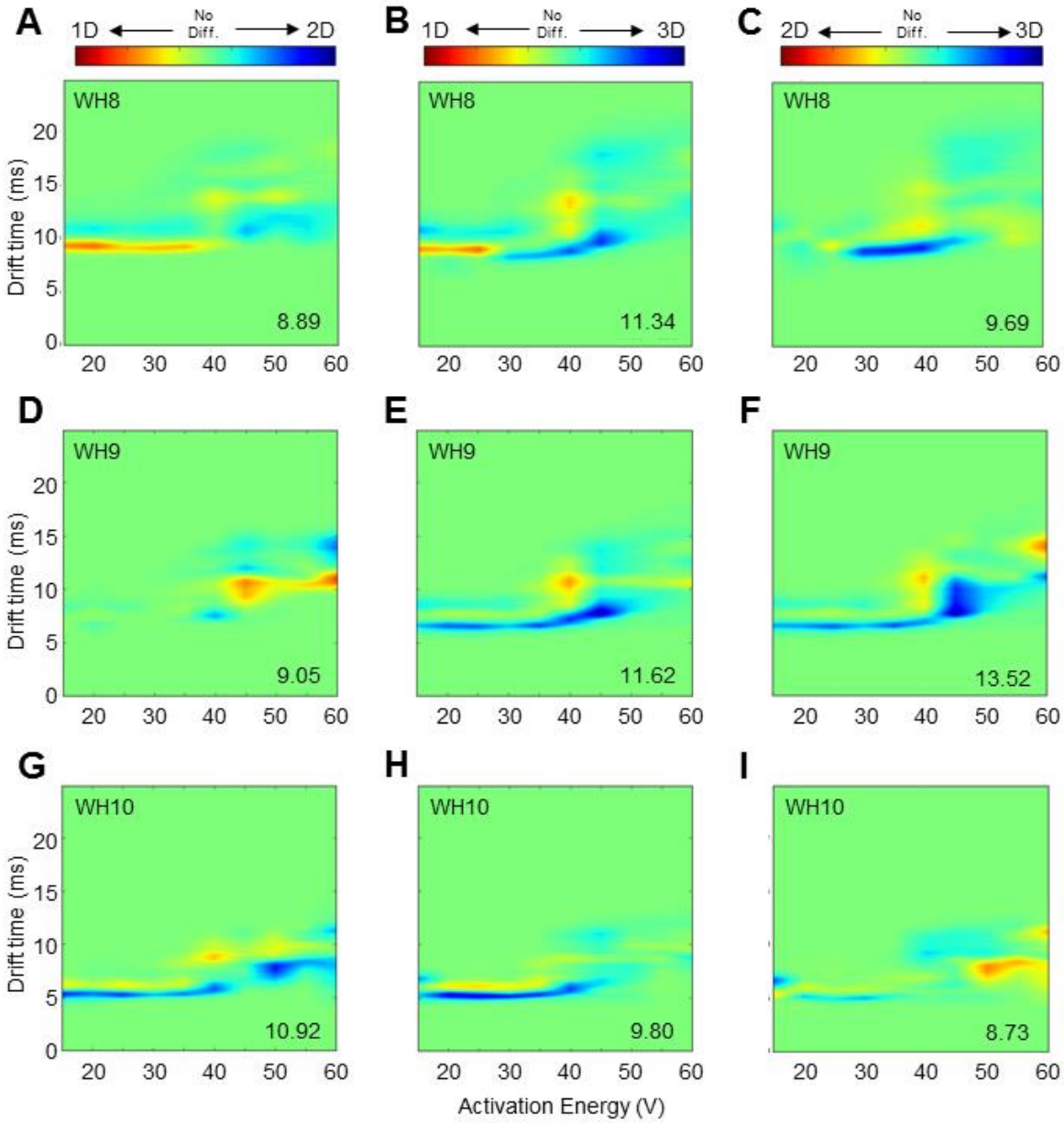

Figure 4.5: Observing the differences in collision-induced unfolding dynamics of $Hsp27_M$ dimers by IM-MS

CIU of $Hsp27_M$ dimers was monitored with increasing activation energy. Heat maps highlight the differences in the unfolding of the $dimer^{13+}$ in the gas-phase between two isoforms at the same wave height (WH in V) (WH8: ***A-C***; WH9: ***D-F***; WH10: ***G-I***). RMSD values (%) (*bottom right corner*) indicate the difference in the unfolding of the dimer between each pair analysed (pairs analysed stated above in heat map scale where greatest difference attributed to one isoform indicated by either dark blue or red). The greatest difference in the unfolding dynamics was observed when Hsp27-1D or Hsp27-2D were compared with Hsp27-3D. Difference plots and RMSD values were calculated using CIUsuite with default settings (Eschweiler *et al.*, 2015).

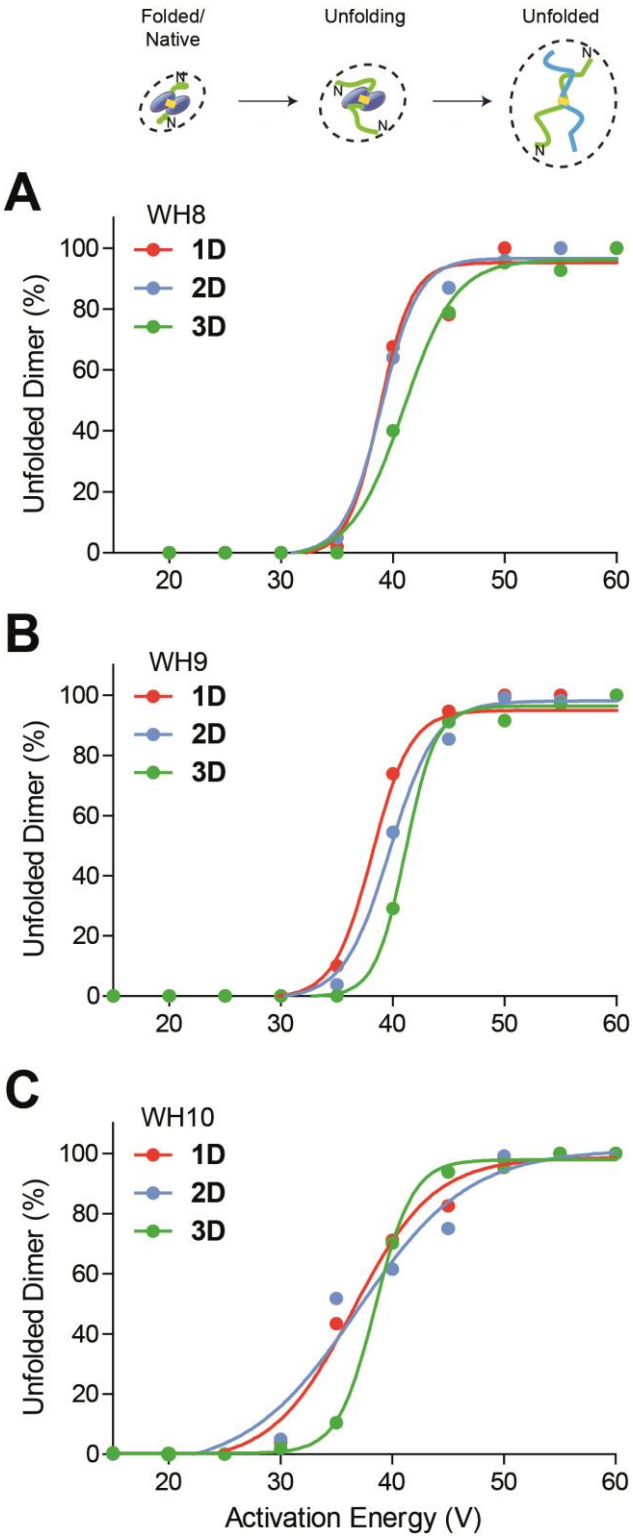

Figure 4.6: Unfolding of $Hsp27_M$ dimers by collision-induced unfolding and as monitored by IM-MS
Unfolding of $Hsp27_M$ dimers was performed using CIU by increasing the activation energy in the trap region of the mass spectrometer. The abundance of unfolded dimer (y-axis) was determined by tracking the loss of folded dimer with increased activation energy. The dimer appears to be more stable (i.e. requires increased activation energy to reach 50% unfolded) with increasing MMP. Each Hsp27 isoform was analysed at a range of wave heights (WH in V) (WH8: ***A***; WH9: ***B***; WH10: ***C***) (n = 1).

4.3.3 **Hsp27-3D and Hsp27-WT undergo subunit-exchange and structural elements are more exposed in Hsp27-3D than WT**

To further explore the dynamics between Hsp27-WT and Hsp27-3D, a bulk-FRET based assay was used to determine whether Hsp27-3D was capable of subunit-exchange with Hsp27-WT. It was observed that Hsp27-3D was capable of subunit-exchange with Hsp27-WT and the rate of exchange (0.2740 ± 0.02 min^{-1}) was faster than WT homo-oligomeric subunit-exchange (0.2289 ± 0.01 min^{-1}) (Figure 4.7A). To confirm that labelled Hsp27-WT and Hsp27-3D were indeed undergoing subunit-exchange, samples from the bulk-FRET experiments were collected and analysed by analytical-SEC with multi-wavelength detection. Analytical-SEC showed that the mixed sample of Hsp27-WT and -3D resulted in a peak eluting from the column at an elution volume (~8 mL), typical of Hsp27-WT oligomers, and that this peak contained both Hsp27 isoforms (Figure 4.7B-C).

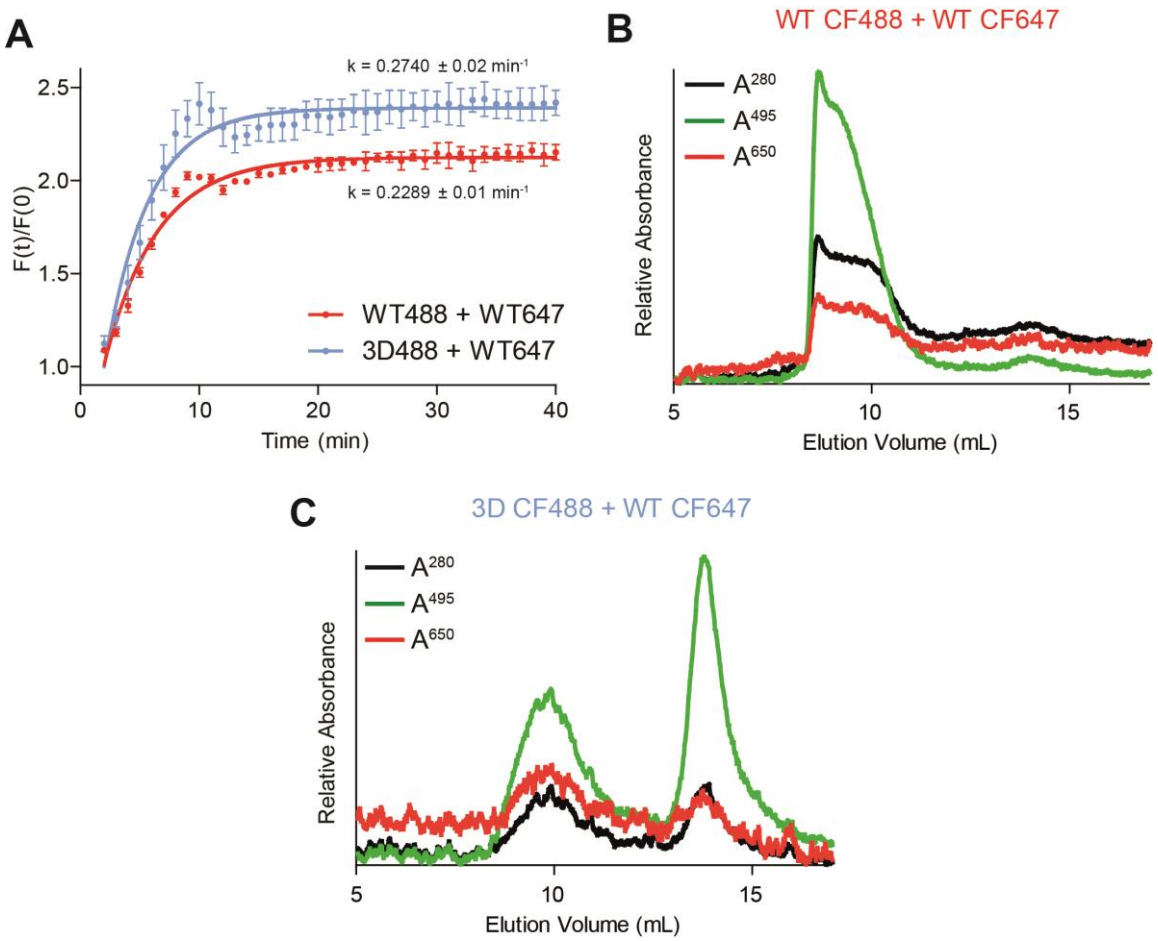

Figure 4.7: Hsp27-WT and Hsp27-3D are capable of undergoing subunit-exchange
***A*:** Bulk-FRET assays indicating that subunit-exchange of Hsp27-WT with Hsp27-3D occurs at a rate faster than WT exchange (n = 3; mean ± SEM). Subunit-exchange was performed at 37 °C at a 1:1 molar ratio (25 µM total protein concentration) in 50 mM phosphate buffer (pH 7.4). The emission fluorescence from Alexa labels was used as a measure of subunit-exchange. ***B*:** Analytical-SEC of Hsp27-WT (CF488) with Hsp27-WT (CF647) after bulk-FRET subunit-exchange ***C*:** Analytical-SEC of Hsp27-3D (CF488) with Hsp27-WT (CF647) after bulk-FRET subunit-exchange. Both B and C were at a 1:1 molar ratio (25 µM total protein concentration) in 50 mM phosphate buffer (pH 7.4). Absorbance was measured at multiple wavelengths (280, 495 and 650 nm).

To further investigate whether there were structural differences between Hsp27 species present in different oligomeric forms, limited proteolysis with trypsin was performed on Hsp27-WT and Hsp27-3D (which consist mainly of large oligomers and dimers, respectively, under the conditions and concentrations (50 µM) used in these experiments). Proteolysis of both Hsp27 isoforms was observed upon addition of trypsin (1000:1 molar ratio; Hsp27:trypsin) by SDS-PAGE (Figure 4.8). However, Hsp27-3D was more susceptible to

proteolysis than Hsp27-WT, evidenced by the more rapid degradation of Hsp27-3D over time, as the ~25 kDa species is still present after 20 min in Hsp27-WT compared to Hsp27-3D. After 30 min of incubation in the presence of trypsin, a distinct band of ~10 kDa was observed by SDS-PAGE in both Hsp27-3D and Hsp27-WT treatments, which persisted for the next 30 min of the assay (Figure 4.8).

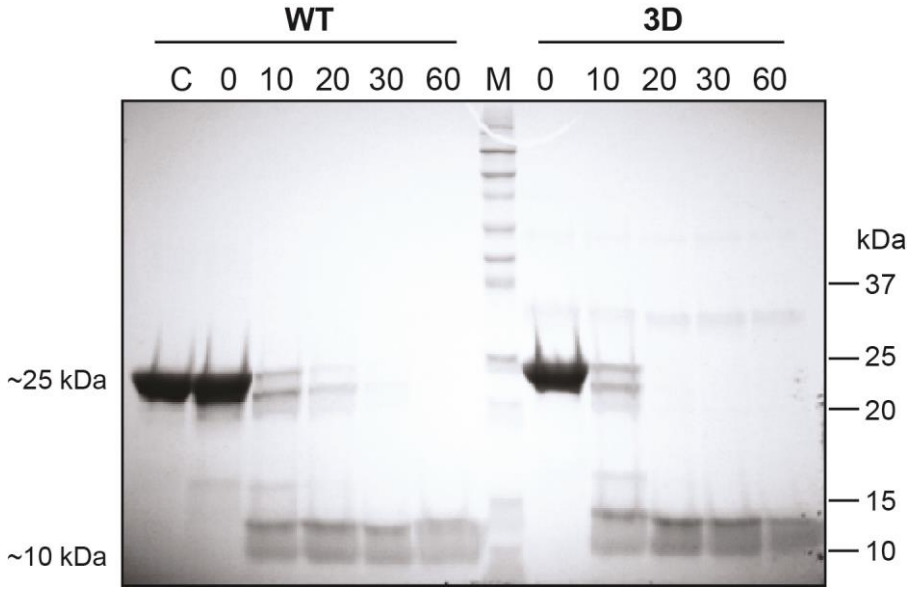

Figure 4.8: Limited proteolysis of Hsp27-WT and Hsp27-3D analysed by SDS-PAGE
SDS-PAGE of trypsin proteolysis (1000:1 molar ratio, Hsp27:trypsin) of Hsp27-WT (WT) and Hsp27-3D (3D) at 37°C (in 50 mM phosphate buffer, pH 7.4) indicates Hsp27-3D (predominantly dimeric) is more prone to proteolysis than Hsp27-WT (predominately large oligomers) under these conditions. A control of Hsp27-WT not exposed to trypsin (C) is also shown on the gel.

In order to identify the proteolytic products present at each time point, MS was utilised for identification of the peptides (Figure 4.9). The rationale for this experiment was that the initial stages of proteolysis (10 min digestion time) would indicate which residues of an oligomer (Hsp27-WT) compared to a dimer (Hsp27-3D) is less exposed. Even during the dead-time of the experiment (i.e. 0 min, which corresponds to the time taken to add the trypsin, mix the sample and then stop the proteolysis reaction by adding PMSF), numerous peptides were observed by MS. Following 10 min of trypsin exposure, both the unstructured

N-terminal (residues 13, 21, 27 and 38) and the flexible C-terminal (residues 172, 189 and 198) domains of Hsp27-WT were readily accessible to cleavage by trypsin (Figure 4.9B). In addition, parts of the αCD were accessible to cleavage by trypsin at residues 112 and 127 in Hsp27-WT (Figure 4.9). The N-terminal domain of Hsp27-3D is more accessible to trypsin cleavage compared to WT, evidenced by shorter peptides (corresponding to cleavage at residues 5, 6, 13, 21, 28, 38, 75 and 80) being detected at 0 min (Figure 4.9). Both the C-terminal domain and αCD of Hsp27-3D are also more accessible to trypsin cleavage compared to Hsp27-WT, as smaller fragments from this region were identified in Hsp27-3D than WT (Figure 4.9). The digestion patterns observed between Hsp27-WT and 3D indicate that WT oligomers are more resistant to proteolysis than Hsp27-3D dimers. The data overall is consistent with a model in which phosphorylation results in an increase in the flexibility of Hsp27 dimers, however, some protection from cleavage may be afforded by the binding interfaces involved in oligomerisation.

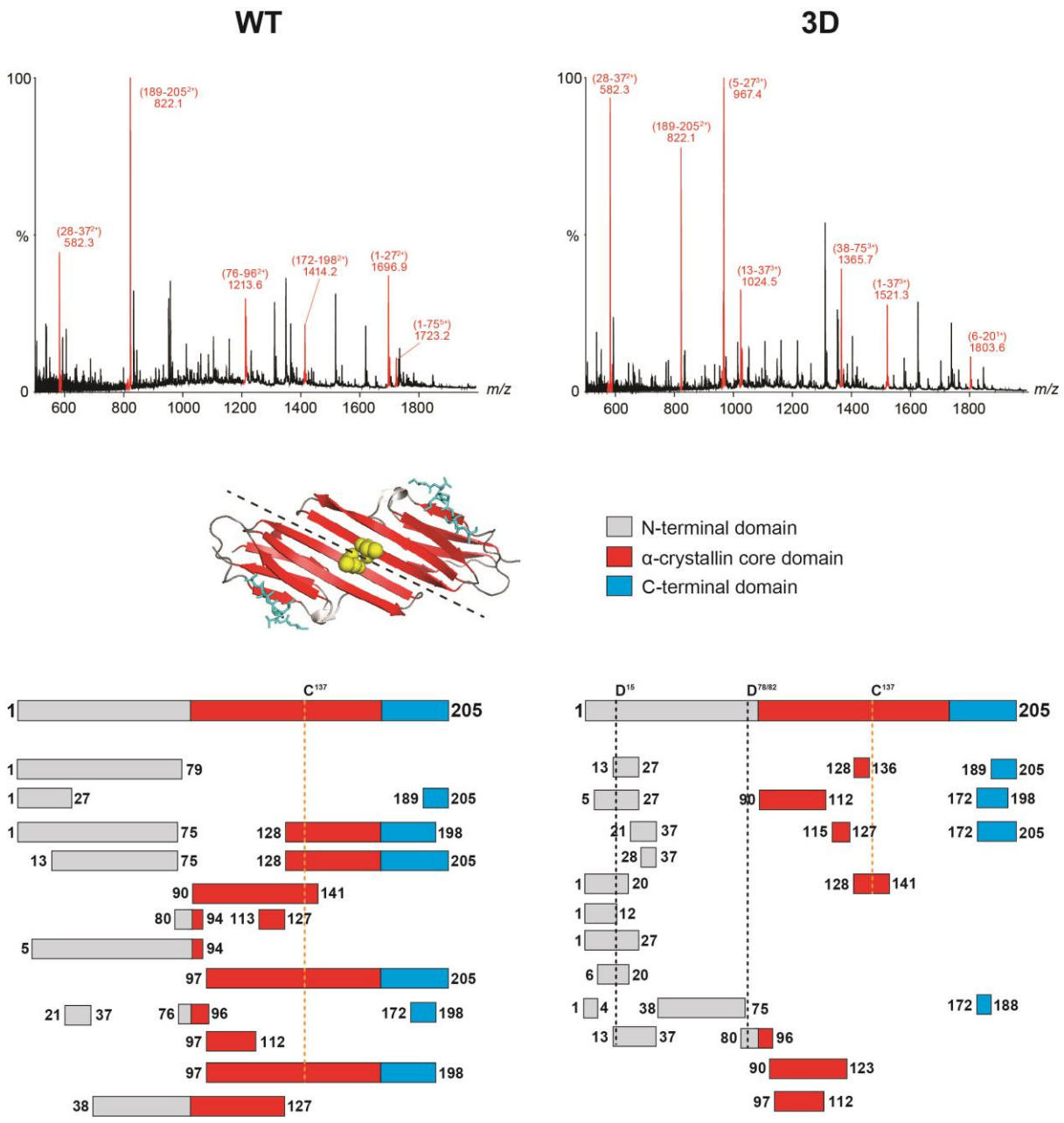

Figure 4.9: Hsp27-WT oligomers are less accessible to proteolysis by trypsin than Hsp27-3D dimers
Peptides from trypsin proteolysis (1000:1 molar ratio, Hsp27:trypsin) of Hsp27-WT and Hsp27-3D at 37°C (in 200 mM NH_4OAc, pH 6.8) were identified by the peaks in each spectrum and compared to the theoretical digestion of Hsp27-WT and Hsp27-3D (performed using BioLynx Protein/Peptide editor V4.1). The core domain of Hsp27 (pdb entry 4MJH, *red*) as well as the N-terminal (residues 80-90 shown in *grey*) and C-terminal (residues 179-185 shown in *blue*) domains are indicated. Peptides generated after 10 min of proteolysis by trypsin and identified by MS are shown. The data show that potential trypsin cleavage sites in WT oligomers are less accessible to proteolysis than in Hsp27-3D. The sites of MMP of Hsp27 are aligned against all peptides identified (*black dashed line*) as well as the disulfide-bond formed between two monomers at Cys137 (*orange dashed line*).

4.3.4 **Blocking of Cys137 alters the oligomeric distribution of Hsp27**

The role of dimerization via disulfide-bonding of Cys137 in the overall quaternary structure and chaperone function of Hsp27 remains unclear. Monomerisation, as a result of disulfide-bond reduction, has been shown to occur in Charcot-Marie Tooth disease-related mutants of Hsp27 (Almeida-Souza *et al.*, 2010). The increase in the amount of monomer was postulated to induce hyperactivity of Hsp27, which then leads to defects in motor neurons. In order to further probe the relationship between monomerisation (via disulfide-bond reduction) and the quaternary structure of Hsp27 a reduction and free thiol-blocking approach was taken. Specifically tris(2-carboxyethyl)phosphine (TCEP), a potent reducing agent to ensure complete reduction of all disulfide bonds, and iodoacetamide (IA) were used to reduce and block Cys137 in order to prevent the disulfide-bond from reforming. To confirm complete reduction and blocking of Cys137, an aliquot of the reaction was taken and analysed by denatured MS. In the absence of TCEP and IA, Hsp27-WT is predominantly dimeric, and this is mediated by the disulfide-bond in the dimer, which was confirmed by non-reducing SDS-PAGE (Figure 4.10A) (charge state overlap between unfolded monomer and dimer, as well as the cleavage of Met1 from recombinant expression of Hsp27 in *E. coli*, cannot distinguish monomer and dimer levels by denatured MS) (Figure 4.10B, top panel). Denatured MS of Hsp27-WT following treatment with TCEP and IA demonstrated that there was complete reduction of the disulfide-bond such that no unfolded dimer was observed (Figure 4.10B, bottom panel). There was an observable increase in mass of the unfolded monomer in this sample attributable to thiol-blocking by IA, which adds ~286 Da to the mass of the monomer.

Following confirmation of the reduction and blocking of Cys137 by TCEP and IA treatment, native MS was utilised to investigate the role this disulfide-bond has in modulating the

quaternary structure of Hsp27. Under low collision energy and in the absence of TCEP and IA (i.e. non-reduced Hsp27), Hsp27-WT is made up of even-sized oligomers ranging from dimers to 24-mers, as previously reported (Figure 4.10C, top panel) (Jovcevski *et al.*, 2015). Following treatment with TCEP and IA, there were observable shifts in the oligomeric distribution of Hsp27, whereby the relative abundance of monomer compared to dimer increases at low collision energies (Figure 4.10C, bottom panel). The reduction and blocking of Cys137 does not disrupt the dimer interface of Hsp27, such that the dimeric structure can still be formed by non-covalent interactions. Also, a significant number of small oligomers, ranging from trimers to 9-mers, were observed following reduction and thiol-blocking of Hsp27, which were not observed previously in Hsp27-WT treated with DTT (Aquilina *et al.*, 2013) (Figure 4.10C, bottom panel). This observation indicates that the dimer interface is weakened due to the reduction of the disulfide-bond. Significantly, for both treatments it was observed that Hsp27 is capable of forming large polydisperse oligomeric assemblies, demonstrating that the reduced form of Hsp27 is still capable of forming large assemblies.

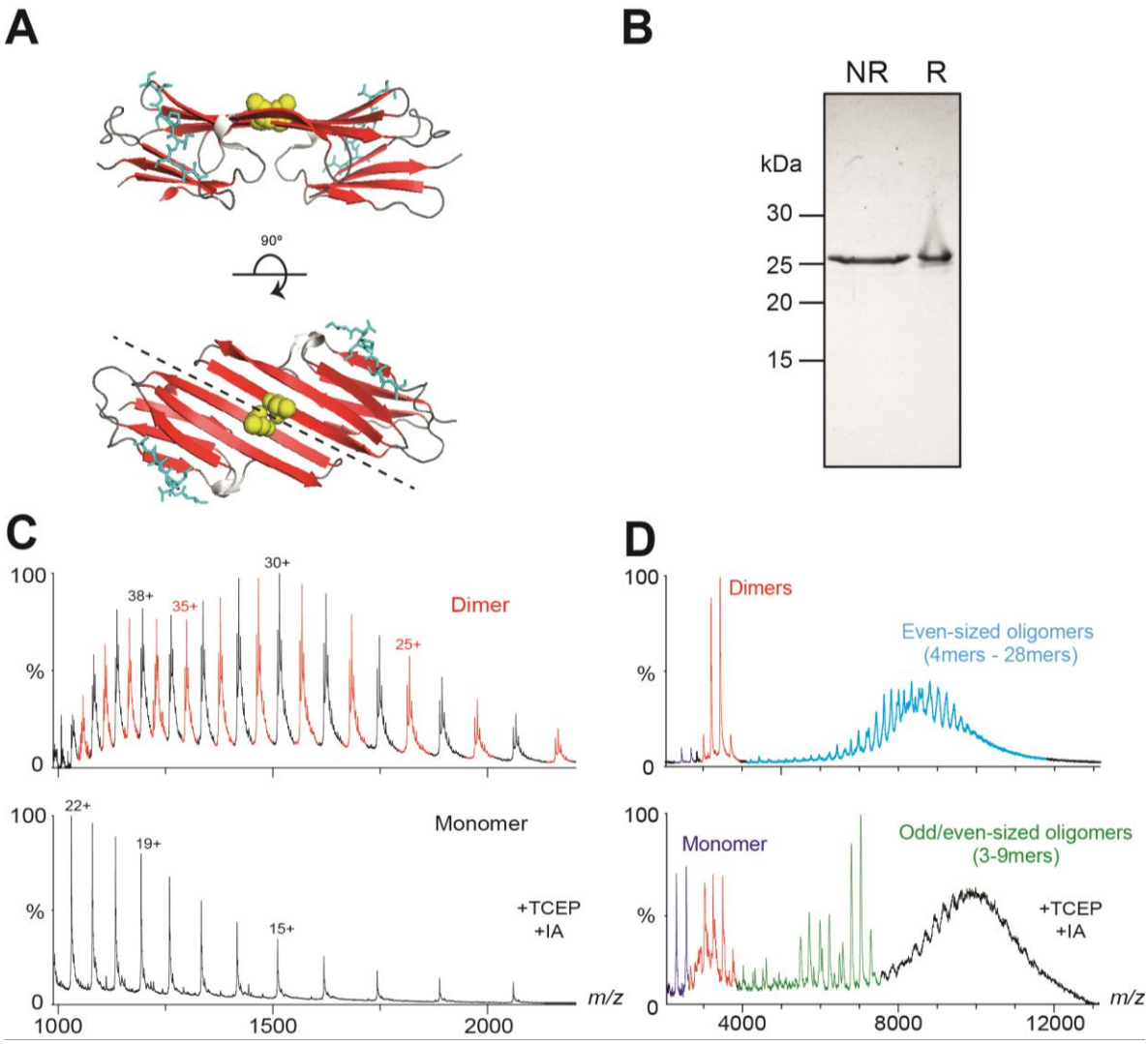

Figure 4.10: TCEP-reduction and IA-blocking of Cys137 shifts the oligomeric equilibrium of Hsp27 towards smaller odd-numbered oligomers

A*:** The core domain of Hsp27 (pdb entry 4MJH) exhibits a curved β-sheet sandwich structure near the dimer interface (*bottom panel, dashed line*) and has an intermolecular disulfide-bond via Cys137 of the β7-sheet of each monomer (*yellow spheres*). ***B: SDS-PAGE of Hsp27-WT after treatment with tris(2-carboxyethyl)phosphine (TCEP) and loaded onto the gel where the SDS-PAGE loading buffer was added to Hsp27 in the absence (NR) and presence (R) of reducing agent (DTT). ***C:*** Denatured MS of Hsp27-WT without the addition of TCEP and IA shows that Hsp27-WT is made up of disulfide-linked dimers (*top panel*), whereas the addition of TCEP and IA results in dimer dissociation such that only monomers are present (*bottom panel*). ***D:*** Native MS shows that the covalent dimeric-building block of oligomers results in the formation of even-sized oligomers (*top panel*) whilst TCEP and IA treatment results in a shift in the oligomer equilibrium towards smaller (and including odd-sized) oligomers (*bottom panel*).

4.4 Discussion

The role of Hsp27 in intracellular proteostasis is inherently dependent on its structural dynamics, whereby changes in structure at the tertiary and quaternary level are linked with its chaperone activity. This work has utilised MMP to investigate the site-specific role phosphorylation has on the structure and chaperone function of Hsp27, demonstrating that increased levels of phosphorylation induce oligomer dissociation into dimers which correlates to enhanced chaperone activity (Chapter 3 and Jovcevski *et al.*, 2015). The work presented in this chapter extends the findings from this previous study by defining the conformation and dynamics of Hsp27 oligomers, in particular chaperone-active dimers. This was done to increase our understanding of the impact PTMs have on the structure of Hsp27 dimers and larger oligomers, and to elucidate how these changes potentially manifest as an increase in chaperone activity. Previous published work in this area has focused on the conformation and dynamics of other ubiquitous human sHsps, in particular αB-c, in order to define the factors that contribute to its polydispersity and function (Baldwin *et al.*, 2011a, Baldwin *et al.*, 2011b, Baldwin *et al.*, 2011c, Jehle *et al.*, 2011, Peschek *et al.*, 2013). However, Hsp27 has received comparatively little attention, despite it also being ubiquitously expressed in tissues and having roles in critical cellular processes, including inhibiting protein aggregation and apoptosis (Rane *et al.*, 2003, Wu *et al.*, 2007). Moreover, there have been no detailed studies investigating the dynamics of a full-length sHsp dimer, which is commonly referred to as the 'basic unit' of large sHsp oligomers.

The overall findings of this work demonstrate that there are distinct differences in the structure of Hsp27 dimers as a result of MMP, whereby with an increasing number of MMP the Hsp27 dimer becomes relatively more unstructured (i.e. flexible) and more stable. These structural changes to the dimer upon phosphorylation may contribute to enhanced

chaperone activity (as reported in Chapter 3 of this thesis), whereby dimers of phosphorylated Hsp27 have an increased capacity to interact with misfolded client proteins to attenuate aggregation. Importantly, however, the changes observed as a result of MMP at the level of the dimer, were not detected in a larger oligomer (12-mer), i.e. the conformation of this 12-mer oligomer was similar for Hsp27-WT and $Hsp27_M$ isoforms.

Since the dimer is Hsp27 is disulfide-bonded it presented an opportunity to study the dynamics of this oligomeric building block and therefore was the focus of this work. Standard biophysical approaches, such as intrinsic tryptophan fluorescence and analytical-SEC, only provide low-resolution structural information on proteins and this is hampered further when dealing with large heterogeneous assemblies such as the sHsps. Both the single and double $Hsp27_M$ isoforms exhibited greater intrinsic tryptophan exposure compared to WT and this increased further for Hsp27-3D at the same concentration (Figure 4.1). However, the levels of tryptophan fluorescence between the single and double $Hsp27_M$ isoforms were near identical. Whilst an enhanced tryptophan exposure with successive MMP was observed, specific differences in the tertiary structure between Hsp27-1D and Hsp27-2D isoforms could not easily be identified with this approach. For example, fluorescence studies, such as tryptophan fluorescence, are unable to discern between individual oligomeric species and thus, increased tryptophan exposure cannot be attributed to a particular species. As a result, the data may reflect the increased proportion of dissociated species that arise due to an increase in the number of MMP, which is similar between single and double $Hsp27_M$ isoforms at the concentrations used in this work. The analytical-SEC data also shows that the quaternary structure of Hsp27 can also be modulated by both pH and buffer systems, particularly Hsp27-3D, where the protein elutes as a mixture of small oligomers and dimers in ammonium acetate. The native MS data (also

performed in ammonium acetate) was unable to detect any oligomers larger than dimers. This may be a result of the associative forces that maintain Hsp27-3D oligomers in ammonium acetate during the solution-phase (i.e. during SEC) are lost during transition into the gas-phase (i.e. during native MS) in the same buffer system.

The ability to observe 'free' Hsp27 dimers by native MS allowed investigation into how the conformation of the full-length dimer varies due to MMP. By exploiting IM-MS, and a comparison of the ATD of various $Hsp27_M$ isoforms (under identical instrument conditions), it was observed that successive MMP result in either an increase in drift time or the expansion of the ATD peak width of the dimer. Together, these data indicate that with an increasing number of MMP, Hsp27 dimers become more unstructured and hence more flexible. Importantly, no discernible differences in the ATD were observed for the 12-mer oligomer between these Hsp27 isoforms. Together these results suggest that at the level of the dimeric building block, cumulative serine phosphorylation of Hsp27 leads to increasing oligomeric dissociation, which in turn causes the dissociated dimer to be more unstructured or loosened. However, within higher-order oligomers there is no detectable change in the shape or stability of the oligomers as a result of phosphorylation. This possibly indicates that the N-terminal domain of Hsp27 is buried within the oligomer irrespective of phosphorylated state. The IM-MS data on Hsp27 dimers and 12-mers was reproducible as the data was acquired on the same instrument, under identical instrument conditions on the same day. When tested on another day under identical instrument conditions on the same instrument, the increase in both ATD and peak widths at half height were observed with increasing MMP. This was also the case for the CIU experiments where an internal RMSD value was determined, indicating that there was a ~5% error between subsequent CIU experiments (Appendix II, Figure 8.3). It should be noted that a single CIU plot is derived

from the acquisition of 10 IM-MS plots (at a single WH) which is then combined and overlayed to generate a single heatmap.

Interestingly, the unfolding dynamics (and by inference, stability) of the Hsp27 dimer differed with an increase in the number of MMP, such that greater activation energy was needed to unfold the Hsp27-3D dimer compared to the Hsp27-1D or -2D dimer. Also, as the activation energy was increased, compaction of the dimer was observed for Hsp27-3D (and to a lesser extent for Hsp27-2D) by a slight decrease in drift time prior to unfolding (Figure 4.4). The compaction of proteins in the gas-phase results from a range of events such as side-chain reorientation, deformation of secondary/tertiary structure or buffer and water molecules being removed from an assembly, all of which can cause a slight collapse in the globular state of the protein. The distinct compaction observed in Hsp27-2D and 3D may be a result of the relatively unstructured N-terminal domains of the dimer, which are believed to be freely exposed in its tertiary structure (Jehle *et al.*, 2011), collapsing or folding into the αCD of the dimer during compaction prior to unfolding in the gas-phase. Overall, the increase in disorder as well as the enhanced stability of the dimer may contribute to enhanced target protein recognition and stabilisation.

Limited proteolysis of Hsp27-WT and Hsp27-3D was performed to elucidate the structural elements that may be more exposed in dimeric (Hsp27-3D) versus oligomeric (Hsp27-WT) assemblies. It was reasoned that fewer structural elements would be exposed in large oligomers (Hsp27-WT) compared to dimers (Hsp27-3D) as a result of packing in the oligomers. Thus, it was expected that the dimer would be more prone to cleavage. The C-terminal domain is readily cleaved and thus accessible in both Hsp27-WT and -3D (at residues 172-198). As the C-terminal domain anchors neighbouring dimers during

oligomerisation, it has been shown previously in other sHsps that this domain is solvent-accessible by NMR and prone to cleavage (Aquilina and Watt, 2007, Baldwin *et al.*, 2011a, Morris and Aquilina, 2010). All the key structural regions of Hsp27-3D (i.e. N-terminal domain, αCD and C-terminal domain) were more accessible to trypsin cleavage than Hsp27-WT, evidenced by larger peptides being identified in Hsp27-WT (indicative of missed cleavage sites by trypsin), whilst much smaller fragments were identified in 3D. The presence of small peptides in 3D, in particular between residues 5-38 in the N-terminal domain, demonstrates that residues are freely accessible to cleavage. In contrast, the absence of these small fragments in Hsp27-WT can be interpreted as the result of these regions being inaccessible to cleavage, presumably because they are buried within an oligomer. However, some of these regions (residues 20-38) may be prone to cleavage as the population of free dimer present during subunit-exchange in Hsp27-WT may be sufficient for proteolytic cleavage. These results demonstrate that both the N-terminal and C-terminal domains of Hsp27 are more accessible to proteolytic cleavage irrespective of oligomerisation state (i.e. dimers and oligomers). More importantly, the results also show that the N-terminal domain of Hsp27-3D dimers remains unstructured and is even more susceptible to proteolysis than Hsp27-WT.

As it was previously shown that MMP enhance oligomer dissociation of Hsp27, it was postulated that oligomeric disassembly is mediated by negative charge repulsion between dimers that result from phosphorylation. As such, it was expected that Hsp27-3D would not undergo subunit-exchange with Hsp27-WT since the negative charge introduced to mimic phosphorylation in Hsp27-3D would prevent it being incorporated into the larger oligomer. Unexpectedly, bulk-FRET analysis and SEC demonstrated that Hsp27-3D is capable of being incorporated into the Hsp27-WT oligomer. This finding indicates that Hsp27 oligomers are

able to withstand nearby negative charge repulsions that are introduced by phosphorylation, at least up to a point. It is postulated that the oligomer would reach a threshold at which the stability of the oligomer is overcome by the negative charge repulsion that Hsp27-3D introduces, leading to dissociation. Whilst studies of αB-c and MMP of this sHsp have demonstrated that these isoforms are capable of subunit-exchange (Ecroyd *et al.*, 2007, Shashidharamurthy *et al.*, 2005), the key difference between αB-c and Hsp27 is that MMP do not lead to dissociation of αB-c oligomers (in contrast to Hsp27). Rather, the rate of subunit-exchange between αB-c oligomers increases substantially with MMP (Ecroyd *et al.*, 2007). Thus, for both Hsp27 and αB-c, the population of dissociated species at any point in time is increased upon the introduction of MMP (and by inference phosphorylation), such that more chaperone-active units are available to interact with, and prevent the aggregation, of client proteins.

Another key PTM of Hsp27 is the formation of an inter-subunit disulfide-bond, mediated by Cys137, which is located along the dimer interface, and results in Hsp27 oligomers being predominantly made up of dimeric building blocks. The disulfide-bonded dimer is the major species produced following recombinant production of Hsp27 in bacteria (Almeida-Souza *et al.*, 2010). However, disulfide-bonded Hsp27 dimers have also been shown to exist *in vivo*; for example, mutations of Hsp27 in Charcot-Marie Tooth disease have been shown to lead to varying levels of disulfide-linked dimers (Almeida-Souza *et al.*, 2010, Evgrafov *et al.*, 2004). The role of dimerization via Cys137 was also examined in this previous study (Almeida-Souza *et al.*, 2010), which showed that reduction results in a gross change in quaternary dynamics, which may contribute to chaperone hyperactivity in cases of disease. This previous study primarily explored the association between disease-related mutants of Hsp27 and reduction of the disulfide-bond (a process the authors referred to as

monomerisation) in cells, since many of these disease-related mutations occur along the dimer interface and close to Cys137 (Almeida-Souza *et al.*, 2010). Using a reduction and thiol-blocking approach in order to generate reduced Hsp27 forms that could not reform the disulfide-bond, the quaternary structure of reduced and non-reduced Hsp27 was probed by native MS in this work. The results show that the quaternary structure of reduced Hsp27-WT is markedly shifted towards the formation of smaller (including odd-sized) oligomers compared to the non-reduced form, indicating a weakening of the dimer interface. These results differ to previous native MS work on reduced Hsp27, whereby treatment with DTT did not result in a significant shift in the oligomeric distribution of the protein nor the formation of odd-sized oligomers (Aquilina *et al.*, 2013). It is possible that in this earlier study the time between DTT treatment and MS analysis was sufficient to allow re-oxidation of the disulfide-bond (Aquilina *et al.*, 2013). Recently, crystal structures of the core domain of Hsp27 disease-associated mutants (R127W, S135F, R136W, T151I and T164A) have indicated that there is no significant difference in the tertiary structure of the mutants compared to the core domain of Hsp27-WT (personal communication from Drs. Heidi Gastall and Justin L.P. Benesch, University of Oxford, UK). However, the susceptibility of the disulfide-bond to reduction was significantly increased as a result of mutation, suggesting that this may play a key role in modulating the quaternary structure and chaperone activity of Hsp27. The data presented here indicates that the inter-subunit disulfide-bond plays a significant role in the quaternary structure of Hsp27 oligomers, whereby a shift in the oligomeric equilibrium resulting from reduction of this disulfide-bond in cells may lead to an increase in chaperone activity due to the formation of smaller oligomers. In the case of disease-related mutants of Hsp27, the increased susceptibility of the disulfide-bond to reduction likely contributes to the observed ’hyperactivity’ of Hsp27, which is a result of the

prolonged and substantial increase in the population of dissociated Hsp27 species able to interact with client proteins. As a result, the disulfide-bond of Hsp27 can regulate the structure of Hsp27, and thus modulate its activity as a chaperone. Future studies should introduce a cysteine to serine mutation (i.e. C137S) in Hsp27, which could be used as a model to further assess the role of the disulfide-bond has on Hsp27 structure and chaperone function.

In this work a wide range of biophysical approaches was used to decipher the impact PTMs, in particular phosphorylation and disulfide-bonding, have on the structure and dynamics of Hsp27. These data suggests that increased levels of phosphorylation of Hsp27 result in subtle changes to the tertiary structure of Hsp27 dimers, such that they become more unstructured and more stable. It is concluded that together these changes lead to an enhanced ability of phosphorylated Hsp27 dimers to recognise and interact with misfolded and aggregating proteins. The disulfide-bond formed between Cys137 in Hsp27 dimers is critical in regulating the activity of Hsp27; reduction of this bond significantly shifts the oligomeric equilibrium towards smaller species, which may be more chaperone-active. The increased susceptibility of disease-related mutants of Hsp27 to be reduced likely contributes to the reports of Hsp27 hyperactivity as a mechanism that underpins these diseases. Overall, PTMs of Hsp27 result in a range of structural changes, at the secondary, tertiary and quaternary level, and these facilitate changes in chaperone activity in cells.

Chapter 5: Results -

N-terminal mutations alter the structure and chaperone function of αB-crystallin

Chapter 5: N-terminal mutations alter the structure and chaperone function of αB-crystallin

5.1 Introduction

The molecular chaperone αB-crystallin (αB-c) is a ubiquitously expressed sHsp which typically exists as large, polydisperse oligomers that undergo constant subunit-exchange (Aquilina *et al.*, 2003, Aquilina *et al.*, 2005, Bhat and Nagineni, 1989, Morris and Aquilina, 2010). In conjunction with other broadly expressed sHsps, such as Hsp27 and Hsp20, αB-c plays a crucial role in the cell's protein quality control (PQC) network by acting as a protein stability sensor (Balch *et al.*, 2008, Kulig and Ecroyd, 2012, McHaourab *et al.*, 2009). Numerous neurodegenerative diseases are associated with the malfunctioning of this quality control network, such as Alzheimer's disease and Parkinson's disease (Iwaki *et al.*, 1992). Mutations in αB-c are also associated with desmin-related cardiomyopathies and cataracts in the lens (Bova *et al.*, 1999, Ecroyd and Carver, 2009). Overall, the association between αB-c and these diseases demonstrates that its chaperone function is critical to the PQC network.

Like most sHsps, αB-c is made up of three key domains, the β-sheet rich αCD (residues 66-149) which is conserved amongst sHsp family members. This domain is flanked by an unstructured N-terminal domain (residues 1-65) which contributes to its polydispersity (Laganowsky *et al.*, 2010) and is also prone to post-translational modification (primarily phosphorylation) (Aquilina *et al.*, 2004, Ecroyd *et al.*, 2007) and a C-terminal flexible domain (residues 150-178) that contains the IXI/V motif which binds to the β4-β8 groove of a neighbouring αCD and is thought to aid in oligomeric stability (Delbecq *et al.*, 2012). The quaternary dynamics of αB-c have also been studied extensively; non-covalent exchange of monomers, mediated by the unstructured N-terminal and C-terminal domains, underpin

subunit-exchange between oligomers (Baldwin *et al.*, 2011a, Baldwin *et al.*, 2011c). In addition, cryo-EM and structural homology modelling has also suggested that residues 54-60 form inter-dimer contacts that maintain a hexameric substructure within an oligomeric assembly (Braun *et al.*, 2011, Peschek *et al.*, 2013).

Numerous structure-function studies on αB-c have shown that various point mutations in the N-terminal domain result in enhanced chaperone activity (against the amorphous aggregation of alcohol dehydrogenase, citrate synthase and insulin) when compared to the αB-c WT (Biswas *et al.*, 2007, Santhoshkumar *et al.*, 2009, Sreelakshmi and Sharma, 2005, Sreelakshmi and Sharma, 2006). However, the majority of these studies use low-resolution techniques (e.g. tryptophan fluorescence, CD spectroscopy and analytical-SEC) to investigate the effect of mutation on the structure of αB-c. Moreover, these studies did not extensively investigate the effect(s) these mutations have on the quaternary structure of αB-c. By contrast, native MS is an ideal technique to study the effect of mutation has on the quaternary structure of αB-c.

A previous study had shown that changing the orientation of residues 54-60 of αB-c significantly reduced its polydispersity, observed by SEC-MALS, and enhanced chaperone activity (Sreelakshmi and Sharma, 2006). It is thought that this region plays a key role in the oligomerisation of αB-c by disrupting the inter-dimer contacts that maintain the oligomer. However, the exact oligomeric distribution and abundance that this mutation introduced was not examined. This study explored the role of the N-terminal domain in the quaternary structure and chaperone function of αB-c by introducing mutations in the region encompassing residues 54 – 60, which is thought to play a key role in αB-c oligomerisation. With this, mutations were designed in order to disrupt the oligomerisation dynamics of αB-c

via changes in size (P58A and S59A), introduction of charge (S59K) or disruption of sequence motifs responsible for oligomerisation (R56S/S59R and invert 54-60). As a result, five different N-terminal domain mutants were generated (P58A, S59A, S59K, R56S/S59R and invert 54-60 of αB-c) and were characterised extensively with respect to structure and chaperone function.

5.2 Methods

Human αB-c WT and N-terminal mutants (P58A, S59A, S59K, R56S/S59R and invert 54-60) were expressed and purified as described previously (section 2.3). Purification and confirmation of the identity of the N-terminal mutations were confirmed by SDS-PAGE (section 2.2.1) and denatured MS (section 2.5.5). The secondary structure of the αB-c isoforms was assessed by far UV-CD spectroscopy (section 2.5.3), thermal stability by dynamic light scattering (DLS) (section 2.5.4) and the tertiary and quaternary structure analysed by intrinsic tryptophan fluorescence and bis-ANS fluorescence (section 2.5.2), analytical-SEC (section 2.5.1) and native MS (section 2.5.6). The chaperone activity of the αB-c isoforms was assessed using *in vitro* aggregation assays as described previously (section 2.6.1).

5.3 Results

5.3.1 Mutations confer changes in secondary and tertiary structure of αB-crystallin

The expression and purification of N-terminal mutants of αB-c (P58A, S59A, S59K, R56S/S59R and invert 54-60) was confirmed by both SDS-PAGE and denatured MS (Figure 5.1). All αB-c mutants were produced with good yields (in excess of 15 mg per 1 L of bacterial culture) and the purity of these proteins was greater than 95 % as determined by denatured MS (Figure 5.1B). Following the expression and purification of these constructs, the structure of these αB-c isoforms was characterised using a range of biophysical

techniques. Far UV-CD spectroscopy was performed to probe the secondary structure of these proteins. Most of the αB-c mutants do not exhibit gross changes in secondary structure compared to WT isoform, with the exception of the invert 54-60 mutant, which showed a dramatic (4-fold) increase in negative ellipticity at 215 – 225 nm (Figure 5.2). The α-helical and β-sheet content for all variants, except for αB-c S59A, was greater than that of WT as evidenced by the increase in negative ellipticity at 225 nm (Figure 5.2). When the CD spectra were deconvoluted using BestSel software to determine secondary structure content, it was observed that the 54-60 invert mutation led to a dramatic overall change in the secondary structure of αB-c compared to the WT protein. The 54-60 invert mutant was found to have a 41 % increase in α-helical content and a 36.7 % decrease in random coil content relative to αB-c WT (Table 5.1).

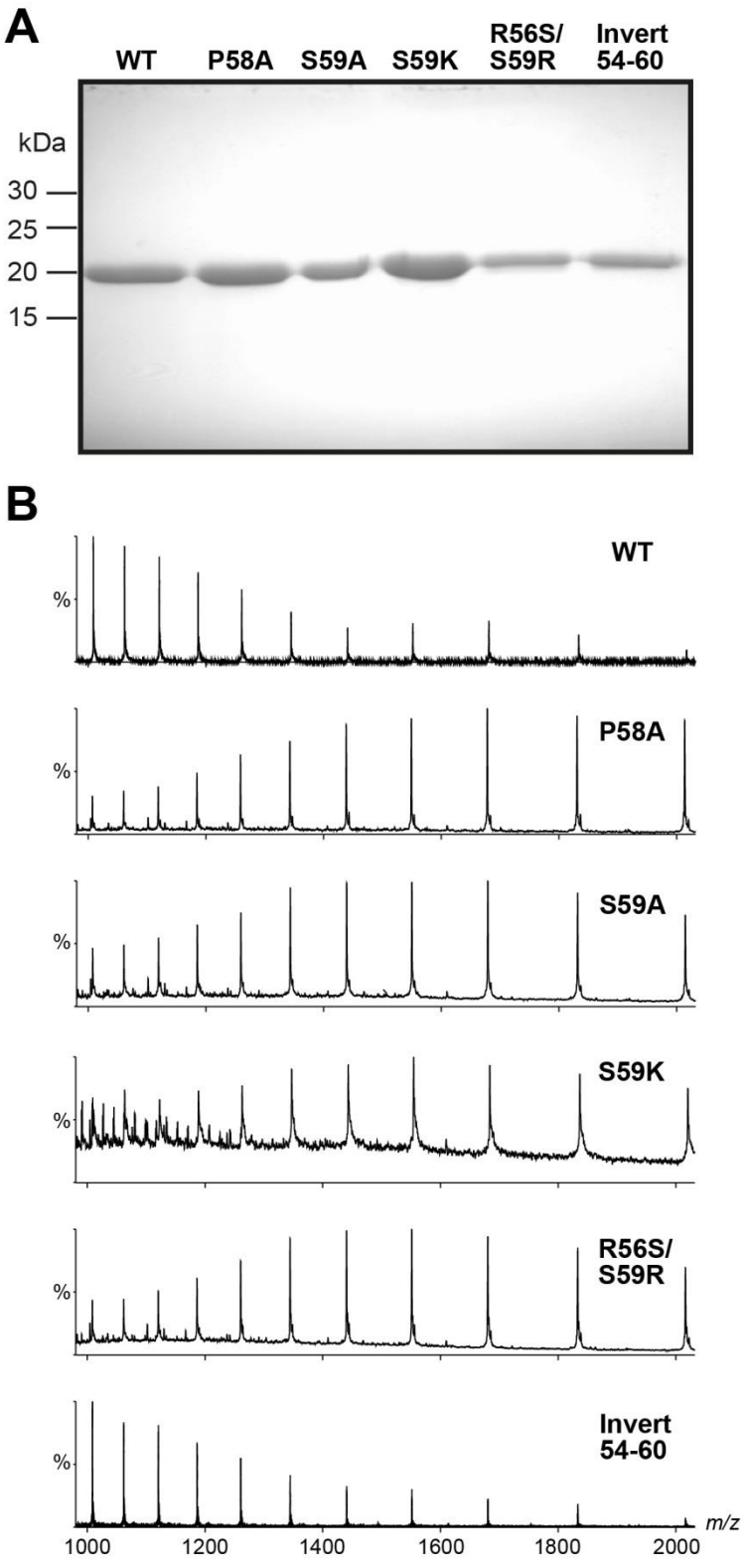

Figure 5.1: SDS-PAGE and denatured MS to assess the purity of αB-c N-terminal mutants
To confirm the purification of the αB-c variants, SDS-PAGE and denatured MS was performed to assess the levels of purity. ***A*:** SDS-PAGE analysis of αB-c variants (50 µM in 50 mM phosphate buffer, pH 7.4). ***B*:** Denatured MS of αB-c variants (50 µM in 200 mM ammonium acetate pH 6.8, 1 % v/v formic acid, 40% v/v acetonitrile). Based on these data the purity of all the variants produced was assessed to be greater than 95%.

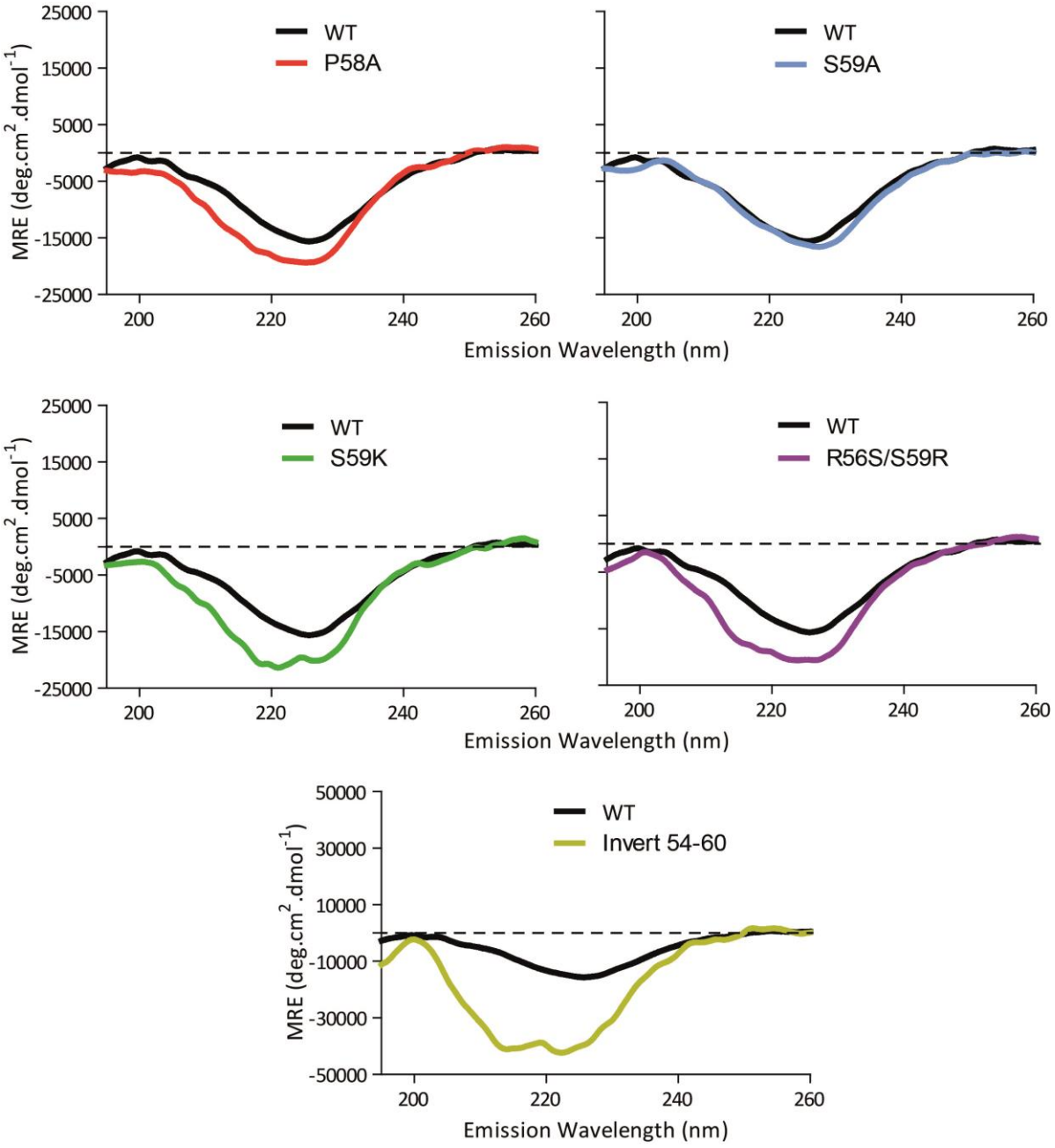

Figure 5.2: Far UV-CD spectroscopy of αB-c N-terminal mutant isoforms reveals differences in secondary structure compared to the wild-type protein

Proteins were incubated at room temperature for 30 min. CD spectra were accumulated from 6 scans, smoothed using Savitzky-Golay smoothing and normalised to protein concentration and results shown are representative of two independent experiments. All variants, with the exception of S59A, exhibited greater negative ellipticity than αB-c WT. The 54-60 inversion mutant exhibited the greatest negative ellipticity compared to WT.

Table 5.1: Deconvolution of the far UV-CD spectra of the αB-c isoforms
CD spectra of the N-terminal αB-c mutants (shown in Figure 5.2) were deconvoluted to determine the content (as a %) of secondary structural motifs (α-helix, β-sheet, turn and random coil) and compared to the wild-type protein. Deconvolution was performed using BeStSel secondary structure prediction software (Micsonai *et al.*, 2015).

	α-helix	β-sheet	Turn	Random coil
WT	6.8	29.8	18.6	45.6
P58A	5.9	41.7	11.0	41.4
S59A	9.5	34.6	17.1	38.8
S59K	6.0	46.2	7.2	40.7
R56S/S59R	7.3	47.1	8.5	37.2
Invert 54-60	47.8	43.2	-	8.9

The relative thermal stability of these isoforms was determined by measuring the mean particle size of the proteins in solution (Z-average) as a function of temperature by DLS (Figure 5.3A). The average size of the αB-c isoforms in solution began to increase exponentially at 60°C (Figure 5.3A). Moreover, there was a greater rate of increase in average particle size in all the mutant isoforms compared to WT such that, at 75 °C the average size of particles formed by αB-c WT was 150 nm whereas it was greater than 250 nm for all the mutant isoforms (Figure 5.3A). The tertiary structure of the αB-c mutants was also examined by intrinsic tryptophan and bis-ANS fluorescence. The S59K and R56S/S59R αB-c isoforms exhibited greater intrinsic tryptophan fluorescence intensity, indicative of greater exposure of the two tryptophan residues (W9 and W60 in αB-c) compared to WT. The other isoforms had an intrinsic tryptophan fluorescence profile similar to WT protein with no observable shift in emission maximum (Figure 5.3B). Interestingly, all αB-c isoforms showed a substantial decrease in bis-ANS fluorescence compared to WT along with a right shift in the emission maximum of the fluorescence spectrum (Figure 5.3B). These results are indicative of a substantial decrease in exposed hydrophobicity of the mutant αB-c isoforms compared to WT.

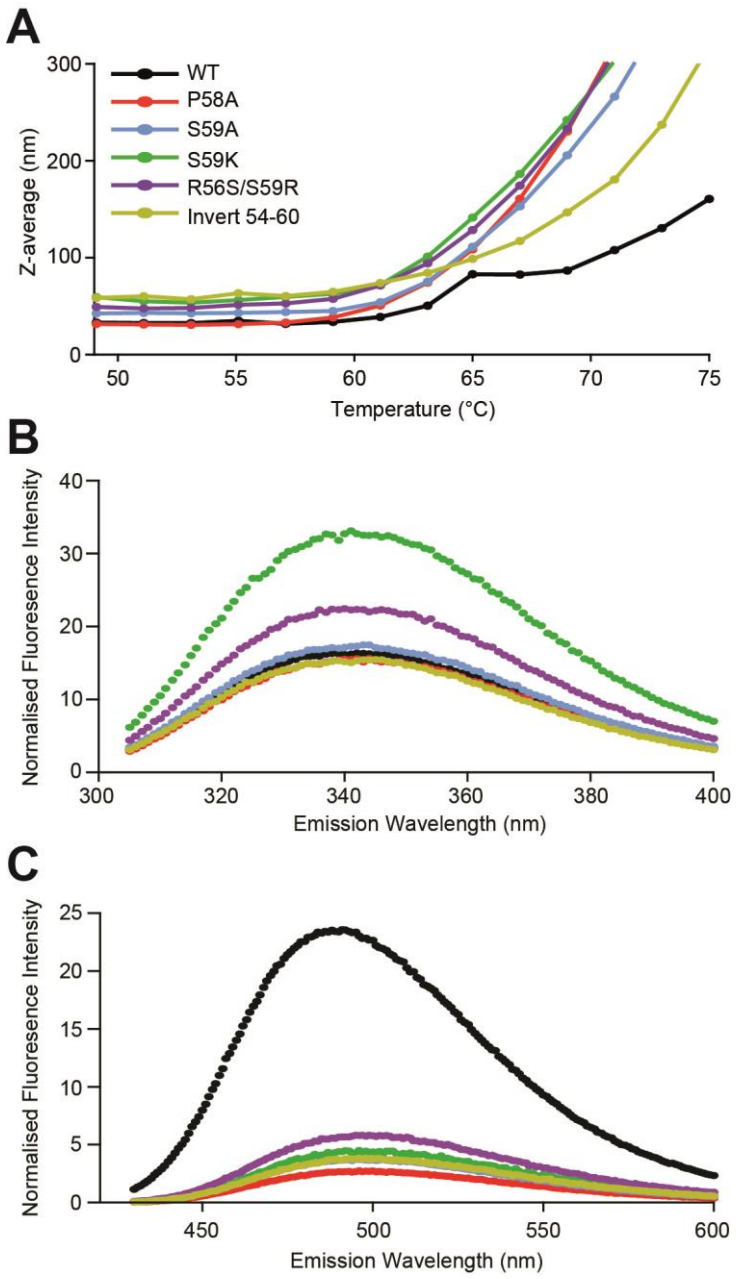

Figure 5.3: N-terminal αB-c variants are less thermostable and adopt a different tertiary and quaternary structure compared to WT

***A*:** Thermal denaturation curves of αB-c isoforms (50 µM in 50 mM phosphate buffer, pH 7.4). The change in average particle size (Z-average) was measured by DLS with increasing temperature (ramp rate 2.5 °C per 15 min). ***B*:** Intrinsic tryptophan fluorescence reveals differences in tertiary structure of some αB-c variants, whereby the R56S/S59R and S59K αB-c mutants have greater tryptophan fluorescence emission compared to WT. ***C*:** bis-ANS fluorescence of αB-c variants reveal that mutations results in decreased hydrophobic exposure compared to WT. Proteins for intrinsic tryptophan and bis-ANS fluorescence studies were incubated (20 µM in 50 mM phosphate buffer, pH 7.4) at room temperature for 15 min prior to measurement. Spectra were normalised to protein concentration and results shown are representative of two independent experiments.

5.3.2 N-terminal mutations alter the quaternary structure of αB-crystallin

In order to extensively characterise the quaternary structure of the N-terminal mutants of αB-c, analytical-SEC and native MS were utilised to determine the oligomeric size and distribution of these proteins. SEC revealed that the mutant αB-c isoforms have a near identical elution profile compared to αB-c WT in both phosphate and ammonium acetate buffer systems. In both cases, eluting as a large broad peak indicative of a large polydisperse assembly, with oligomeric masses ranging from 200 – 700 kDa (Figure 5.4A). A slight variation in elution volume between phosphate (used in other structural studies and aggregation assays) and ammonium acetate (used in native MS experiments) buffers was also observed (Figure 5.4A-B). Native MS and CID (as described previously; section 3.1.3), allows the oligomeric state and distribution of these polydisperse proteins to be observed and quantified. Multiple MS studies on αB-c have demonstrated its polydisperse nature; the size of the oligomers range from 10-mers to 40-mers and there is a preference for even-sized stoichiometries under the condition used in this study (Aquilina *et al.*, 2003, Baldwin *et al.*, 2011c). Under low collision energies, all αB-c isoforms exhibited a charge state distribution envelope ranging from 8,000 – 12,000 *m/z*, which is typical of a large polydisperse species such as αB-c WT (Figure 5.4B). The complexity of the MS spectra was overcome by employing CID, which strips a monomeric subunit off an oligomer and allows the identification and quantification of all the oligomers present (Aquilina *et al.*, 2003). It was found that the oligomeric distribution of the N-terminal isoforms was similar to αB-c WT, with oligomers ranging from 14-mers to 33-mers observed (Figure 5.4C) (Appendix III; Figure 8.4). The 20-mer and the 22-mer were the most abundant oligomers present in all the αB-c isoforms (Figure 5.4C). The inversion mutant of αB-c displayed an atypical

oligomeric distribution whereby there was a considerable decrease in the abundance of oligomers ranging from 14-mers to 18-mers (Figure 5.4C).

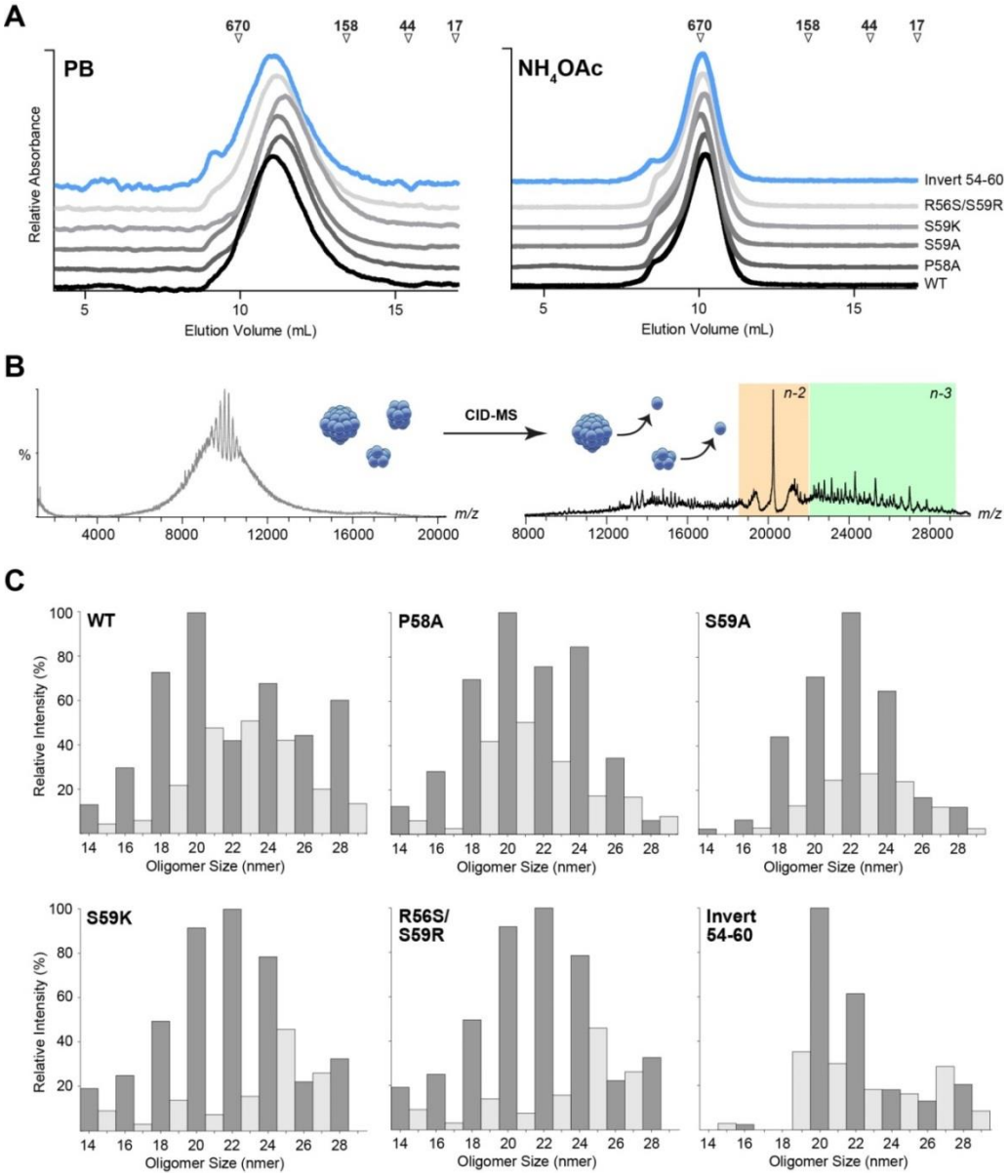

Figure 5.4: Native MS reveals changes in quaternary structure between αB-c variants
***A*:** Analytical-SEC of N-terminal αB-c variants (50 µM) in 50 mM phosphate buffer (PB, pH 7.4) (*left panel*) and 200 mM ammonium acetate (NH_4OAc; pH 6.8) (*right panel*) which illustrates the presence of large oligomers in solution. ***B*:** Native MS of αB-c variants (50 µM) under low collision energy (αB-c P58A in this instance) (25 V), present as large polydisperse oligomers ranging from 5,000 - 14,000 *m/z* (*left panel*). Collision-induced dissociation (CID) MS of αB-c variants under a higher accelerating voltage (180 V) results in the signal in the *n*-2 (orange box) and *n*-3 (green box) regions being well resolved (*right panel*). ***C*:** Oligomeric distributions of αB-c variants, with large oligomers ranging from 14-mers to 29-mers present. There is a preference of even-sized oligomers (dark grey) over odd-sized oligomers (light grey). Protein samples were prepared in 200 mM NH_4OAc (pH 6.8) for the MS experiments. Distribution and abundance data was deconvoluted using UniDec (Marty *et al.*, 2015).

5.3.3 N-terminal mutations are just as chaperone able compared to wildtype αB-crystallin

The ability of the N-terminal αB-c mutants to prevent amorphous and fibrillar protein aggregation was also analysed. In order to assess the chaperone activity of these isoforms, insulin was used as a model protein for amorphous aggregation and αS was used to model fibril forming protein. In the absence of chaperone, insulin was observed to aggregate rapidly upon reduction with DTT such that, after ~15 min the light scatter associated with its aggregation into large insoluble particles had reached a plateau (Figure 5.5A, left panel). In the absence of client protein, no increase in light scatter and ThT fluorescence associated with aggregation was observed (Appendix III; Figure 8.5). There was no significant difference in chaperone efficacy between αB-c isoforms in preventing amorphous insulin aggregation (Figure 5.5B) with the exception of the 54-60 inversion mutant isoform, which was significantly less effective at preventing insulin aggregation compared to WT (Figure 5.5B). The ability of the N-terminal αB-c mutants to prevent fibrillar aggregation was ascertained by monitoring the inhibition of seeded αS aggregation. Essentially, this assay measures the ability of αB-c to inhibit the elongation of αS fibrils using preformed αS seed fibrils (Buell *et al.*, 2014). In the absence of chaperone, αS was observed to completely aggregate over ~16 h, indicated by the change in ThT fluorescence associated with fibrillar aggregation reaching a plateau after this time (Figure 5.5A, right panel). In the presence of chaperone, there was a decrease in the change in ThT fluorescence associated with αS fibril formation. However, there was no significant difference in chaperone activity between the αB-c isoforms in preventing seeded αS aggregation (Figure 5.5C). Therefore, mutation of the N-terminal region of αB-c appears to not have a significant effect on its ability to act as a

molecular chaperone, with the exception of the 54-60 invert mutant which was less effective in preventing insulin aggregation.

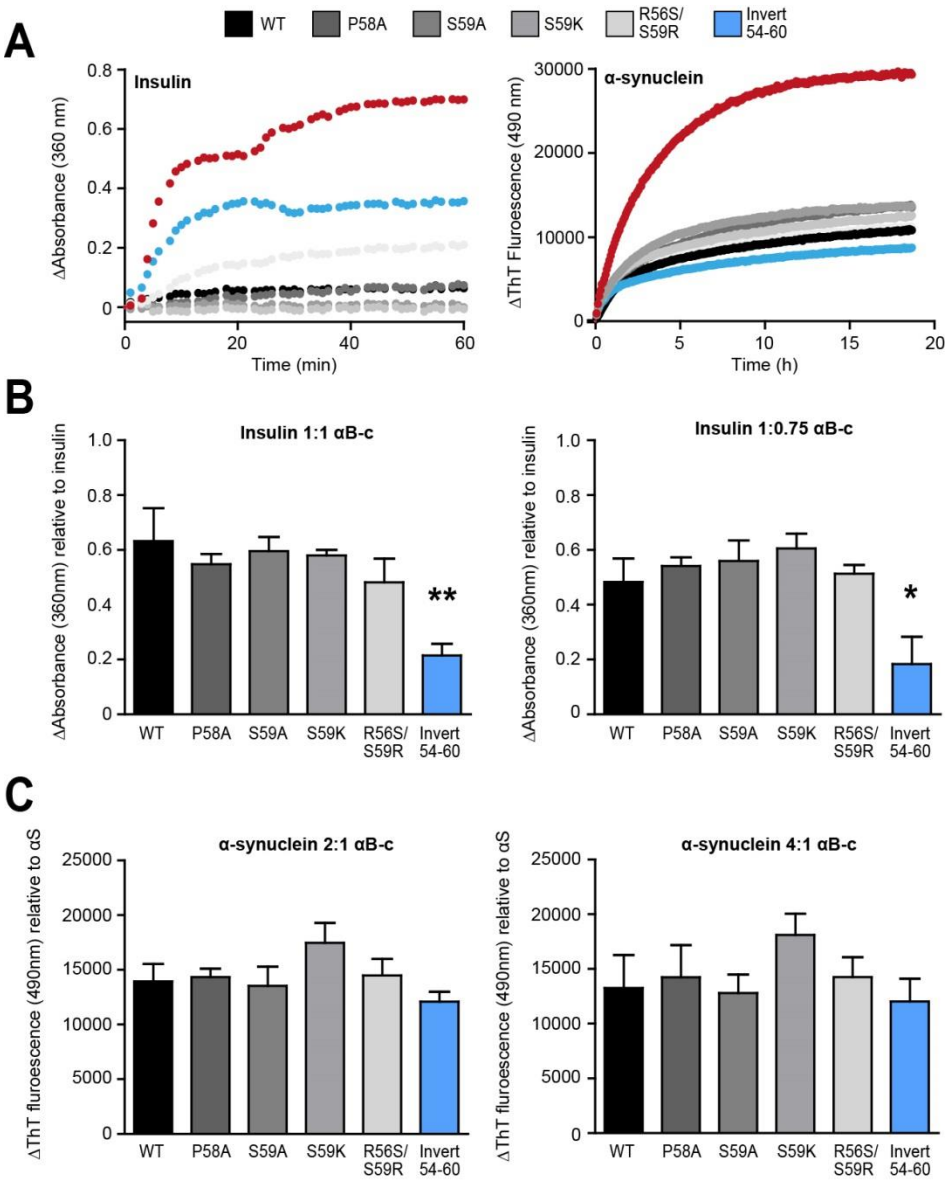

Figure 5.5: The ability of the N-terminal αB-c variants to inhibit the amorphous and fibrillar aggregation of client proteins

***A*:** Inhibition of the reduction-induced amorphous aggregation of insulin was monitored by the change in light scatter at 360 nm (*left panel*), whilst fibrillar αS aggregation was measured by the change in ThT fluorescence emission at 490 nm (excitation at 440 nm) (*right panel*). ***B*:** The invert 54-60 mutant of αB-c showed a significant decrease in the ability to inhibit insulin aggregation at various molar ratios compared to αB-c WT (*left panel, red*). ***C*:** There was no significant difference in the ability of αB-c isoforms to inhibit αS seeded aggregation (10% w/w seed relative to αS monomer concentration) at either molar ratios tested (*right panel, red*). Amorphous and fibrillar aggregation assays were performed in 50 mM phosphate buffer (pH 7.4) at 37 °C. Molar ratios between αS and αB-c to ascertain chaperone activity is stated above each histogram. Data in B and C are mean ± SEM (n = 3) (*$p < 0.05$; **$p < 0.01$).

5.4 Discussion

The aim of this work was to examine the effect(s) of mutations have in the region from 54-60 in the N-terminal domain of αB-c have on its structure and chaperone function. The rationale for this was based on various studies that have demonstrated that residues 54-60 potentially play a critical role in oligomerisation of αB-c by forming inter-dimer contacts which maintain αB-c oligomers (Braun *et al.*, 2011). Moreover, another study, using SEC-MALS, indicated that the inversion of αB-c residues 54-60 significantly reduced its polydispersity (Sreelakshmi and Sharma, 2006). Thus, five different mutant isoforms were generated for this work, namely P58A, S59A, S59K, R56S/S59R and invert 54-60 αB-c. This study showed that mutation of these residues does confer slight changes in secondary and tertiary structure to αB-c. However, native MS showed that there was no observable difference in polydispersity and quaternary structure of these αB-c mutants compared to αB-c WT, the exception being the 54-60 invert mutation of αB-c, which led to a decreased abundance of oligomers smaller than 19-mers. Moreover, the ability of these isoforms to prevent amorphous and fibrillar aggregation of client proteins was not significantly different to αB-c WT (again, with the exception of the 54-60 invert mutant which was less efficient than WT at preventing the amorphous aggregation of insulin). These results suggest that whilst mutations may alter the structure of αB-c at the secondary and tertiary level, the detailed quaternary level information is extremely valuable in delineating the structure-function relationship in αB-c. Therefore, it is concluded that the quaternary structure is a key determinant of αB-c chaperone activity.

After expression and purification of these isoforms, changes in secondary structure (in comparison to αB-c WT) were assessed by far-UV CD spectroscopy. The data shows that all the mutant isoforms, with the exception of αB-c S59A, induce slight changes in secondary

structure of αB-c. The inversion of residues 54-60 resulted in the most significant difference in secondary structure compared to αB-c WT, substantially increasing the α-helical content and decreasing the proportion of random coil in the protein, in agreement with the earlier study of this mutant αB-c isoform (Sreelakshmi and Sharma, 2006). All of the N-terminal mutations were found to increase the overall β-sheet content compared to αB-c WT.

These changes in secondary structure were accompanied by more significant changes in the tertiary structure of the N-terminal mutants compared to αB-c WT, as assessed by intrinsic tryptophan and bis-ANS fluorescence. The intrinsic tryptophan fluorescence data show that the S59K and R56S/S59R isoforms have a significant increase in tryptophan fluorescence intensity (one-fold and two-fold increase, respectively) compared to αB-c WT. There are only two tryptophan residues in αB-c (W9 and W60), and thus these primarily report on the solvent exposure of the N-terminal region of αB-c. It is likely that the S59K and R56S/S59R mutations primarily effect the packing of W60, since they are very close to this residue, making it more solvent exposed. The introduction of the basic residues lysine and arginine (which have large side chains) proximal to W60 is likely to reduce the flexibility of this region, resulting in increased solvent exposure. Interestingly, other mutations, including inversion of residues 54-60, which includes W60, did not have a significant effect on solvent accessibility of the tryptophan residues in αB-c.

In stark contrast to the intrinsic fluorescence data, the result from the bis-ANS experiments demonstrate that all the mutants isoforms studied in this work have decreased exposed surface hydrophobicity compared to αB-c WT. This indicates that the tertiary structure of these αB-c mutants differs significantly to that of WT. Surprisingly; the large difference in bis-ANS fluorescence did not translate to changes in chaperone activity, which is thought to

be driven by hydrophobic interactions. This could be a result of the mutant isoforms shielding their hydrophobic regions (in both oligomeric and dissociated states of αB-c) in the absence of an aggregating client protein and undergoing a tertiary and/or quaternary structure change when in the presence of exposed hydrophobicity from the client protein. Also, non-hydrophobic interactions (e.g. charged interactions) may also be responsible for the chaperone activity observed of these N-terminal mutants. It also indicates that the quaternary structure and dynamics primarily drives the chaperone activity of the N-terminal αB-c isoforms. However, both these fluorescence-based techniques provide relatively low resolution information on the tertiary and quaternary structure of large polydisperse proteins like αB-c. This polydispersity, as well as the constant subunit-exchange dynamics that underpin the quaternary structure of αB-c, cannot be studied using these low resolution approaches. Therefore, the differences observed by intrinsic and bis-ANS fluorescence could pertain to changes at the level of the dimeric building block of αB-c and/or the various oligomeric states that αB-c populates, or both.

Analytical-SEC demonstrated that αB-c elutes as a large, broad peak, which has previously been shown and is typical of large polydisperse oligomers of αB-c (Aquilina *et al.*, 2004, Ecroyd *et al.*, 2007, Santhoshkumar *et al.*, 2009). In order to ascertain the effect that these mutations have on the quaternary structure of αB-c, native MS was used to determine the oligomeric state of the N-terminal mutant αB-c isoforms. Native MS allows the structural heterogeneity of large polydisperse proteins, such as αB-c, to be interrogated (Aquilina *et al.*, 2004, Baldwin *et al.*, 2011c, Benesch *et al.*, 2010, Jovcevski *et al.*, 2015). This work shows that the polydispersity and oligomeric distribution of αB-c does not change significantly with the N-terminal mutations introduced in this work. This indicates that the observed changes in secondary and tertiary structure of these αB-c isoforms relative to αB-c WT do not

translate to changes in quaternary structure. It is concluded that the differences in secondary and tertiary structure may be due to differences in subunit-exchange rates, whereby the structural elements of smaller species (e.g. dimers) are more abundant in certain mutants when measured using averaged, fluorescence-based techniques. For example, the significant increase in tryptophan fluorescence of the R56S/S59R mutant may be a result of an increase in subunit-exchange rate where structural elements in smaller species are more abundant during measurement at room temperature. Thus, the subunit-exchange rate of some of these isoforms (S59K, R56S/S59R and invert 54-60) may be faster than the other isoforms tested; including WT. The increase in subunit-exchange is reflected by the relative abundance of odd-sized oligomers, which is much lower than even-sized oligomers in these isoforms. This indicates that the intra-dimer interface (site of dimerization) is stronger than the inter-dimer 'edge' interface (dimer-dimer contact regions), resulting in an increase in dimeric subunit-exchange rate. Surprisingly, this increase in subunit-exchange did not translate to enhanced chaperone activity when tested against the client proteins used in this study. The data demonstrates that the choice of client protein is crucial in determining the chaperone efficacy of these N-terminal αB-c mutants, which can vary depending on the client protein chosen (Ecroyd *et al.*, 2007). In light of this, the chaperone activity of these mutants should be tested against other client proteins to gain a greater picture of how effective the N-terminal mutants are at inhibiting aggregation.

After extensively characterising the structure of the N-terminal αB-c mutants, we sought to assess their ability to inhibit the amorphous and fibrillar aggregation of target proteins. It was found that the ability of these mutants to prevent amorphous insulin and fibrillar αS aggregation was comparable to WT, with the exception of the 54-60 inversion mutant which had a significantly reduced capacity to inhibit the reduction-induced amorphous aggregation

of insulin, but not the seeded fibrillar aggregation of αS. Overall, these data show that the quaternary structure and dynamics of αB-c is a key indicator of chaperone activity since it also was found not to change significantly with mutation (as the dimeric and oligomeric form cannot be distinguished in this case). Thus, despite observing distinct changes in secondary and tertiary structure of the N-terminal αB-c mutants compared to αB-c WT, the similarity of the mutant isoforms to αB-c WT in quaternary structure mirrored the similarity measured in chaperone activity. The decrease in the ability of the 54-60 inversion mutant to prevent insulin amorphous aggregation may be attributable to specific changes in the tertiary structure between residues 54-60 in this isoform, which alters the ability of the protein to recognise and/or interact (via. hydrophobic exposure or charged interactions) with aggregation-prone monomeric insulin. The relative absence of small oligomers in 54-60 invert αB-c may also be responsible for the reduction in the relative chaperone activity of this mutant, as it has been previously shown that oligomer dissociation and increased subunit-exchange is crucial to inhibiting aggregation (Ecroyd *et al.*, 2007, Jovcevski *et al.*, 2015).

The data also suggests that the mechanisms by which αB-c inhibits αS aggregation differs from the inhibition of amorphous insulin aggregation. Interestingly, this data implies that a different region of αB-c is responsible for interacting with αS to prevent its fibrillar aggregation, since the invert mutant had a similar chaperone efficacy to αB-c WT in this assay. Moreover, in preventing the amorphous aggregation of insulin, αB-c form a high molecular mass complex with this client protein (i.e. holdase type activity), whereas recent work has shown that αB-c interacts with aggregation-prone monomeric αS in a transient manner (i.e. no high molecular mass complex is formed and thus, it does not involve a holdase type mechanism) (Cox *et al.*, 2016). Therefore, in the case of the inversion mutation

of αB-c, the holdase-like activity appears to be compromised whereas the transient-like interaction mechanism with client proteins is maintained. A recent study suggested that region of αB-c involved in binding to aggregation-prone proteins is dependent on the morphology of the aggregating substrate protein (Mainz *et al.*, 2015). Using deletion mutants of αB-c and solid-state NMR correlation spectroscopy, it was shown that the N-terminal domain was responsible for the recognition and interaction with aggregation prone (i.e. reduced) lysozyme (which aggregates amorphously), whereas both the N-terminal domain and αCD interact with and are involved in preventing the fibrillar aggregation of the $A\beta^{1-40}$ peptide (Mainz *et al.*, 2015). Therefore, it is possible that the 54-60 inversion mutation of αB-c reduces its ability to recognise and form a stable high molecular mass complex with amorphously aggregating substrate proteins.

The unstructured N-terminal domain of αB-c is thought to play a key role in the structure and chaperone activity of sHsps. Previous studies proposed that residues 54-60 form inter-dimer contacts in αB-c, and therefore maintain oligomeric stability and modulate oligomeric polydispersity. By introducing a variety of mutations in this region of the N-terminal domain (residues 54-60) this work has investigated the potential effects that these mutations have on the structure and chaperone function of αB-c. Despite mutations in this region leading to significant changes in secondary and tertiary structure of αB-c relative to αB-c WT, the quaternary structure and chaperone activity of these mutants was similar to αB-c WT. These results highlight the fundamental link between quaternary structure and chaperone activity of sHsps.

Chapter 6:

Overall Discussion and Conclusions

Chapter 6: Overall Discussion

The primary focus of this thesis was to study the quaternary structure and dynamics of the human sHsps, Hsp27 and αB-c, in order to rationalise the effects these have on the capacity of these proteins to act as a molecular chaperones by inhibiting protein aggregation. Due to the large and heterogeneous nature of these mammalian sHsps, this work primarily employed native MS to study the structure and dynamics of these molecular chaperones. A detailed analysis was undertaken on the effect PTMs, in particular phosphorylation and disulfide-bonding on the structure of Hsp27. The results of this work highlight the pivotal role that PTMs have in regulating Hsp27 structure and hence chaperone function. In addition, the role of the N-terminal domain in modulating the structure and function of αB-c was assessed. Overall, the results of the work presented here emphasises the key role the quaternary structure has on the function of these mammalian sHsps, both of which are crucial parts of the network that acts to maintain proteostasis in cells.

6.1 The site-specific effect phosphorylation has on Hsp27 structure and chaperone function

The sHsp Hsp27 is an important member of the cells PQC network that aids in maintaining intracellular proteostasis. One key PTM that occurs in some human sHsps, including Hsp27, is phosphorylation. This PTM changes the quaternary structure and dynamics of Hsp27, whereby phosphorylation at all three serine residues decreases the size of Hsp27 oligomers (Hayes *et al.*, 2009, McDonald *et al.*, 2012, Rogalla *et al.*, 1999). However, up until the work described in this thesis (Chapter 3), there had not been a comprehensive survey performed on the specific effect(s) phosphorylation at each serine residue had on the oligomer size, oligomer distribution and chaperone function of Hsp27. Consequently, the first aim of this

thesis (Chapter 3) was to systematically examine the site-specific effects of phosphorylation on Hsp27.

In order to ascertain the role phosphorylation has on Hsp27 structure and chaperone function, seven distinct variants were produced in which phosphorylatable serine residues were substituted with aspartic acid residues, i.e. S15D, S78D and S82D, collectively referred to as isoforms with MMP. To assess the effect of phosphorylation on Hsp27 quaternary structure, native MS was used to examine how MMP changes the oligomeric distribution of Hsp27. Native MS was also used to observe the concentration-dependent dissociation of Hsp27 oligomers with successive MMP. This work showed that substitution at two serine residues had a significant impact on Hsp27 quaternary structure, reducing the size of Hsp27 oligomers, whilst substitution at three serine residues (i.e. Hsp27-3D) led to complete dissociation of oligomers into dimers. A strong correlation between oligomer dissociation (via increased MMP) and enhanced chaperone activity against amorphous and fibrillar client proteins was also observed. The results of this work support a model whereby the dimer is a more effective chaperone than the larger oligomers. This enhanced function, combined with dissociation, suggests that the inter-dimer contacts maintained in oligomeric Hsp27 are disrupted by the negative charges introduced by phosphorylation. It appears that the large oligomers act as reservoirs of these chaperone-active dimers. As a result, it is proposed that phosphorylation acts as a molecular switch, activating Hsp27 under conditions of cellular stress in order to boost the overall PQC network in the cell.

6.2 Post-translational modifications modulate the structure and dynamics of Hsp27 dimers and oligomers

This aspect of the project, described by the results presented in chapter 4 of this thesis, built on from the previous work (Chapter 3) in which it was concluded that Hsp27 dimers

were more chaperone-active than the larger oligomers. This work sought to address whether the enhanced chaperone activity of Hsp27 dimers is attributable to the dissociation of the large oligomers into dimers (differences in quaternary structure) or whether there are distinct differences in the structure and/or conformation of Hsp27 dimers (differences in tertiary structure) upon phosphorylation. Low resolution approaches (i.e. far UV-CD spectroscopy and intrinsic tryptophan fluorescence), despite being unable to discern between dimers and oligomers, showed that there are differences in the secondary and tertiary structure of Hsp27 with increased MMP. However, there is no conclusive evidence to indicate whether these observed changes in structure specifically alter the conformation of Hsp27 dimers. As a result, IM-MS was employed to identify potential differences in the conformation of Hsp27 dimers and oligomers. This study found that MMP make Hsp27 dimers more unstructured (i.e. more flexible) and more stable. However, there was no discernible difference in the overall conformation of Hsp27 12mers (and by inference all oligomers) with MMP. Thus, it is concluded that differences in the conformation and stability of Hsp27 dimers upon phosphorylation contribute to their enhanced chaperone activity.

The data presented in Chapter 4 conclusively shows that an increase in the number of MMP results in variation to the conformation of Hsp27 dimers; the dimer of Hsp27 becomes increasingly unstructured with MMP. This may be favourable for the recognition of misfolded proteins since the dimers are more adaptable and flexible. Previous studies which have shown that MMP, as well as phosphorylated forms of Hsp27, are more efficient at inhibiting the amorphous and fibrillar aggregation of client proteins compared to Hsp27-WT (Hayes *et al.*, 2009, Jovcevski *et al.*, 2015, McDonald *et al.*, 2012, Rogalla *et al.*, 1999). The increase in flexibility of the Hsp27 dimer observed in this work may facilitate Hsp27-3D

subunit-exchanging with Hsp27-WT. A Hsp27 oligomer comprising both phosphorylated and non-phosphorylated dimers must reach a critical point whereby the number of phosphorylated dimers incorporated into an oligomer leads to negative charge repulsions and hence dissociation. Interestingly, the observed rates of subunit-exchange between Hsp27-3D and Hsp27-WT oligomers were comparable to those between WT oligomers and with other subunit-exchange studies of other sHsps (Bova *et al.*, 1997, Bova *et al.*, 2000, Shashidharamurthy *et al.*, 2005). However, it must be noted that the bulk-FRET method of monitoring subunit-exchange of WT and 3D was performed by covalently-labelling lysine residues, which results in the subunit-exchange of labelled disulfide-linked dimers. Consequently, the subunit-exchange dynamics of disulfide-linked dimers may differ significantly to that of reduced Hsp27 in which monomers and dimers can exchange. Unfortunately, an MS-based approach could not be used for this experiment as the ionisation efficiency of Hsp27-3D is significantly greater than that of WT, resulting in the poor resolution of the Hsp27-WT/3D hetero-oligomer at high *m/z*.

Hsp27 is unique amongst the sHsp family in that dimerization also occurs via inter-molecular disulfide bonding of Cys137 that is located along the β6 sheet of the αCD (Hochberg *et al.*, 2014). This is in contrast to the dimer of αB-c, which is mediated only by a charged network along the β6+7 sheets (Bagneris *et al.*, 2009, Hochberg *et al.*, 2014). The effect of reduction of Cys137 is thought to contribute towards the increase in proportion of monomer in mutant Hsp27, which leads to chaperone hyperactivity in Charcot-Marie Tooth disease (Almeida-Souza *et al.*, 2010). In addition, Hsp27 has been shown to form disulfide-linked dimers in HeLa cell lysates (Arrigo, 2011). This highlights the importance of dimerization via Cys137 in Hsp27; however, no previous studies have extensively investigated the effects of reduction in terms of Hsp27 quaternary structure. As a result, the role of disulfide-bonding

in modulating the quaternary structure and dynamics of Hsp27 was investigated. By preventing the re-oxidation of the disulfide-bond with IA, a significant shift in the oligomeric equilibrium of Hsp27 occurred, such that smaller odd-sized species were observed. The generally accepted mechanism of action by which sHsps become chaperone-active is by oligomeric dissociation and enhanced rate of subunit-exchange, whereby the population of smaller 'chaperone-active' species (i.e. monomers and dimers) are responsible for inhibiting protein aggregation (Figure 6.1). However, the aggregating client protein is just as important in ascertaining how effective a sHsp is at inhibiting aggregation and must be taken into account when assessing sHsp function. In the case of Hsp27, disulfide-bond reduction at Cys137 is crucial as it contributes to the increased abundance of monomers, where a shift in the oligomeric equilibrium, towards smaller species, was observed. Based on the findings in this thesis, it is proposed that the abundance of smaller oligomers in disease mutants of Hsp27 to become 'hyperactive' such that it co-aggregates with client proteins (Almeida-Souza *et al.*, 2010, Benesch *et al.*, 2008). Thus, the abundance of dissociated Hsp27 in the cell, as well as the proportion of monomer and dimer, must be tightly regulated in order to avoid hyperactivity and hence disease. Overall, both phosphorylation and disulfide-bonding of Hsp27 lead to a range of structural transitions in the protein. These changes in structure underlie the increase in chaperone activity of Hsp27 during periods of cell stress, as well as in disease.

Future directions with this aspect of the project should focus on investigating the conformation of Hsp27 monomers post-reduction using IM-MS, with MMP used as the model system. Such an approach may reveal more observable differences in the flexibility of the dimer with MMP. It should be noted that such an approach should not be limited to just monomers and dimer. Other higher assemblies, particularly hexamers would be of

significant interest as many oligomeric models of αB-c (24-mer) are based upon the formation of hexamers prior to higher order oligomerisation (Braun *et al.*, 2011, Jehle *et al.*, 2011) and also may provide information on role of the N-terminal domain in maintaining the hexameric structure of Hsp27. Also, subunit-exchange analyses (via bulk-FRET and MS) between Hsp27-WT with single and double $Hsp27_M$ isoforms should be performed to determine whether the degree of MMP modulates the rate of subunit-exchange. In light of the role dimerization has on modulating Hsp27 quaternary structure, all the above analyses should also be performed under both reduced and reduced/thiol-blocked conditions. In addition, chaperone activity assays against amorphous and fibrillar client proteins (seeded αS, $A\beta^{1\text{-}40/42}$, insulin, BSA, κ-casein) should be performed to determine whether reduced and thiol-blocked Hsp27 becomes 'hyperactive' across a range of client proteins. Put together, these studies would reflect a greater physiological relevance in the cell as the population and abundance of all these potential protein species are likely to occur and interact *in vivo.*

6.3 The role of the N-terminal domain (residues 54-60) on the structure and chaperone function of αB-c

The work presented in Chapter 5 of this thesis aimed to determine the role of residues 54-60 in the N-terminal domain of αB-c with regards to the structure and chaperone function of the protein. Many studies have structurally and functionally characterised various point mutations of αB-c that have led to an apparent increase or decrease in chaperone function (Biswas *et al.*, 2007, Bova *et al.*, 1999, Horwitz *et al.*, 1998a, Santhoshkumar *et al.*, 2009, Sreelakshmi and Sharma, 2005, Sreelakshmi and Sharma, 2006). However, these studies typically employed relatively low-resolution approaches to characterise the tertiary and quaternary structure of αB-c. To address this, five distinct isoforms harbouring mutations in the disordered N-terminal domain of αB-c (P58A, S59A, S59K, R56S/S59R and invert 54-60)

were constructed and the structure and chaperone function of these isoforms was thoroughly characterised. The biophysical studies undertaken on these mutant αB-c isoforms demonstrate that these mutations result in various changes to the secondary and tertiary structure of αB-c. As the majority of these techniques are unable to overcome the structural heterogeneity of αB-c, native MS was utilised to observe any distinct changes in the quaternary structure of these isoforms resulting from mutation. However, there was no significant difference observed in quaternary structure of these mutant isoforms compared to αB-c WT, with the exception of the invert 54-60 mutation, which was skewed towards larger species. The ability of these isoforms to prevent amorphous and fibrillar aggregation was also not significantly different from αB-c WT, again with the exception of the invert 54-60 mutant which had a decreased ability to prevent the reduction-induced amorphous aggregation of insulin compared to αB-c WT. Overall, the lack of difference in the point mutant isoforms compared to αB-c WT with regards to quaternary structure correlates strongly with the mutants having a similar chaperone activity to αB-c WT. Therefore, it is concluded that the quaternary structure is the key determinant of αB-c chaperone activity. Support for this conclusion can be found in work using MMP of αB-c in which enhanced chaperone activity was a result of enhanced subunit-exchange, where the increased abundance of dissociated forms of αB-c (presumably dimers) contribute to its enhanced chaperone activity (Ecroyd *et al.*, 2007).

Future work, measuring the subunit-exchange rate of the mutant αB-c isoforms by native MS, will help to define whether the presence of dissociated species is either enhanced or diminished with mutation. As the mass of the monomeric form of these mutant isoforms are very close to that of αB-c WT (< 200 Da difference between the two isoforms), a labelling approach (e.g. ^{15}N or ^{13}C) should be used to provide clear resolution between

labelled and unlabelled αB-c. Another key future direction is to test the chaperone function of the N-terminal αB-c mutants against other client proteins such as κ-casein, $A\beta^{1-40/42}$, creatine phosphatase kinase, alcohol dehydrogenase and α-lactalbumin. This is particularly important as the chaperone activity of αB-c is also dependent on the aggregating client protein. Also, utilising IM-MS to observe whether there are any distinct differences in quaternary architecture with N-terminal mutation should also be examined and performing dilution native MS experiments would supplement this information in terms of whether N-terminal mutations significantly weaken the inter-dimer contacts that maintain αB-c oligomers.

Overall, the results of the work presented in this chapter indicates that the unstructured N-terminal domain of αB-c plays a key role in dictating oligomeric structure and dynamics of the protein, both of which are determinants of chaperone activity. Mutations at residues 54-60 translate the gross changes in both secondary and tertiary structure. These changes did not translate to large rearrangements in quaternary structure. The similarity in quaternary structure translated well with chaperone activity when compared to αB-c WT. The data suggests that there is an interlinked relationship between quaternary structure and dynamics with chaperone activity, to a point where the partially unstructured state of αB-c overcomes the effect of mutation and demonstrates the robustness nature of αB-c to effectively prevent protein aggregation.

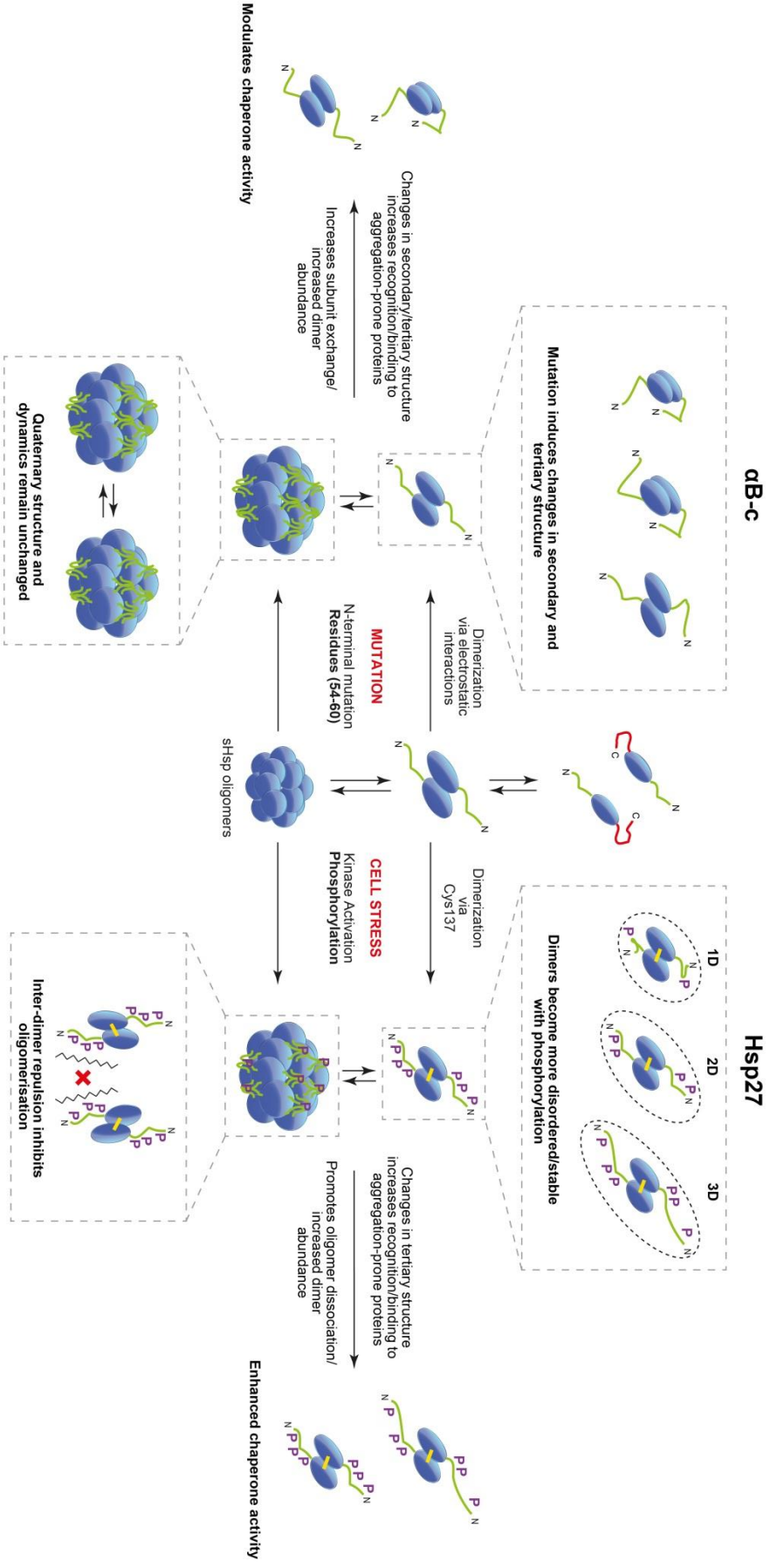
αB-c
Hsp27
Mutation induces changes in secondary and tertiary structure
Dimers become more disordered/stable with phosphorylation
1D
2D
3D
Dimerization via electrostatic interactions
Dimerization via Cys137
MUTATION
N-terminal mutation Residues (54-60)
CELL STRESS
Kinase Activation Phosphorylation
sHsp oligomers
Changes in secondary/tertiary structure increases recognition/binding to aggregation-prone proteins
Increases subunit exchange/ increased dimer abundance
Changes in tertiary structure increases recognition/binding to aggregation-prone proteins
Promotes oligomer dissociation/ increased dimer abundance
Modulates chaperone activity
Enhanced chaperone activity
Quaternary structure and dynamics remain unchanged
Inter-dimer repulsion inhibits oligomerisation

Figure 6.1: Modifications at the primary sequence level significantly alter the quaternary structure and dynamics of Hsp27 and αB-c which modulate chaperone activity.
The modification of sHsps is a defining factor in regulating sHsp structure and consequent chaperone function. The tertiary structure of sHsp monomers is comprised of the αCD (*blue ellipses/spheres*) and is flanked by the unstructured N-terminal (*green*) and flexible C-terminal (*red*) domains. Dimerization is mediated by either electrostatic interactions (αB-c) or disulfide-linkage (Hsp27; *yellow*) along the dimer interface on the αCD. Mutations in the N-terminal domain of αB-c results in the alteration of secondary and tertiary structure compared to WT. However, the quaternary structure remains relatively unchanged with mutation, which confers to comparable levels of chaperone activity. In the case of Hsp27, phosphorylation (P) at serine residues in the N-terminal domain results in oligomeric dissociation into dimers (via negative charged inter-dimer repulsions). Increased levels of phosphorylation also results in the dimers becoming more unstructured and more stable. These changes in structure aid in enhanced recognition and binding of misfolded proteins, contributing to its enhanced chaperone activity.

6.4 Concluding Remarks and Future Directions

Defining the structure-function relationship of sHsps is crucial to understanding the mechanisms involved in maintaining intracellular proteostasis. More importantly, delineating this relationship has the potential to inform therapeutic design, whereby the activation of sHsps is enhanced to combat neurodegenerative diseases that are associated with protein aggregation. For example, drugs could potentially be designed that trigger the dissociation of large sHsp oligomers into chaperone-active dimers, which would be ideal to inhibit and prevent protein aggregation.

A common problem in the sHsp literature is that many mammalian sHsps are ‘painted with the same brush’; conclusions as to the structure and chaperone function of all human sHsps tend to be based purely on information attained from studies of αB-c. The work in this thesis has shown that this should not be the case. There are significant differences in the structure and dynamics of Hsp27 compared to αB-c. For example, phosphorylation induces a range of downstream structural changes in Hsp27 that do not occur in αB-c, e.g. complete oligomeric dissociation. In addition, Hsp27 phosphorylation induces the 'chaperone-active' dimers to adopt a different conformation, becoming more unstructured and flexible with

increased levels of phosphorylation. However, it has yet to be established whether the structure of the monomer and/or dimer also changes upon phosphorylation of αB-c. These structural transitions significantly boost the chaperone activity of Hsp27 by enhancing the adaptability of dimers to recognise and interact with misfolded proteins, thereby preventing aggregation.

In light of this, there is much more work that needs to be done to further our understanding of the structure, function and interactions of sHsps within the cell. It is well-known that various sHsp family members are able to undergo subunit-exchange *in vitro* and *in vivo* to form large hetero-oligomers. Some of these hetero-oligomers have been previously studied, predominately Hsp27/αB-c (Aquilina *et al.*, 2013, Bova *et al.*, 2000), αA-c/αB-c (Aquilina *et al.*, 2005, Morris and Aquilina, 2010), Hsp16.9/Hsp18.1 (Sobott *et al.*, 2002) and more recently Hsp27/Hsp20 (Bukach *et al.*, 2009, Heirbaut *et al.*, 2016). However, all of the aforementioned studies have only investigated the WT isoforms of each sHsp; the hetero-oligomerisation dynamics between WT and phosphorylated isoforms has not been addressed. It is very likely that there are distinct populations of sHsp oligomers in cells that contain both non-phosphorylated and phosphorylated forms of various sHsps. These likely form a wide range of oligomeric forms of sHsps in cells, much more complicated than the 'simple' oligomers that have been studied in most work to date. Studies of the structure-function relationship, akin to those highlighted in this thesis, should be performed in these more complex hetero-oligomers. The detection, separation and sensitivity of technology present in mass spectrometers has significantly improved in recent years with the emergence of new generation Orbitrap mass spectrometers which can provide the necessary baseline resolution to detect hetero-oligomeric species without the use of labels,

particularly when analysing hetero-oligomeric species formed between single and double $Hsp27_M$ isoforms.

Our current understanding of sHsp structure and dynamics has largely been attained using purified recombinant proteins in relatively simple buffer systems. However, it remains to be determined whether the structure and dynamics of sHsps is similar when in the presence of other non-interacting proteins and/or crowding agents that can mimic the intracellular environment. An optimal crowding agent or non-interacting protein would be one that does not undergo subunit-exchange with sHsps, does not covalently attach to or modify sHsp residues, and does not directly contribute to aggregation, e.g. polyethylene glycol (PEG). Such a system would enable several unresolved questions to be answered. For example, does the concentration-dependent dissociation of Hsp27 also occur in the presence of crowding agents? Are subunit-exchange dynamics and chaperone activity of sHsps affected by molecular crowding? Previous work has shown that the molecular crowding agent trimethylamine N-oxide (TMAO) induced oligomerisation of Hsp20-WT, but had no effect on the oligomerisation state of phosphorylated Hsp20 (Sluchanko *et al.*, 2015). However, this study did not investigate how these changes in structure in the presence of crowding agent affected chaperone activity. Previous studies have also looked at the effect of crowding agents on the subunit-exchange of α-crystallin using dextran (Ghahghaei *et al.*, 2007), PEG, Ficoll and TMAO (Roman *et al.*, 2011). Both studies showed that the presence of these crowding agents lowered subunit-exchange rate and decreased chaperone activity (Ghahghaei *et al.*, 2007, Roman *et al.*, 2011). However, both studies only tested a single client protein (ovotransferrin and glycogen phosphorylase *b*) to measure the chaperone activity of α-crystallin in the presence of crowding agents. These studies also did not

determine the effect of crowding agents has on the oligomeric distribution of α-crystallin by SEC-MALS or MS. Of particular interest is the effect molecular crowding has on the structure and function of phosphorylated Hsp27 since the rationale for the enhanced chaperone activity of phosphorylated Hsp27 is the dissociation of large oligomers into dimers. Whilst this dissociation has been consistently observed by native-PAGE, analytical-SEC and native MS, it remains to be established whether dissociation occurs within the crowded environment of the cell. Overall, investigating the effects of molecular crowding on sHsp structure and function would provide a more relevant picture of the structural characteristics of sHsps, and how changes that occur to structure translate to differences in chaperone activity.

It is concluded that Hsp27-3D would be a useful model sHsp for use in a wide range of biophysical studies aimed at establishing precisely how sHsps interact with client proteins to prevent aggregation. For example, the stoichiometries of sHsp/client protein complexes may be able to be resolved using this dimeric form of Hsp27 through techniques such as native MS, X-ray co-crystallisation, single molecule fluorescence microscopy or NMR dispersion/relaxation experiments. These studies could also aid in determining the specific residues of Hsp27-3D involved in client protein binding and interaction. Similar experiments have been recently performed in order to investigate the regions of αB-c involved in binding to preventing the aggregation of lysozyme (amorphous) and $A\beta^{1-40}$ (fibrillar) (Mainz *et al.*, 2015). The advantage of using Hsp27-3D over αB-c is that these experiments did not use a predominantly dimeric sHsp; therefore regions that are involved in oligomerisation can confound the analyses, in particular since the oligomerisation state itself may vary in the presence of client proteins. Generally, binding to the aggregation-prone client protein that is

observed *in vitro* is highly dependent on the client protein of choice (Ecroyd *et al.*, 2007, Kulig and Ecroyd, 2012). Therefore, studies as stated above should be performed against a wide range of client proteins, in order to determine whether the specific residues of Hsp27-3D that are involved in the interaction with the client proteins are generic or specific for certain client proteins.

In conclusion, this thesis has demonstrated that modification of the unstructured N-terminal domain, by PTMs or mutation, of Hsp27 and αB-c induces changes in sHsp structure from the secondary to the quaternary level. It is concluded that, in general, factors that act to dissociate large oligomeric forms of these sHsps enhance chaperone activity. This work has increased our understanding of the roles PTMs have in regulating sHsp structure, and, in turn, modulating its chaperone activity. A better understanding of the mechanisms involved in regulating the structure-function relationship of sHsps provides new targets for therapeutic development. Enhancing the ability of sHsps to inhibit and prevent protein aggregation may one day lead to the development of a drug to treat a range of devastating neurodegenerative diseases.

Chapter 7:

References

Chapter 7: References

Ahmad, M. F., Raman, B., Ramakrishna, T. & Rao Ch, M. 2008. Effect of phosphorylation on alpha b-crystallin: Differences in stability, subunit exchange and chaperone activity of homo and mixed oligomers of alpha b-crystallin and its phosphorylation-mimicking mutant. *J Mol Biol,* 375**,** 1040-1051.

Almeida-Souza, L., Goethals, S., De Winter, V., Dierick, I., Gallardo, R., Van Durme, J., Irobi, J., Gettemans, J., Rousseau, F., Schymkowitz, J., Timmerman, V. & Janssens, S. 2010. Increased monomerization of mutant hspb1 leads to protein hyperactivity in charcot-marie-tooth neuropathy. *J Biol Chem,* 285**,** 12778-12786.

Anfinsen, C. B. 1973. Principles that govern the folding of protein chains. *Science,* 181**,** 223-230.

Aquilina, J. A., Benesch, J. L., Bateman, O. A., Slingsby, C. & Robinson, C. V. 2003. Polydispersity of a mammalian chaperone: Mass spectrometry reveals the population of oligomers in alphab-crystallin. *Proc Natl Acad Sci U S A,* 100**,** 10611-10616.

Aquilina, J. A., Benesch, J. L., Ding, L. L., Yaron, O., Horwitz, J. & Robinson, C. V. 2004. Phosphorylation of alphab-crystallin alters chaperone function through loss of dimeric substructure. *J Biol Chem,* 279**,** 28675-28680.

Aquilina, J. A., Benesch, J. L., Ding, L. L., Yaron, O., Horwitz, J. & Robinson, C. V. 2005. Subunit exchange of polydisperse proteins: Mass spectrometry reveals consequences of alphaa-crystallin truncation. *J Biol Chem,* 280**,** 14485-14491.

Aquilina, J. A., Shrestha, S., Morris, A. M. & Ecroyd, H. 2013. Structural and functional aspects of hetero-oligomers formed by the small heat shock proteins alphab-crystallin and hsp27. *J Biol Chem,* 288**,** 13602-13609.

Aquilina, J. A. & Watt, S. J. 2007. The n-terminal domain of alphab-crystallin is protected from proteolysis by bound substrate. *Biochem Biophys Res Commun,* 353**,** 1115-1120.

Arrigo, A. P. 2011. Structure-functions of hspb1 (hsp27). *Methods Mol Biol,* 787**,** 105-119.

Arrigo, A. P., Simon, S., Gibert, B., Kretz-Remy, C., Nivon, M., Czekalla, A., Guillet, D., Moulin, M., Diaz-Latoud, C. & Vicart, P. 2007. Hsp27 (hspb1) and alphab-crystallin (hspb5) as therapeutic targets. *FEBS Lett,* 581**,** 3665-3674.

Arts, H. J., Hollema, H., Lemstra, W., Willemse, P. H., De Vries, E. G., Kampinga, H. H. & Van Der Zee, A. G. 1999. Heat-shock-protein-27 (hsp27) expression in ovarian carcinoma: Relation in response to chemotherapy and prognosis. *Int J Cancer,* 84**,** 234-238.

Bagneris, C., Bateman, O. A., Naylor, C. E., Cronin, N., Boelens, W. C., Keep, N. H. & Slingsby, C. 2009. Crystal structures of alpha-crystallin domain dimers of alphab-crystallin and hsp20. *J Mol Biol,* 392**,** 1242-1252.

Balch, W. E., Morimoto, R. I., Dillin, A. & Kelly, J. W. 2008. Adapting proteostasis for disease intervention. *Science,* 319**,** 916-919.

Baldwin, A. J., Hilton, G. R., Lioe, H., Bagneris, C., Benesch, J. L. & Kay, L. E. 2011a. Quaternary dynamics of alphab-crystallin as a direct consequence of localised tertiary fluctuations in the c-terminus. *J Mol Biol,* 413**,** 310-320.

Baldwin, A. J., Lioe, H., Hilton, G. R., Baker, L. A., Rubinstein, J. L., Kay, L. E. & Benesch, J. L. 2011b. The polydispersity of alphab-crystallin is rationalized by an interconverting polyhedral architecture. *Structure,* 19**,** 1855-1863.

Baldwin, A. J., Lioe, H., Robinson, C. V., Kay, L. E. & Benesch, J. L. 2011c. Alphab-crystallin polydispersity is a consequence of unbiased quaternary dynamics. *J Mol Biol,* 413**,** 297-309.

Baranova, E. V., Weeks, S. D., Beelen, S., Bukach, O. V., Gusev, N. B. & Strelkov, S. V. 2011. Three-dimensional structure of alpha-crystallin domain dimers of human small heat shock proteins hspb1 and hspb6. *J Mol Biol,* 411**,** 110-122.

Basha, E., Jones, C., Wysocki, V. & Vierling, E. 2010. Mechanistic differences between two conserved classes of small heat shock proteins found in the plant cytosol. *J Biol Chem,* 285**,** 11489-11497.

Basha, E., O'neill, H. & Vierling, E. 2012. Small heat shock proteins and alpha-crystallins: Dynamic proteins with flexible functions. *Trends Biochem Sci,* 37**,** 106-117.

Beckmann, R. P., Mizzen, L. E. & Welch, W. J. 1990. Interaction of hsp 70 with newly synthesized proteins: Implications for protein folding and assembly. *Science,* 248**,** 850-854.

Benesch, J. L. 2009. Collisional activation of protein complexes: Picking up the pieces. *J Am Soc Mass Spectrom,* 20**,** 341-348.

Benesch, J. L., Aquilina, J. A., Baldwin, A. J., Rekas, A., Stengel, F., Lindner, R. A., Basha, E., Devlin, G. L., Horwitz, J., Vierling, E., Carver, J. A. & Robinson, C. V. 2010. The quaternary organization and dynamics of the molecular chaperone hsp26 are thermally regulated. *Chem Biol,* 17**,** 1008-1017.

Benesch, J. L., Aquilina, J. A., Ruotolo, B. T., Sobott, F. & Robinson, C. V. 2006. Tandem mass spectrometry reveals the quaternary organization of macromolecular assemblies. *Chem Biol,* 13**,** 597-605.

Benesch, J. L., Ayoub, M., Robinson, C. V. & Aquilina, J. A. 2008. Small heat shock protein activity is regulated by variable oligomeric substructure. *J Biol Chem,* 283**,** 28513-28517.

Benesch, J. L. & Ruotolo, B. T. 2011. Mass spectrometry: Come of age for structural and dynamical biology. *Curr Opin Struct Biol,* 21**,** 641-649.

Berry, V., Francis, P., Reddy, M. A., Collyer, D., Vithana, E., Mackay, I., Dawson, G., Carey, A. H., Moore, A., Bhattacharya, S. S. & Quinlan, R. A. 2001. Alpha-b crystallin gene (cryab) mutation causes dominant congenital posterior polar cataract in humans. *Am J Hum Genet,* 69**,** 1141-1145.

Bhat, S. P. & Nagineni, C. N. 1989. Alpha b subunit of lens-specific protein alpha-crystallin is present in other ocular and non-ocular tissues. *Biochem Biophys Res Commun,* 158**,** 319-325.

Binger, K. J., Ecroyd, H., Yang, S., Carver, J. A., Howlett, G. J. & Griffin, M. D. 2013. Avoiding the oligomeric state: Alphab-crystallin inhibits fragmentation and induces dissociation of apolipoprotein c-ii amyloid fibrils. *FASEB J,* 27**,** 1214-1222.

Biswas, A., Goshe, J., Miller, A., Santhoshkumar, P., Luckey, C., Bhat, M. B. & Nagaraj, R. H. 2007. Paradoxical effects of substitution and deletion mutation of arg56 on the structure and chaperone function of human alphab-crystallin. *Biochemistry,* 46**,** 1117-1127.

Bloemendal, H. 1977. The vertebrate eye lens. *Science,* 197**,** 127-137.

Boncoraglio, A., Minoia, M. & Carra, S. 2012. The family of mammalian small heat shock proteins (hspbs): Implications in protein deposit diseases and motor neuropathies. *Int J Biochem Cell Biol,* 44**,** 1657-1669.

Bova, M. P., Ding, L. L., Horwitz, J. & Fung, B. K. 1997. Subunit exchange of alphaa-crystallin. *J Biol Chem,* 272**,** 29511-29517.

Bova, M. P., Mchaourab, H. S., Han, Y. & Fung, B. K. 2000. Subunit exchange of small heat shock proteins. Analysis of oligomer formation of alphaa-crystallin and hsp27 by fluorescence resonance energy transfer and site-directed truncations. *J Biol Chem,* 275**,** 1035-1042.

Bova, M. P., Yaron, O., Huang, Q., Ding, L., Haley, D. A., Stewart, P. L. & Horwitz, J. 1999. Mutation r120g in alphab-crystallin, which is linked to a desmin-related myopathy, results in an irregular structure and defective chaperone-like function. *Proc Natl Acad Sci U S A,* 96**,** 6137-6142.

Braun, N., Zacharias, M., Peschek, J., Kastenmuller, A., Zou, J., Hanzlik, M., Haslbeck, M., Rappsilber, J., Buchner, J. & Weinkauf, S. 2011. Multiple molecular architectures of the eye lens chaperone alphab-crystallin elucidated by a triple hybrid approach. *Proc Natl Acad Sci U S A,* 108**,** 20491-20496.

Buchner, J. 1996. Supervising the fold: Functional principles of molecular chaperones. *FASEB J,* 10**,** 10-19.

Buell, A. K., Galvagnion, C., Gaspar, R., Sparr, E., Vendruscolo, M., Knowles, T. P., Linse, S. & Dobson, C. M. 2014. Solution conditions determine the relative importance of nucleation and growth processes in alpha-synuclein aggregation. *Proc Natl Acad Sci U S A,* 111**,** 7671-7676.

Bukach, O. V., Glukhova, A. E., Seit-Nebi, A. S. & Gusev, N. B. 2009. Heterooligomeric complexes formed by human small heat shock proteins hspb1 (hsp27) and hspb6 (hsp20). *Biochim Biophys Acta,* 1794**,** 486-495.

Bukach, O. V., Seit-Nebi, A. S., Marston, S. B. & Gusev, N. B. 2004. Some properties of human small heat shock protein hsp20 (hspb6). *Eur J Biochem,* 271**,** 291-302.

Carver, J. A., Lindner, R. A., Lyon, C., Canet, D., Hernandez, H., Dobson, C. M. & Redfield, C. 2002. The interaction of the molecular chaperone alpha-crystallin with unfolding alpha-lactalbumin: A structural and kinetic spectroscopic study. *J Mol Biol,* 318**,** 815-827.

Cassiman, J. J., Marynen, P., Brugmans, M., Van Leuven, F. & Van Den Berghe, H. 1981. Role of the alpha 2m-receptor in attachment and spreading of human fibroblasts. *Cell Biol Int Rep,* 5**,** 901-911.

Caughey, B. & Lansbury, P. T. 2003. Protofibrils, pores, fibrils, and neurodegeneration: Separating the responsible protein aggregates from the innocent bystanders. *Annu Rev Neurosci,* 26**,** 267-298.

Chen, Q., Ma, J., Yan, M., Mothobi, M. E., Liu, Y. & Zheng, F. 2009. A novel mutation in cryab associated with autosomal dominant congenital nuclear cataract in a chinese family. *Mol Vis,* 15**,** 1359-1365.

Cheng, M. Y., Hartl, F. U., Martin, J., Pollock, R. A., Kalousek, F., Neupert, W., Hallberg, E. M., Hallberg, R. L. & Horwich, A. L. 1989. Mitochondrial heat-shock protein hsp60 is essential for assembly of proteins imported into yeast mitochondria. *Nature,* 337**,** 620-625.

Chiti, F. & Dobson, C. M. 2006. Protein misfolding, functional amyloid, and human disease. *Annu Rev Biochem,* 75**,** 333-366.

Clark, A. R., Naylor, C. E., Bagneris, C., Keep, N. H. & Slingsby, C. 2011. Crystal structure of r120g disease mutant of human alphab-crystallin domain dimer shows closure of a groove. *J Mol Biol,* 408**,** 118-134.

Clark, J. I. & Muchowski, P. J. 2000. Small heat-shock proteins and their potential role in human disease. *Curr Opin Struct Biol,* 10**,** 52-59.

Cornford, P. A., Dodson, A. R., Parsons, K. F., Desmond, A. D., Woolfenden, A., Fordham, M., Neoptolemos, J. P., Ke, Y. & Foster, C. S. 2000. Heat shock protein expression independently predicts clinical outcome in prostate cancer. *Cancer Res,* 60**,** 7099-7105.

Cox, D., Selig, E., Griffin, M. D., Carver, J. A. & Ecroyd, H. 2016. Small heat shock proteins prevent alpha-synuclein aggregation via transient interactions and their efficacy is affected by the rate of aggregation. *J Biol Chem*.

Csermely, P., Soti, C., Kalmar, E., Papp, E., Pato, B., Vermes, A. & Sreedhar, A. S. 2003. Molecular chaperones, evolution and medicine *J Mol Struct,* 666-667**,** 373-380.

Datskevich, P. N., Mymrikov, E. V., Sluchanko, N. N., Shemetov, A. A., Sudnitsyna, M. V. & Gusev, N. B. 2012. Expression, purification and some properties of fluorescent chimeras of human small heat shock proteins. *Protein Expr Purif,* 82**,** 45-54.

De Jong, W. W., Van Kleef, F. S. & Bloemendal, H. 1974. Intracellular carboxy-terminal degradation of the alpha a chain of alpha-crystallin. *Eur J Biochem,* 48**,** 271-276.

Delaye, M. & Tardieu, A. 1983. Short-range order of crystallin proteins accounts for eye lens transparency. *Nature,* 302**,** 415-417.

Delbecq, S. P., Jehle, S. & Klevit, R. 2012. Binding determinants of the small heat shock protein, alphab-crystallin: Recognition of the 'ixi' motif. *EMBO J,* 31**,** 4587-4594.

Delbecq, S. P. & Klevit, R. E. 2013. One size does not fit all: The oligomeric states of alphab crystallin. *FEBS Lett,* 587**,** 1073-1080.

Devi, R. R., Yao, W., Vijayalakshmi, P., Sergeev, Y. V., Sundaresan, P. & Hejtmancik, J. F. 2008. Crystallin gene mutations in indian families with inherited pediatric cataract. *Mol Vis,* 14**,** 1157-1170.

Dinner, A. R., Sali, A., Smith, E. J., Dobson, C. M. & Karplus, M. 2000. Understanding protein folding via free-energy surfaces from theroy and experiment. *Trends Biochem Sci,* 25**,** 331-339.

Dobson, C. M. 1999. Protein misfolding, evolution and disease. *Trends Biochem Sci,* 24**,** 329-332.

Dobson, C. M. 2003. Protein folding and misfolding. *Nature,* 426**,** 884-890.

Dobson, C. M. 2004. Experimental investigation of protein folding and misfolding. *Methods,* 34**,** 4-14.

Doshi, B. M., Hightower, L. E. & Lee, J. 2010. Hspb1, actin filament dynamics, and aging cells. *Ann N Y Acad Sci,* 1197**,** 76-84.

Ecroyd, H. & Carver, J. A. 2008. The effect of small molecules in modulating the chaperone activity of alphab-crystallin against ordered and disordered protein aggregation. *FEBS J,* 275**,** 935-947.

Ecroyd, H. & Carver, J. A. 2009. Crystallin proteins and amyloid fibrils. *Cell Mol Life Sci,* 66**,** 62-81.

Ecroyd, H., Koudelka, T., Thorn, D. C., Williams, D. M., Devlin, G., Hoffmann, P. & Carver, J. A. 2008. Dissociation from the oligomeric state is the rate-limiting step in fibril formation by kappa-casein. *J Biol Chem,* 283**,** 9012-9022.

Ecroyd, H., Meehan, S., Horwitz, J., Aquilina, J. A., Benesch, J. L., Robinson, C. V., Macphee, C. E. & Carver, J. A. 2007. Mimicking phosphorylation of alphab-crystallin affects its chaperone activity. *Biochem J,* 401**,** 129-141.

Edwards, H. V., Cameron, R. T. & Baillie, G. S. 2011. The emerging role of hsp20 as a multifunctional protective agent. *Cell Signal,* 23**,** 1447-1454.

Eschweiler, J. D., Rabuck-Gibbons, J. N., Tian, Y. & Ruotolo, B. T. 2015. Ciusuite: A quantitative analysis package for collision induced unfolding measurements of gas-phase protein ions. *Anal Chem,* 87**,** 11516-11522.

Evgrafov, O. V., Mersiyanova, I., Irobi, J., Van Den Bosch, L., Dierick, I., Leung, C. L., Schagina, O., Verpoorten, N., Van Impe, K., Fedotov, V., Dadali, E., Auer-Grumbach, M., Windpassinger, C., Wagner, K., Mitrovic, Z., Hilton-Jones, D., Talbot, K., Martin, J. J., Vasserman, N., Tverskaya, S., Polyakov, A., Liem, R. K., Gettemans, J., Robberecht, W., De Jonghe, P. & Timmerman, V. 2004. Mutant small heat-shock protein 27 causes axonal charcot-marie-tooth disease and distal hereditary motor neuropathy. *Nat Genet,* 36**,** 602-606.

Fenton, W. A., Kashi, Y., Furtak, K. & Horwich, A. L. 1994. Residues in chaperonin groel required for polypeptide binding and release. *Nature,* 371**,** 614-619.

Fink, A. 1999. Chaperone-mediated protein folding. *Physiol Rev,* 79**,** 425-449.

Fitzpatrick, A. W., Debelouchina, G. T., Bayro, M. J., Clare, D. K., Caporini, M. A., Bajaj, V. S., Jaroniec, C. P., Wang, L., Ladizhansky, V., Muller, S. A., Macphee, C. E., Waudby, C. A., Mott, H. R., De Simone, A., Knowles, T. P., Saibil, H. R., Vendruscolo, M., Orlova, E. V., Griffin, R. G. & Dobson, C. M. 2013. Atomic structure and hierarchical assembly of a cross-beta amyloid fibril. *Proc Natl Acad Sci U S A,* 110**,** 5468-5473.

Gaestel, M., Schroder, W., Benndorf, R., Lippmann, C., Buchner, K., Hucho, F., Erdmann, V. A. & Bielka, H. 1991. Identification of the phosphorylation sites of the murine small heat shock protein hsp25. *J Biol Chem,* 266**,** 14721-14724.

Garrido, C. 2002. Size matters: Of the small hsp27 and its large oligomers. *Cell Death Differ,* 9**,** 483-485.

Garrido, C., Bruey, J. M., Fromentin, A., Hammann, A., Arrigo, A. P. & Solary, E. 1999. Hsp27 inhibits cytochrome c-dependent activation of procaspase-9. *FASEB J,* 13**,** 2061-2070.

Garrido, C., Ottavi, P., Fromentin, A., Hammann, A., Arrigo, A. P., Chauffert, B. & Mehlen, P. 1997. Hsp27 as a mediator of confluence-dependent resistance to cell death induced by anticancer drugs. *Cancer Res,* 57**,** 2661-2667.

Garrido, C., Paul, C., Seigneuric, R. & Kampinga, H. H. 2012. The small heat shock proteins family: The long forgotten chaperones. *Int J Biochem Cell Biol,* 44**,** 1588-1592.

Gasteiger E., H. C., Gattiker A., Duvaud S., Wilkins M.R., Appel R.D., Bairoch A.; 2005. *Protein identification and analysis tools on the expasy server*, Humana Press

Ghahghaei, A., Rekas, A., Price, W. E. & Carver, J. A. 2007. The effect of dextran on subunit exchange of the molecular chaperone alphaa-crystallin. *Biochim Biophys Acta,* 1774**,** 102-111.

Graceffa, P. 2011. Hsp27-actin interaction. *Biochem Res Int,* 2011**,** 901572.

Gregersen, N., Bross, P., Vang, S. & Christensen, J. H. 2006. Protein misfolding and human disease. *Annual Review of Genomics and Human Genetics,* 7**,** 103-124.

Guo, Y., Hernandez, I., Isermann, B., Kang, T., Medved, L., Sood, R., Kerschen, E. J., Holyst, T., Mosesson, M. W. & Weiler, H. 2009. Caveolin-1-dependant apoptosis induced by fibrin degradation products. *Blood,* 113**,** 4431-4439.

Haley, D. A., Horwitz, J. & Stewart, P. L. 1998. The small heat-shock protein, alphab-crystallin, has a variable quaternary structure. *J Mol Biol,* 277**,** 27-35.

Hartl, F. U., Martin, J. & Neupert, W. 1992. Protein folding in the cell: The role of molecular chaperones hsp70 and hsp60. *Annu Rev Biophys Biomol Struct,* 21**,** 293-322.

Hayes, D., Napoli, V., Mazurkie, A., Stafford, W. F. & Graceffa, P. 2009. Phosphorylation dependence of hsp27 multimeric size and molecular chaperone function. *J Biol Chem,* 284**,** 18801-18807.

Heirbaut, M., Lermyte, F., Martin, E. M., Beelen, S., Verschueren, T., Sobott, F., Strelkov, S. V. & Weeks, S. D. 2016. The preferential heterodimerization of human small heat shock proteins hspb1 and hspb6 is dictated by the n-terminal domain. *Arch Biochem Biophys,* 610**,** 41-50.

Hickey, E., Brandon, S. E., Potter, R., Stein, G., Stein, J. & Weber, L. A. 1986. Sequence and organization of genes encoding the human 27 kda heat shock protein. *Nucleic Acids Res,* 14**,** 4127-4145.

Hilton, G. R. & Benesch, J. L. 2012. Two decades of studying non-covalent biomolecular assemblies by means of electrospray ionization mass spectrometry. *J R Soc Interface,* 9**,** 801-816.

Hilton, G. R., Hochberg, G. K., Laganowsky, A., Mcginnigle, S. I., Baldwin, A. J. & Benesch, J. L. 2013. C-terminal interactions mediate the quaternary dynamics of alphab-crystallin. *Philos Trans R Soc Lond B Biol Sci,* 368**,** 20110405.

Hochberg, G. K. & Benesch, J. L. 2014. Dynamical structure of alphab-crystallin. *Prog Biophys Mol Biol*.

Hochberg, G. K., Ecroyd, H., Liu, C., Cox, D., Cascio, D., Sawaya, M. R., Collier, M. P., Stroud, J., Carver, J. A., Baldwin, A. J., Robinson, C. V., Eisenberg, D. S., Benesch, J. L. & Laganowsky, A. 2014. The structured core domain of alphab-crystallin can prevent amyloid fibrillation and associated toxicity. *Proc Natl Acad Sci U S A,* 111**,** E1562-1570.

Horwitz, J., Bova, M., Huang, Q. L., Ding, L., Yaron, O. & Lowman, S. 1998a. Mutation of alpha b-crystallin: Effects on chaperone-like activity. *Int J Biol Macromol,* 22**,** 263-269.

Horwitz, J., Bova, M. P., Ding, L. L., Haley, D. A. & Stewart, P. L. 1999. Lens alpha-crystallin: Function and structure. *Eye (Lond),* 13 (Pt 3b)**,** 403-408.

Horwitz, J., Huang, Q. L., Ding, L. & Bova, M. P. 1998b. Lens alpha-crystallin: Chaperone-like properties. *Methods Enzymol,* 290**,** 365-383.

Houlden, H., Laura, M., Wavrant-De Vrieze, F., Blake, J., Wood, N. & Reilly, M. M. 2008. Mutations in the hsp27 (hspb1) gene cause dominant, recessive, and sporadic distal hmn/cmt type 2. *Neurology,* 71**,** 1660-1668.

Ikeda, Y., Abe, A., Ishida, C., Takahashi, K., Hayasaka, K. & Yamada, M. 2009. A clinical phenotype of distal hereditary motor neuronopathy type ii with a novel hspb1 mutation. *J Neurol Sci,* 277**,** 9-12.

Inagaki, N., Hayashi, T., Arimura, T., Koga, Y., Takahashi, M., Shibata, H., Teraoka, K., Chikamori, T., Yamashina, A. & Kimura, A. 2006. Alpha b-crystallin mutation in dilated cardiomyopathy. *Biochem Biophys Res Commun,* 342**,** 379-386.

Inoue, R., Takata, T., Fujii, N., Ishii, K., Uchiyama, S., Sato, N., Oba, Y., Wood, K., Kato, K., Fujii, N. & Sugiyama, M. 2016. New insight into the dynamical system of alphab-crystallin oligomers. *Sci Rep,* 6**,** 29208.

Ito, H., Okamoto, K., Nakayama, H., Isobe, T. & Kato, K. 1997. Phosphorylation of alphab-crystallin in response to various types of stress. *J Biol Chem,* 272**,** 29934-29941.

Iwaki, T., Wisniewski, T., Iwaki, A., Corbin, E., Tomokane, N., Tateishi, J. & Goldman, J. E. 1992. Accumulation of alpha b-crystallin in central nervous system glia and neurons in pathologic conditions. *Am J Pathol,* 140**,** 345-356.

Jakob, U., Gaestel, M., Engel, K. & Buchner, J. 1993. Small heat-shock proteins are molecular chaperones. *J Biol Chem,* 268**,** 1517-1520.

James, P. A., Rankin, J. & Talbot, K. 2008. Asymmetrical late onset motor neuropathy associated with a novel mutation in the small heat shock protein hspb1 (hsp27). *J Neurol Neurosurg Psychiatry,* 79**,** 461-463.

Jehle, S., Rajagopal, P., Bardiaux, B., Markovic, S., Kuhne, R., Stout, J. R., Higman, V. A., Klevit, R. E., Van Rossum, B. J. & Oschkinat, H. 2010. Solid-state nmr and saxs studies provide a structural basis for the activation of alphab-crystallin oligomers. *Nat Struct Mol Biol,* 17**,** 1037-1042.

Jehle, S., Vollmar, B. S., Bardiaux, B., Dove, K. K., Rajagopal, P., Gonen, T., Oschkinat, H. & Klevit, R. E. 2011. N-terminal domain of alphab-crystallin provides a conformational switch for multimerization and structural heterogeneity. *Proc Natl Acad Sci U S A,* 108**,** 6409-6414.

Jonak, C., Mildner, M., Klosner, G., Paulitschke, V., Kunstfeld, R., Pehamberger, H., Tschachler, E. & Trautinger, F. 2011. The hsp27 kd heat shock protein and p38-mapk signalling are required for regular epidermal differentiation. *J Dermatol Sci,* 61**,** 32-37.

Jovcevski, B., Kelly, M. A., Rote, A. P., Berg, T., Gastall, H. Y., Benesch, J. L., Aquilina, J. A. & Ecroyd, H. 2015. Phosphomimics destabilize hsp27 oligomeric assemblies and enhance chaperone activity. *Chem Biol,* 22**,** 186-195.

Kampinga, H. H., Brunsting, J. F., Stege, G. J., Konings, A. W. & Landry, J. 1994. Cells overexpressing hsp27 show accelerated recovery from heat-induced nuclear protein aggregation. *Biochem Biophys Res Commun,* 204**,** 1170-1177.

Kato, K., Inaguma, Y., Ito, H., Iida, K., Iwamoto, I., Kamei, K., Ochi, N., Ohta, H. & Kishikawa, M. 2001. Ser-59 is the major phosphorylation site in alphab-crystallin accumulated in the brains of patients with alexander's disease. *J Neurochem,* 76**,** 730-736.

Kato, K., Shinohara, H., Goto, S., Inaguma, Y., Morishita, R. & Asano, T. 1992. Copurification of small heat shock protein with alpha b crystallin from human skeletal muscle. *J Biol Chem,* 267**,** 7718-7725.

Kato, K., Shinohara, H., Kurobe, N., Inaguma, Y., Shimizu, K. & Ohshima, K. 1991. Tissue distribution and developmental profiles of immunoreactive alpha b crystallin in the rat determined with a sensitive immunoassay system. *Biochim Biophys Acta,* 1074**,** 201-208.

Kelly, J. W. 1997. Amyloid fibril formation and protein misassembly: A structural quest for insights into amyloid and prion diseases. *Structure,* 5**,** 595-600.

Khan, A. O., Abu Safieh, L. & Alkuraya, F. S. 2010. Later retinal degeneration following childhood surgical aphakia in a family with recessive cryab mutation (p.R56w). *Ophthalmic Genet,* 31**,** 30-36.

Kijima, K., Numakura, C., Goto, T., Takahashi, T., Otagiri, T., Umetsu, K. & Hayasaka, K. 2005. Small heat shock protein 27 mutation in a japanese patient with distal hereditary motor neuropathy. *J Hum Genet,* 50**,** 473-476.

Kim, P. S. & Baldwin, R. L. 1982. Specific intermediates in the folding reactions of small proteins and the mechanism of protein folding. *Ann Rev Biochem,* 51**,** 459-489.

Koteiche, H. A. & Mchaourab, H. S. 2003. Mechanism of chaperone function in small heat-shock proteins. Phosphorylation-induced activation of two-mode binding in alphab-crystallin. *J Biol Chem,* 278**,** 10361-10367.

Krishna, M. M. G., Lin, Y. & Englander, W. 2004. Protein misfolding: Optimal barriers, misfolded intermediates and pathway heterogeneity. *J Mol Biol,* 343**,** 1095-1109.

Kulig, M. & Ecroyd, H. 2012. The small heat-shock protein alphab-crystallin uses different mechanisms of chaperone action to prevent the amorphous versus fibrillar aggregation of alpha-lactalbumin. *Biochem J,* 448**,** 343-352.

Laganowsky, A., Benesch, J. L., Landau, M., Ding, L., Sawaya, M. R., Cascio, D., Huang, Q., Robinson, C. V., Horwitz, J. & Eisenberg, D. 2010. Crystal structures of truncated alphaa and alphab crystallins reveal structural mechanisms of polydispersity important for eye lens function. *Protein Sci,* 19**,** 1031-1043.

Lambert, H., Charette, S. J., Bernier, A. F., Guimond, A. & Landry, J. 1999. Hsp27 multimerization mediated by phosphorylation-sensitive intermolecular interactions at the amino terminus. *J Biol Chem,* 274**,** 9378-9385.

Landry, J., Lambert, H., Zhou, M., Lavoie, J. N., Hickey, E., Weber, L. A. & Anderson, C. W. 1992a. Human hsp27 is phosphorylated at serines 78 and 82 by heat shock and mitogen-activated kinases that recognize the same amino acid motif as s6 kinase ii. *J Biol Chem,* 267**,** 794-803.

Landry, S. J., Jordan, R., Mcmacken, R. & Gierasch, L. M. 1992b. Different conformations for the same polypeptide bound to chaperones dnak and groel. *Nature,* 355**,** 455-457.

Langer, T., Lu, C., Echols, H., Flanagan, J., Hayer, M. K. & Hartl, F. U. 1992a. Successive action of dnak, dnaj and groel along the pathway of chaperone-mediated protein folding. *Nature,* 356**,** 683-689.

Langer, T., Pfeifer, G., Martin, J., Baumeister, W. & Hartl, F. U. 1992b. Chaperonin-mediated protein folding: Groes binds to one end of the groel cylinder, which accommodates the protein substrate within its central cavity. *EMBO J,* 11**,** 4757-4765.

Lelj-Garolla, B. & Mauk, A. G. 2006. Self-association and chaperone activity of hsp27 are thermally activated. *J Biol Chem,* 281**,** 8169-8174.

Lindner, R. A., Kapur, A. & Carver, J. A. 1997. The interaction of the molecular chaperone, alpha-crystallin, with molten globule states of bovine alpha-lactalbumin. *J Biol Chem,* 272**,** 27722-27729.

Liu, Y., Graetz, M., Ho, L. & Pukala, T. L. 2015. Ion mobility-mass spectrometry-based screening for inhibition of alpha- synuclein aggregation. *Eur J Mass Spectrom (Chichester),* 21**,** 255-264.

Liu, Y., Zhang, X., Luo, L., Wu, M., Zeng, R., Cheng, G., Hu, B., Liu, B., Liang, J. J. & Shang, F. 2006. A novel alphab-crystallin mutation associated with autosomal dominant congenital lamellar cataract. *Invest Ophthalmol Vis Sci,* 47**,** 1069-1075.

Luigetti, M., Fabrizi, G. M., Madia, F., Ferrarini, M., Conte, A., Del Grande, A., Tasca, G., Tonali, P. A. & Sabatelli, M. 2010. A novel hspb1 mutation in an italian patient with cmt2/dhmn phenotype. *J Neurol Sci,* 298**,** 114-117.

Mainz, A., Peschek, J., Stavropoulou, M., Back, K. C., Bardiaux, B., Asami, S., Prade, E., Peters, C., Weinkauf, S., Buchner, J. & Reif, B. 2015. The chaperone alphab-crystallin uses different interfaces to capture an amorphous and an amyloid client. *Nat Struct Mol Biol,* 22**,** 898-905.

Makin, O. S., Atkins, E., Sikorski, P., Johansson, J. & Serpell, L. C. 2005. Molecular basis for amyloid fibril formation and stability. *PNAS,* 102**,** 315-320.

Markossian, K. A. & Kurganov, B. I. 2004. Protein folding, misfolding and aggregation. Formation of inclusion bodies and aggresomes. *Biochemistry (Moscow),* 69**,** 971-984.

Markossian, K. A., Yudin, I. K. & Kurganov, B. I. 2009. Mechanism of suppression of protein aggregation by α-crystallin. *Int J Mol Sci,* 10**,** 1314-1345.

Martin, J., Mayhew, M., Langer, T. & Hartl, F. U. 1993. The reaction cycle of groel and groes in chaperonin-assisted protein folding. *Nature,* 366**,** 228-233.

Marty, M. T., Baldwin, A. J., Marklund, E. G., Hochberg, G. K., Benesch, J. L. & Robinson, C. V. 2015. Bayesian deconvolution of mass and ion mobility spectra: From binary interactions to polydisperse ensembles. *Anal Chem,* 87**,** 4370-4376.

Masuda, M., Dohmae, N., Nonaka, T., Oikawa, T., Hisanaga, S., Goedert, M. & Hasegawa, M. 2006. Cysteine misincorporation in bacterially expressed human alpha-synuclein. *FEBS Lett,* 580**,** 1775-1779.

Mayhew, M., Da Silva, A. C., Martin, J., Erdjument-Bromage, H., Tempst, P. & Hartl, F. U. 1996. Protein folding in the central cavity of the groel-groes chaperonin complex. *Nature,* 379**,** 420-426.

Mcalary, L., Yerbury, J. J. & Aquilina, J. A. 2013. Glutathionylation potentiates benign superoxide dismutase 1 variants to the toxic forms associated with amyotrophic lateral sclerosis. *Sci Rep,* 3**,** 3275.

Mcdonald, E. T., Bortolus, M., Koteiche, H. A. & Mchaourab, H. S. 2012. Sequence, structure, and dynamic determinants of hsp27 (hspb1) equilibrium dissociation are encoded by the n-terminal domain. *Biochemistry,* 51**,** 1257-1268.

Mchaourab, H. S., Godar, J. A. & Stewart, P. L. 2009. Structure and mechanism of protein stability sensors: Chaperone activity of small heat shock proteins. *Biochemistry,* 48**,** 3828-3837.

Micsonai, A., Wien, F., Kernya, L., Lee, Y. H., Goto, Y., Refregiers, M. & Kardos, J. 2015. Accurate secondary structure prediction and fold recognition for circular dichroism spectroscopy. *Proc Natl Acad Sci U S A,* 112**,** E3095-3103.

Miesbauer, L. R., Zhou, X., Yang, Z., Yang, Z., Sun, Y., Smith, D. L. & Smith, J. B. 1994. Post-translational modifications of water-soluble human lens crystallins from young adults. *J Biol Chem,* 269**,** 12494-12502.

Morris, A. M. & Aquilina, J. A. 2010. Evidence for specific subunit distribution and interactions in the quaternary structure of alpha-crystallin. *Proteins,* 78**,** 2546-2553.

Muchowski, P. J., Bassuk, J. A., Lubsen, N. H. & Clark, J. I. 1997. Human alphab-crystallin. Small heat shock protein and molecular chaperone. *J Biol Chem,* 272**,** 2578-2582.

Numoto, N., Kita, A., Fujii, N. & Miki, K. 2012. A p39r mutation at the n-terminal domain of human alphab-crystallin regulates its oligomeric state and chaperone-like activity. *Biochem Biophys Res Commun,* 425**,** 601-606.

Ojha, J., Masilamoni, G., Dunlap, D., Udoff, R. A. & Cashikar, A. G. 2011. Sequestration of toxic oligomers by hspb1 as a cytoprotective mechanism. *Mol Cell Biol,* 31**,** 3146-3157.

Parcellier, A., Schmitt, E., Brunet, M., Hammann, A., Solary, E. & Garrido, C. 2005. Small heat shock proteins hsp27 and alphab-crystallin: Cytoprotective and oncogenic functions. *Antioxid Redox Signal,* 7**,** 404-413.

Pasta, S. Y., Raman, B., Ramakrishna, T. & Rao Ch, M. 2004. The ixi/v motif in the c-terminal extension of alpha-crystallins: Alternative interactions and oligomeric assemblies. *Mol Vis,* 10**,** 655-662.

Peschek, J., Braun, N., Franzmann, T. M., Georgalis, Y., Haslbeck, M., Weinkauf, S. & Buchner, J. 2009. The eye lens chaperone alpha-crystallin forms defined globular assemblies. *Proc Natl Acad Sci U S A,* 106**,** 13272-13277.

Peschek, J., Braun, N., Rohrberg, J., Back, K. C., Kriehuber, T., Kastenmuller, A., Weinkauf, S. & Buchner, J. 2013. Regulated structural transitions unleash the chaperone activity of alphab-crystallin. *Proc Natl Acad Sci U S A,* 110**,** E3780-3789.

Pilotto, A., Marziliano, N., Pasotti, M., Grasso, M., Costante, A. M. & Arbustini, E. 2006. Alphab-crystallin mutation in dilated cardiomyopathies: Low prevalence in a consecutive series of 200 unrelated probands. *Biochem Biophys Res Commun,* 346**,** 1115-1117.

Pivovarova, A. V., Chebotareva, N. A., Chernik, I. S., Gusev, N. B. & Levitsky, D. I. 2007. Small heat shock protein hsp27 prevents heat-induced aggregation of f-actin by forming soluble complexes with denatured actin. *FEBS J,* 274**,** 5937-5948.

Pivovarova, A. V., Mikhailova, V. V., Chernik, I. S., Chebotareva, N. A., Levitsky, D. I. & Gusev, N. B. 2005. Effects of small heat shock proteins on the thermal denaturation and aggregation of f-actin. *Biochem Biophys Res Commun,* 331**,** 1548-1553.

Radford, S. E. & Dobson, C. M. 1999. From computer simulations to human disease: Emerging themes in protein folding. *Cell,* 97**,** 291-298.

Rane, M. J., Coxon, P. Y., Powell, D. W., Webster, R., Klein, J. B., Pierce, W., Ping, P. & Mcleish, K. R. 2001. P38 kinase-dependent mapkapk-2 activation functions as 3-phosphoinositide-dependent kinase-2 for akt in human neutrophils. *J Biol Chem,* 276**,** 3517-3523.

Rane, M. J., Pan, Y., Singh, S., Powell, D. W., Wu, R., Cummins, T., Chen, Q., Mcleish, K. R. & Klein, J. B. 2003. Heat shock protein 27 controls apoptosis by regulating akt activation. *J Biol Chem,* 278**,** 27828-27835.

Renkawek, K., Bosman, G. J. & De Jong, W. W. 1994a. Expression of small heat-shock protein hsp 27 in reactive gliosis in alzheimer disease and other types of dementia. *Acta Neuropathol,* 87**,** 511-519.

Renkawek, K., Voorter, C. E., Bosman, G. J., Van Workum, F. P. & De Jong, W. W. 1994b. Expression of alpha b-crystallin in alzheimer's disease. *Acta Neuropathol,* 87**,** 155-160.

Rocchi, P., Jugpal, P., So, A., Sinneman, S., Ettinger, S., Fazli, L., Nelson, C. & Gleave, M. 2006. Small interference rna targeting heat-shock protein 27 inhibits the growth of prostatic cell lines and induces apoptosis via caspase-3 activation in vitro. *BJU Int,* 98**,** 1082-1089.

Rogalla, T., Ehrnsperger, M., Preville, X., Kotlyarov, A., Lutsch, G., Ducasse, C., Paul, C., Wieske, M., Arrigo, A. P., Buchner, J. & Gaestel, M. 1999. Regulation of hsp27 oligomerization, chaperone function, and protective activity against oxidative stress/tumor necrosis factor alpha by phosphorylation. *J Biol Chem,* 274**,** 18947-18956.

Roman, S. G., Chebotareva, N. A., Eronina, T. B., Kleymenov, S. Y., Makeeva, V. F., Poliansky, N. B., Muranov, K. O. & Kurganov, B. I. 2011. Does the crowded cell-like environment reduce the chaperone-like activity of alpha-crystallin? *Biochemistry,* 50**,** 10607-10623.

Rose, R. J., Labrijn, A. F., Van Den Bremer, E. T., Loverix, S., Lasters, I., Van Berkel, P. H., Van De Winkel, J. G., Schuurman, J., Parren, P. W. & Heck, A. J. 2011. Quantitative analysis of the interaction strength and dynamics of human igg4 half molecules by native mass spectrometry. *Structure,* 19**,** 1274-1282.

Ross, C. A. & Poirier, M. A. 2004. Protein aggregation and neurodegenerative disease. *Nat Med,* S**,** 10-17.

Ruotolo, B. T., Benesch, J. L., Sandercock, A. M., Hyung, S. J. & Robinson, C. V. 2008. Ion mobility-mass spectrometry analysis of large protein complexes. *Nat Protoc,* 3**,** 1139-1152.

Sakuma, K., Watanabe, K., Totsuka, T. & Kato, K. 1998. Pathological changes in levels of three small stress proteins, alphab crystallin, hsp 27 and p20, in the hindlimb muscles of dy mouse. *Biochim Biophys Acta,* 1406**,** 162-168.

Santhoshkumar, P., Murugesan, R. & Sharma, K. K. 2009. Deletion of (54)flrapswf(61) residues decreases the oligomeric size and enhances the chaperone function of alphab-crystallin. *Biochemistry,* 48**,** 5066-5073.

Schepers, H., Geugien, M., Van Der Toorn, M., Bryantsev, A. L., Kampinga, H. H., Eggen, B. J. & Vellenga, E. 2005. Hsp27 protects aml cells against vp-16-induced apoptosis through modulation of p38 and c-jun. *Exp Hematol,* 33**,** 660-670.

Selcen, D. & Engel, A. G. 2003. Myofibrillar myopathy caused by novel dominant negative alpha b-crystallin mutations. *Ann Neurol,* 54**,** 804-810.

Serpell, L. C., Sunde, M. & Blake, C. C. 1997. The molecular basis of amyloidosis. *Cell Mol Life Sci,* 53**,** 871-887.

Shammas, S. L., Waudby, C. A., Wang, S., Buell, A. K., Knowles, T. P., Ecroyd, H., Welland, M. E., Carver, J. A., Dobson, C. M. & Meehan, S. 2011. Binding of the molecular chaperone alphab-crystallin to abeta amyloid fibrils inhibits fibril elongation. *Biophys J,* 101**,** 1681-1689.

Shashidharamurthy, R., Koteiche, H. A., Dong, J. & Mchaourab, H. S. 2005. Mechanism of chaperone function in small heat shock proteins: Dissociation of the hsp27 oligomer is required for recognition and binding of destabilized t4 lysozyme. *J Biol Chem,* 280**,** 5281-5289.

Shukla, A. K. & Futrell, J. H. 2000. Tandem mass spectrometry: Dissociation of ions by collisional activation. *J Mass Spectrom,* 35**,** 1069-1090.

Siezen, R. J., Bindels, J. G. & Hoenders, H. J. 1978. The quaternary structure of bovine alpha-crystallin. Size and charge microheterogeneity: More than 1000 different hybrids? *Eur J Biochem,* 91**,** 387-396.

Sluchanko, N. N., Chebotareva, N. A. & Gusev, N. B. 2015. Quaternary structure of human small heat shock protein hspb6 (hsp20) in crowded media modeled by trimethylamine n-oxide (tmao): Effect of protein phosphorylation. *Biochimie,* 108**,** 68-75.

Sobott, F., Benesch, J. L., Vierling, E. & Robinson, C. V. 2002. Subunit exchange of multimeric protein complexes. Real-time monitoring of subunit exchange between small heat shock proteins by using electrospray mass spectrometry. *J Biol Chem,* 277**,** 38921-38929.

Sreelakshmi, Y. & Sharma, K. K. 2005. Recognition sequence 2 (residues 60-71) plays a role in oligomerization and exchange dynamics of alphab-crystallin. *Biochemistry,* 44**,** 12245-12252.

Sreelakshmi, Y. & Sharma, K. K. 2006. The interaction between alphaa- and alphab-crystallin is sequence-specific. *Mol Vis,* 12**,** 581-587.

Stefani, M. & Dobson, C. M. 2003. Protein aggregation and aggregate toxicity: New insights into protein folding, misfolding diseases and biological evolution. *Journal of Molecular Medicine,* 81**,** 678-699.

Stengel, F., Baldwin, A. J., Painter, A. J., Jaya, N., Basha, E., Kay, L. E., Vierling, E., Robinson, C. V. & Benesch, J. L. 2010. Quaternary dynamics and plasticity underlie small heat shock protein chaperone function. *Proc Natl Acad Sci U S A,* 107**,** 2007-2012.

Stirling, P. C., Lundin, V. F. & Leroux, M. R. 2003. Getting a grip on non-native proteins. *EMBO Rep,* 4**,** 565-570.

Stranks, S. D., Ecroyd, H., Van Sluyter, S., Waters, E. J., Carver, J. A. & Von Smekal, L. 2009. Model for amorphous aggregation processes. *Phys Rev E Stat Nonlin Soft Matter Phys,* 80**,** 051907.

Sun, Y. & Macrae, T. H. 2005. Small heat shock proteins: Molecular structure and chaperone function. *Cell Mol Life Sci,* 62**,** 2460-2476.

Sunde, M., Serpell, L. C., Bartlam, M., Fraser, P. E., Pepys, M. B. & Blake, C. C. 1997. Common core structure of amyloid fibrils by synchrotron x-ray diffraction. *J Mol Biol,* 273**,** 729-739.

Tang, B., Liu, X., Zhao, G., Luo, W., Xia, K., Pan, Q., Cai, F., Hu, Z., Zhang, C., Chen, B., Zhang, F., Shen, L., Zhang, R. & Jiang, H. 2005. Mutation analysis of the small heat shock protein 27 gene in chinese patients with charcot-marie-tooth disease. *Arch Neurol,* 62**,** 1201-1207.

Theriault, J. R., Lambert, H., Chavez-Zobel, A. T., Charest, G., Lavigne, P. & Landry, J. 2004. Essential role of the nh2-terminal wd/epf motif in the phosphorylation-activated protective function of mammalian hsp27. *J Biol Chem,* 279**,** 23463-23471.

Thompson, J. D., Higgins, D. G. & Gibson, T. J. 1994. Clustal w: Improving the sensitivity of progressive multiple sequence alignment through sequence weighting, position-specific gap penalties and weight matrix choice. *Nucleic Acids Res,* 22**,** 4673-4680.

Thulasiraman, V., Yang, C. F. & Frydman, J. 1999. In vivo newly translated polypeptides are sequestered in a protected folding environment. *EMBO J,* 18**,** 85-95.

Treweek, T. M., Meehan, S., Ecroyd, H. & Carver, J. A. 2015. Small heat-shock proteins: Important players in regulating cellular proteostasis. *Cell Mol Life Sci,* 72**,** 429-451.

Treweek, T. M., Rekas, A., Lindner, R. A., Walker, M. J., Aquilina, J. A., Robinson, C. V., Horwitz, J., Perng, M. D., Quinlan, R. A. & Carver, J. A. 2005. R120g alphab-crystallin promotes the unfolding of reduced alpha-lactalbumin and is inherently unstable. *FEBS J,* 272**,** 711-724.

Vicart, P., Caron, A., Guicheney, P., Li, Z., Prevost, M. C., Faure, A., Chateau, D., Chapon, F., Tome, F., Dupret, J. M., Paulin, D. & Fardeau, M. 1998. A missense mutation in the alphab-crystallin chaperone gene causes a desmin-related myopathy. *Nat Genet,* 20**,** 92-95.

Walsh, D. M., Klyubin, I., Fadeeva, J. V., Cullen, W. K., Anwyl, R., Wolfe, M. S., Rowan, M. J. & Selkoe, J. 2002. Naturally secreted oligomers of amyloid b protein potentially inhibit hippocampal long-term potentiation in vivo. *Nature,* 416**,** 535-539.

Waudby, C. A., Knowles, T. P., Devlin, G. L., Skepper, J. N., Ecroyd, H., Carver, J. A., Welland, M. E., Christodoulou, J., Dobson, C. M. & Meehan, S. 2010. The interaction of alphab-crystallin with mature alpha-synuclein amyloid fibrils inhibits their elongation. *Biophys J,* 98**,** 843-851.

Wilson, M. R., Yerbury, J. J. & Poon, S. 2008. Potential roles of abundant extracellular chaperones in the control of amyloid formation and toxicity. *Molecular BioSystems,* 4**,** 42-52.

Wu, R., Kausar, H., Johnson, P., Montoya-Durango, D. E., Merchant, M. & Rane, M. J. 2007. Hsp27 regulates akt activation and polymorphonuclear leukocyte apoptosis by scaffolding mk2 to akt signal complex. *J Biol Chem,* 282**,** 21598-21608.

Xia, Y., Liu, Y., Wan, J., Wang, M., Rocchi, P., Qu, F., Iovanna, J. L. & Peng, L. 2009. Novel triazole ribonucleoside down-regulates heat shock protein 27 and induces potent anticancer activity on drug-resistant pancreatic cancer. *J Med Chem,* 52**,** 6083-6096.

Yang, W. Y. & Gruebele, M. 2003. Folding at the speed limit. *Nature,* 423**,** 193-197.

Chapter 8:

Appendices

Chapter 8: Appendices

8.1 Appendix I –Hsp27 structure and function supplementary material

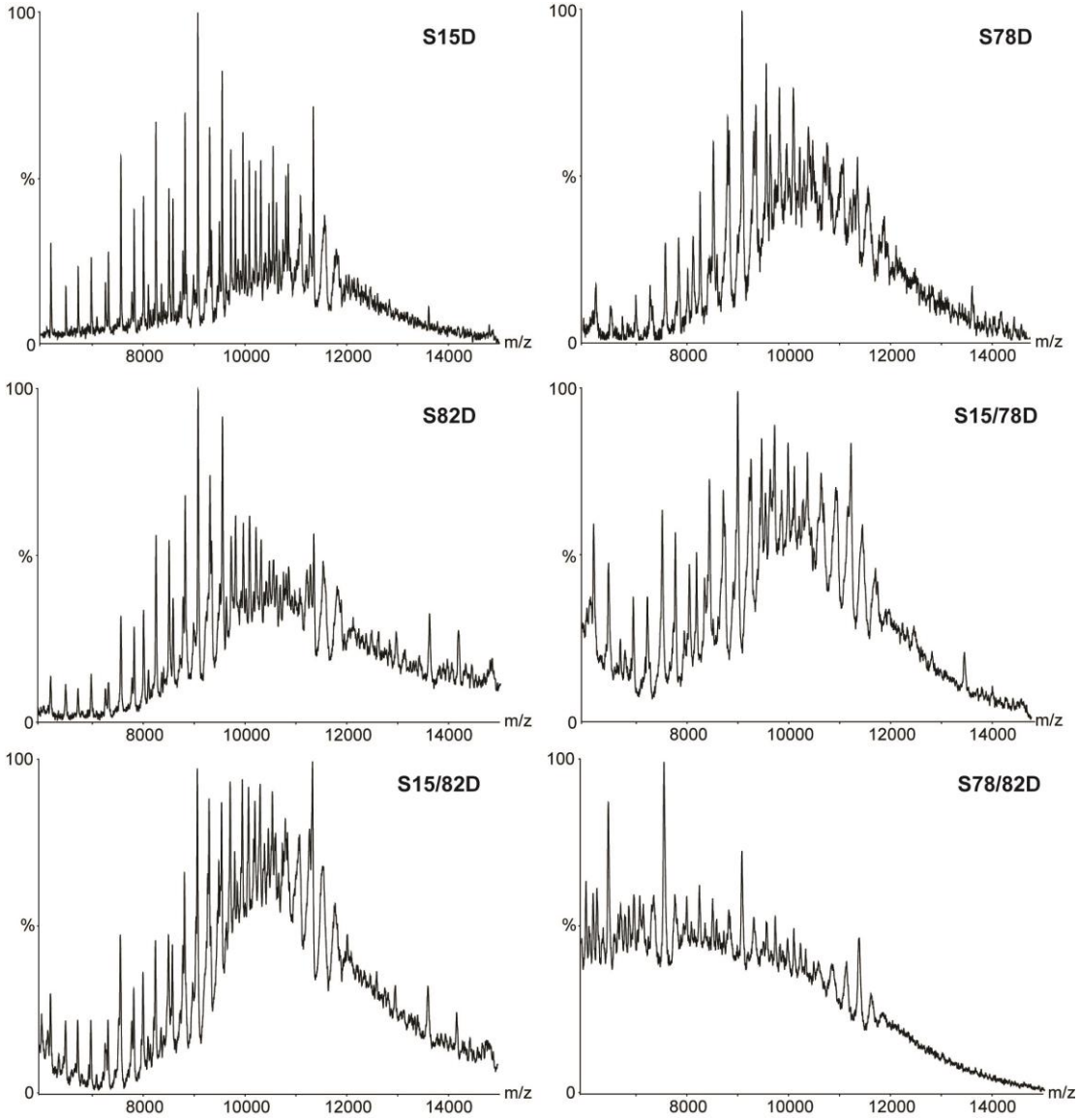

Figure 8.1 (related to Chapter 3, Figure 3.3, page 67): Collision-induced dissociation mass spectrometry of Hsp27 phosphomimics
Spectra were acquired at higher accelerating voltage (200 V) where signal in the *n* region (6,000 – 14,000 *m/z*) were substantially resolved. The charge state distributions in this region were used to identify and determine the relative abundance of $Hsp27_M$.

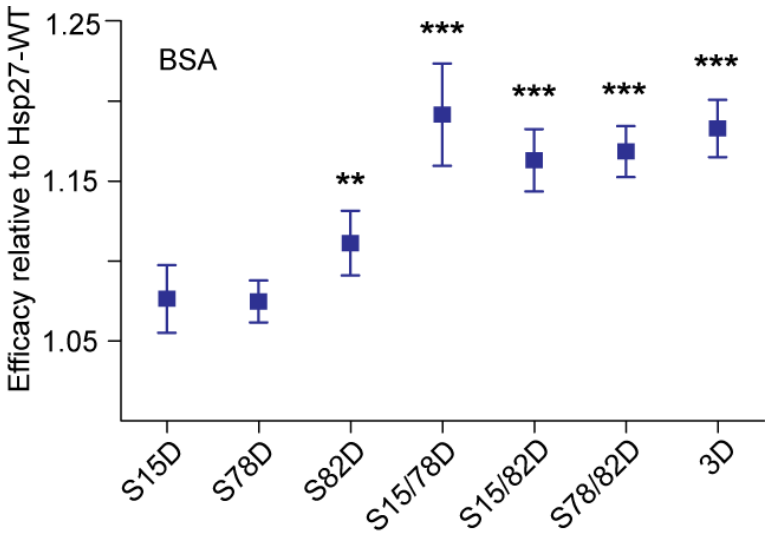

Figure 8.2 (related to Chapter 3, Figure 3.5, page 72): Chaperone activity of Hsp27-WT and phosphomimics against amorphous BSA aggregation
Chaperone efficacy of the Hsp27 isoforms containing MMP was determined relative to Hsp27-WT for the target protein (BSA). Inhibition of amorphously aggregating BSA was monitored by the change in light scatter at 340 nm. Variants that showed a significant increase in activity compared to Hsp27-WT are indicated (*= $p < 0.05$; **= $p < 0.01$; ***= $p < 0.001$) (n = 3 – 5; mean ± SEM).

8.2 Appendix II – Hsp27 structural dynamics supplementary material

Table 8.1 (related to Chapter 4, Figure 4.3, page 86): Drift time analysis of Hsp27 dimers and 12-mers by IM-MS

Arrival time and peak width at half height of $Hsp27_M$ dimers and 12-mers as determined by IM-MS. The increase in both arrival time and peak width at half height confers to an increase in the unstructured state of the species of $Hsp27_M$.

Dimer^{13+}	Arrival time (ms)			Peak width at half height (ms)		
	WH8	WH9	WH10	WH8	WH9	WH10
Hsp27-1D	9.87	7.31	5.9	1.68	1.42	0.92
Hsp27-2D	10.13	7.42	5.52	1.52	1.55	1.22
Hsp27-3D	10.39	7.38	5.9	1.8	2.18	1.76
12-mer^{31+}	Arrival time (ms)			Peak width at half height (ms)		
	WH11.5		WH13	WH11.5		WH13
Hsp27-WT	13.07		9.23	2.1		1.17
Hsp27-1D	12.81		9.22	2.0		1.22
Hsp27-2D	12.81		9.22	2.0		1.39

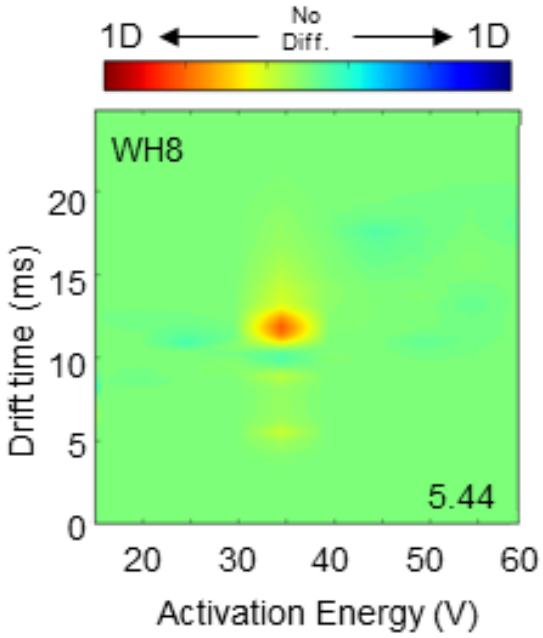

Figure 8.3 (related to Chapter 4, Figure 4.5, page 89): Internal RMSD determination of the collision-induced unfolding dynamics of $Hsp27_M$ dimers by IM-MS

CIU of $Hsp27_M$ dimers was monitored with increasing activation energy. Heat maps highlight the differences in the unfolding of the dimer^{13+} in the gas-phase between the same isoform (Hsp27-S15D; Hsp27-1D) calculated on two different occasions at the same WH (V). RMSD values (%) (*bottom right corner*) indicate the difference in the unfolding of the dimer between each pair analysed (pairs analysed where greatest difference attributed to one isoform indicated by either dark blue or red). Difference plots and RMSD values were calculated using CIUsuite with default settings (Eschweiler *et al.*, 2015).

8.3 Appendix III – αB-c N-terminal mutation structure and function supplementary material

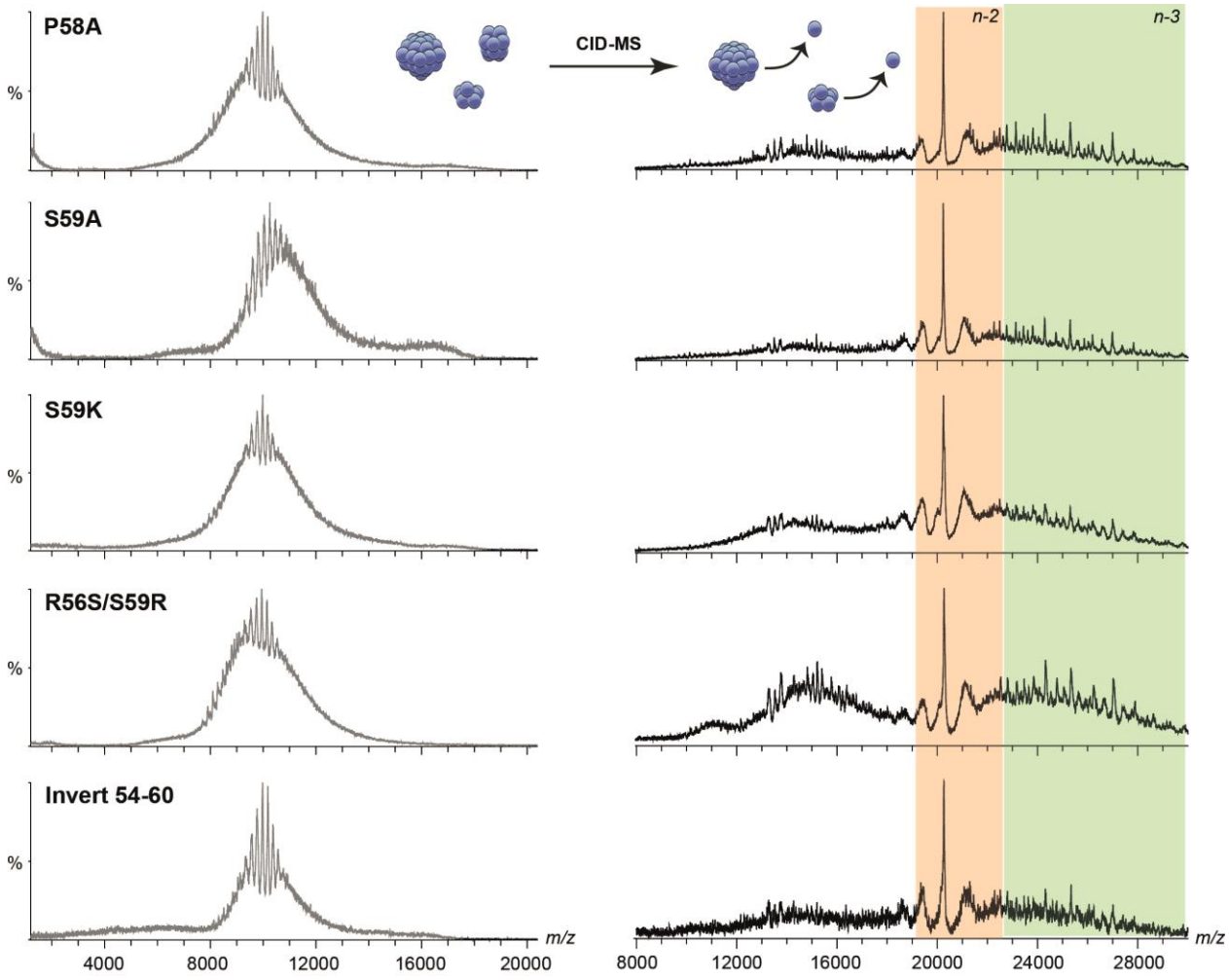

Figure 8.4 (related to Chapter 5, Figure 5.4, page 117): Collision-induced dissociation mass spectrometry of αB-c N-terminal domain mutants
Spectra were acquired at both lower activation energy (20 V; *left panels*) and at higher activation energies (200 V; *right panels*) where signal in the *n-2* (*orange*) *and n-3* (*green*) regions (19,000 – 30,000 *m/z*) were substantially resolved. The charge state distributions in this region were used to identify and determine the relative abundance of αB-c mutant isoforms.

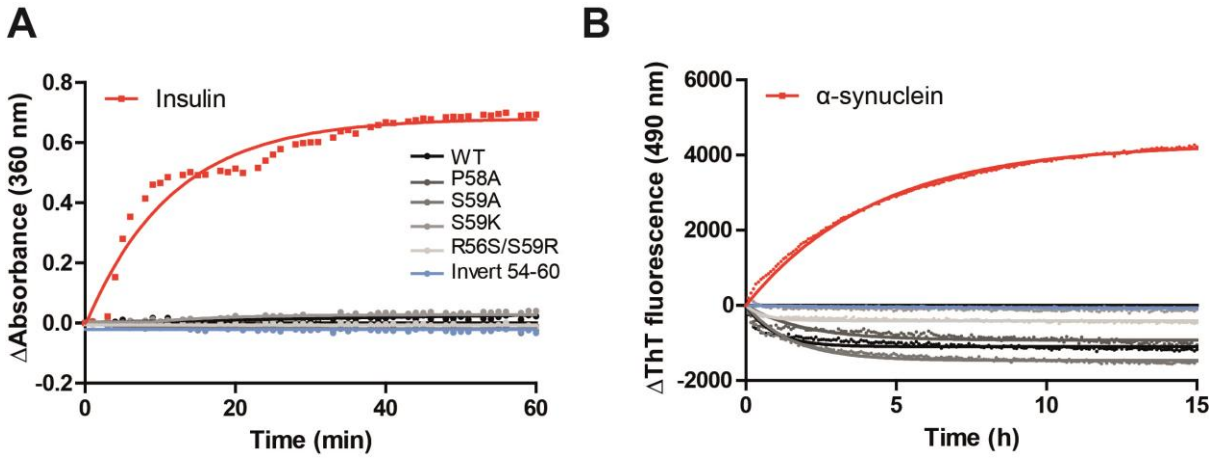

Figure 8.5 (related to Chapter 5, Figure 5.5, page 119): The aggregation propensity of the N-terminal αB-c variants in the absence of amorphous and fibrillar client proteins

***A*:** In the absence of client protein (insulin) there was no observable increase in light scatter at 360 nm of αB-c isoforms (75 µM). ***B*:** In the absence of client protein (seeded αS, 10% w/w seed relative to αS monomer) there was no observable increase in ThT fluorescence at 490 nm of αB-c isoforms (25 µM). Amorphous and fibrillar aggregation assays were performed in 50 mM phosphate buffer (pH 7.4) at 37 °C.

8.4 Appendix IV – Media and buffer compositions

Luria-Bertani (LB) broth

Tryptone	10 g/L
Yeast Extract	5 g/L
NaCl	10 g/L

LB agar

Tryptone	10 g/L
Yeast Extract	5 g/L
NaCl	10 g/L
Agar	15 g/L

1 × Phosphate buffered saline (PBS) (pH 7.4)

NaCL	8 g/L
KCl	0.2 g/L
Na_2HPO_4	1.44 g/L
KH_2PO_4	0.24 g/L

50 mM phosphate buffer (pH 7.4)

NaH_2PO_4	1.58 g/L
Na_2HPO_4	6.37 g/L

5 × SDS-PAGE sample buffer

Tris-HCl (pH 6.8)	200 mM
Glycerol	50 % (v/v)
SDS	1 g/L
2-Mercaptoethanol	300 mM
Bromophenol blue	0.4 % (w/v)

Coomassie blue stain

Coomassie blue	2 g/L
Methanol	40 % (v/v)
Glacial acetic acid	10 % (v/v)

Rapid destain

Methanol	40 % (v/v)
Glacial acetic acid	10 % (v/v)

200 mM ammonium acetate (pH 6.8)

7.5 M NH_4OAc	2.66 % (v/v)